Production of Scalar Leptons at Linear Colliders

Dissertation

zur Erlangung des Doktorgrades

des Fachbereichs Physik

der Universität Hamburg

vorgelegt von

Ayres Freitas

aus Aurich

Hamburg

2002

Gutachter der Dissertation:	Prof. Dr. P. M. Zerwas Prof. Dr. B. A. Kniehl
Gutachter der Disputation:	Prof. Dr. P. M. Zerwas Prof. Dr. J. Bartels
Datum der Disputation:	09.07.2002
Dekan des Fachbereichs Physik:	Prof. Dr. F.-W. Büßer
Vorsitzender des Promotionsausschusses:	Prof. Dr. G. Huber

Abstract

This thesis presents an analysis of precision physics in pair production of scalar leptons at e^+e^- and e^-e^- linear colliders. From the measurement of the production cross-sections near threshold and in the continuum it is possible to determine the masses and couplings of the scalar leptons with high precision. This is important for the experimental establishment of supersymmetry and the investigation of the fundamental source of supersymmetry breaking.

In order to provide reliable theoretical predictions for the excitation curves near threshold, the treatment of non-zero width and Coulomb rescattering effects is studied with special emphasis on the preservation of gauge-invariance. The influence of backgrounds both from Standard Model and supersymmetric sources is investigated, and it is shown how they can be controlled with suitable cuts and beam polarization. Secondly, the complete next-to-leading order radiative corrections to the production of right-chiral selectrons and smuons in the Minimal Supersymmetric Standard Model (MSSM) are presented. This comprises a first step towards a firm theoretical understanding of the scalar lepton cross-sections in the continuum. The corrections are found to be sizeable for the expected experimental accuracy. The third major part discusses the precision of the mass determination in threshold scans and the information about supersymmetric couplings that can be obtained from scalar lepton production.

Zusammenfassung

In dieser Arbeit werden Untersuchungen zu Präzisionsphysik bei der Paar-Produktion von skalaren Leptonen an e^+e^- und e^-e^- Linearcollidern vorgestellt. Durch die Messung der Produktions-Wirkungsquerschnitte an der Schwelle und im Kontinuum können die Massen und Kopplungen der skalaren Leptonen mit hoher Präzision bestimmt werden. Dies ist von grundlegender Bedeutung für die experimentelle Identifikation von Supersymmetrie und die Untersuchung des zugrundeliegenden Mechanismus, der für die Brechung von Supersymmetrie verantwortlich ist.

Für eine zuverlässige theoretische Vorhersage der Anregungskurve an der Schwelle wird die Behandlung von Breiten- und Coulomb-Streuungs-Effekten diskutiert, wobei im besonderen die Erhaltung der Eichinvarianz berücksichtigt wird. Außerdem wird der Einfluß von sowohl Standardmodell- als auch supersymmetrischen Hintergründen untersucht, und gezeigt, wie diese durch geeignete Schnitte und Strahl-Polarisation kontrolliert werden können. Des weiteren werden die vollständigen Strahlungskorrekturen zur Produktion von rechts-chiralen Selektronen und Smyonen in nächstführender Ordnung im Minimalen Supersymmetrischen Standardmodell (MSSM) vorgestellt. Dies stellt einen ersten Schritt für ein fundiertes theoretisches Verständnis der Wirkungsquerschnitte der skalaren Leptonen im Kontinuum dar. Die Korrekturen ergeben einen wichtigen Effekt, der deutlich über der erwarteten experimentellen Präzision liegt. Ein dritter Schwerpunkt beschäftigt sich mit der Präzision der Massenbestimmung in Schwellen-Scans und der Frage, welche Informationen über supersymmetrische Kopplungen aus der Produktion von skalaren Leptonen erhalten werden können.

Contents

1 Introduction **1**

2 Supersymmetric extensions of the Standard Model **5**
2.1 The Standard Model of electroweak interactions 5
2.2 The minimal supersymmetric extension of the Standard Model 7
2.3 Supersymmetry breaking schemes 14

3 Phenomenology of sleptons at linear colliders **19**

4 Predictions for off-shell slepton pair production **25**
4.1 Finite width effects and gauge invariance 25
4.2 Leading radiative corrections 27
4.3 The Monte Carlo program 32
4.4 Signatures and backgrounds 36
4.5 Analysis of smuon and selectron pair production near threshold 41

5 Radiative corrections to on-shell slepton pair production **45**
5.1 Renormalization of the MSSM 45
5.2 Outline of the calculation 59
5.3 Results for smuon pair production 62
5.4 Results for selectron pair production 62
5.5 Superoblique corrections 65

6 Determination of supersymmetric masses and couplings **71**
6.1 Measurement of masses in threshold scans 71
6.2 Testing the equivalence of SM gauge and MSSM Yukawa couplings 76

7 Conclusions **83**

Appendix **85**

A Reference scenarios **87**

Bibliography **93**

Chapter 1

Introduction

For more than two decades the Standard Model of electroweak interactions [1] in conjunction with the theory of Quantum Chromodynamics [2] has been widely tested and established in parts up to the quantum level in various collider and low-energy experiments (see [3] for more information). Nevertheless, despite its enormous success, the Standard Model cannot be regarded as the ultimate theory of nature because of several conceptual problems. In particular in the context of Grand Unified Theories, which combine the electroweak and strong forces in one gauge group, and in the attempt to include gravity, severe difficulties arise within the Standard Model.

The introduction of supersymmetry [4] provides a framework which naturally resolves the aforementioned problems. Supersymmetry extends the conventional Poincaré symmetry of space-time [5] by relating fermionic and bosonic states. As a consequence, in a supersymmetric extension of the Standard Model all known particles are accompanied by a partner which differs in the spin quantum number by 1/2. The partners of the gauge and Higgs bosons would be gauginos and higgsinos with spin 1/2 while the leptons and quarks are paired with scalar companions called scalar leptons (sleptons) and scalar quarks (squarks).

If supersymmetry is realized in nature it obviously has to be broken since none of the superpartner particles have been observed yet in experiment. The construction of a viable mechanism as source of supersymmetry breaking is a difficult issue. While a variety of breaking schemes has been proposed they mostly require the introduction of additional unobserved degrees of freedom. For phenomenological purposes the breaking of supersymmetry is therefore usually parametrized by the most general explicit breaking terms in the Lagrangian. The structure of the breaking terms is constrained by the preservation of gauge symmetry and the requirement of stabilization against quantum corrections from higher scales. This leads to a set of so-called soft-breaking terms [6]. The stability of quantum corrections furthermore implies that at least some of the supersymmetric partners are relatively light, with a mass around 1 TeV or less, and thus within reach of this or the next generation of high-energy colliders.

As a consequence of the soft-breaking, a large number of additional parameters are introduced, resulting in a complex phenomenology and rich spectroscopy of states. If supersymmetry is detected at a future collider it will therefore be an enormous task to investigate the masses, couplings and quantum numbers of the superpartners. Here

the concept of a high-energy e^+e^- linear collider [7–9] is of particular interest since it opens up the possibility of precision measurements of supersymmetric particle properties [10–12]. The accurate determination of the soft-breaking parameters could then be used to reconstruct the underlying breaking mechanism [13], which would probably be inaccessible to direct measurements.

The scalar leptons are particularly suited for precision measurements because of their clean final state signature consisting of few leptons plus nothing else. Thus, one of the main challenges in the exploration of the slepton sector will be the accurate determination of their characteristic properties, in particular their masses and couplings.

With a high luminosity linear collider it is possible to experimentally extract particle masses from the measurement of the pair production cross-section near the kinematical threshold [10]. The steep and distinct rise of the excitation curve allows a very precise determination of the slepton masses in these so-called threshold scans.

In contrast to the masses of the superpartners, their couplings cannot be directly modified by soft-breaking terms. As a consequence, supersymmetry predicts the Standard Model gauge couplings and their supersymmetric counterparts to be equal. More precisely, the usual gauge coupling between a vector boson V and fermionic current f, $g(Vff)$, is accompanied by the gauge coupling between the vector boson V and the scalar fermion $\tilde{f}$, $\bar{g}(V\tilde{f}\tilde{f})$, as well as the Yukawa coupling between the gaugino partner $\tilde{V}$ of the vector boson, the fermion f and the sfermion $\tilde{f}$, $\hat{g}(\tilde{V}f\tilde{f})$. Within supersymmetry all three kinds of couplings are required to be identical, $g = \bar{g} = \hat{g}$.

To establish supersymmetry experimentally, it is therefore necessary to measure the couplings of the superpartners precisely so as to test the predicted coupling relations. For the strongly interacting sector this has been investigated in Ref. [14]. The production cross-sections for scalar leptons, on the other hand, are sensitive to the supersymmetric gauge and Yukawa couplings of the electroweak sector. A comparison of accurate cross-section measurements with precise theoretical predictions would thus allow one to constrain the values of these couplings and test their equivalence with the known Standard Model couplings.

This thesis focuses on the theoretical requirements to obtain sufficiently accurate and reliable theoretical predictions for the aforementioned precision measurements in the scalar lepton sector. It covers three main topics:

The first main part is devoted to a careful analysis of excitation curves for sleptons pair production near threshold. In this region the cross-sections are significantly modified by the decay width of the sleptons. It is therefore studied how non-zero slepton widths can be incorporated in theoretical predictions while preserving gauge-invariance. Additionally, the most important higher order effects near threshold are taken into account, notably Coulomb rescattering effects among the produced slepton pairs. The final state signatures can be contaminated by substantial backgrounds both from Standard Model and supersymmetric sources. They are taken into account including non-leading and interference contributions and it is discussed how they can be reduced by appropriate cuts.

Secondly, the production of scalar leptons in the continuum far above threshold is studied. A precise prediction of the cross-sections in this region is relevant for the measurement of the slepton couplings. For this purpose the complete next-to-leading order electroweak radiative corrections to the on-shell pair production of right-chiral smuons

and selectrons are presented, including both virtual loop corrections and real photon emission contributions. As a prerequisite, the on-shell renormalization of the relevant supersymmetric contributions is discussed in detail.

In a third part the precision that can be achieved in the determination of slepton masses and couplings is reexamined. The investigations of previous studies on threshold mass measurements [15–18] are improved by incorporating the theoretical corrections discussed in the first part. The determination of supersymmetric couplings has only scarcely been addressed in the literature so far. The couplings that can be extracted from the smuon and selectron cross-section are discussed and the achievable precision is explored.

The thesis is organized as follows: After an introduction into supersymmetric extensions of the Standard Model and defining the notations and conventions in chapter 2, the phenomenology of sleptons at a linear collider is recapitulated in chapter 3. Chapter 4 deals with the investigation of the threshold behaviour of slepton pair production, while in chapter 5 the $\mathcal{O}(\alpha)$ corrections to these processes in the continuum are presented. The determination of the slepton masses and couplings is analyzed in chapter 6. Finally the conclusions are drawn in chapter 7. The appendix lists the input values used for the numerical studies in this thesis.

Chapter 2

Supersymmetric extensions of the Standard Model

2.1 The Standard Model of electroweak interactions

The electroweak Standard Model [1] is a gauge theory with the gauge group $\mathrm{SU(2)_I} \times \mathrm{U(1)_Y}$. In combination with the $\mathrm{SU(3)_C}$ symmetry of Quantum Chromodynamics [2] (QCD) it is compatible with all available experimental observations from collider experiments (see [3] for details). The only deviation is the experimental evidence for neutrino masses (see below), which however can easily be embedded in the Standard Model by introducing appropriate mass terms.

The left-handed fermion matter fields form doublets $L = (\nu_l, l)$, $Q = (q_\mathrm{u}, q_\mathrm{d})$ under the $\mathrm{SU(2)_I}$ group while the right-handed components are singlets with respect to this group. Here $\nu_l, l, q_\mathrm{u}, q_\mathrm{d}$ denote the fields of neutrino, charged lepton, up-type and down-type quarks, respectively.

The Lagrangian for the fermionic sector reads

$$\mathcal{L}_\mathrm{f} = \overline{L}_\mathrm{L} i\gamma_\mu D_\mu L_\mathrm{L} + \overline{Q}_\mathrm{L} i\gamma^\mu D_\mu Q_\mathrm{L} + \overline{l}_\mathrm{R} i\gamma^\mu D_\mu l_\mathrm{R} + \overline{q}_{u,R} i\gamma^\mu D_\mu q_{u,R} + \overline{q}_{d,R} i\gamma^\mu D_\mu q_{d,R}. \quad (2.1)$$

Each lepton and quark exists in three generations. Right-handed neutrinos are singlets under all gauge groups and thus do not interact with the other particles of the Standard Model. However, the existence of right-handed neutrinos has been proven by recent experimental evidence for mixing between the three neutrino generations [19]. Nevertheless, since the neutrino masses are restricted to be very small, they will be neglected throughout this thesis and therefore do not appear in the Lagrangian. The requirement of local gauge symmetries leads to the introduction of gauge fields $W_\mu^{1,2,3}, B_\mu$ in the covariant derivatives D_μ,

$$D_\mu = \partial_\mu - igI^a W_\mu^a + ig'\frac{Y}{2}B_\mu. \quad (2.2)$$

where Y and I^a are the generators of the U(1) hypercharge and SU(2) isospin groups in their adjoint representation. The fermions can be classified according to their quantum numbers with respect to the hypercharge Y and the third component of the weak isospin I^3 as shown in table 2.1.

			I^3	Y	Q
$\begin{pmatrix}\nu_e\\ e^-\end{pmatrix}_{\mathrm{L}}$	$\begin{pmatrix}\nu_\mu\\ \mu^-\end{pmatrix}_{\mathrm{L}}$	$\begin{pmatrix}\nu_\tau\\ \tau^-\end{pmatrix}_{\mathrm{L}}$	$1/2$ $-1/2$	$-1/2$ $-1/2$	0 -1
$\nu_{e\mathrm{R}}$	$\nu_{\mu\mathrm{R}}$	$\nu_{\tau\mathrm{R}}$	0	0	0
e_{R}	μ_{R}	τ_{R}	0	-1	-1
$\begin{pmatrix}u\\ d\end{pmatrix}_{\mathrm{L}}$	$\begin{pmatrix}c\\ s\end{pmatrix}_{\mathrm{L}}$	$\begin{pmatrix}t\\ b\end{pmatrix}_{\mathrm{L}}$	$1/2$ $-1/2$	$1/6$ $1/6$	$2/3$ $-1/3$
u_{R}	c_{R}	t_{R}	0	$2/3$	$2/3$
d_{R}	s_{R}	b_{R}	0	$-1/3$	$-1/3$

Table 2.1: *Quantum numbers of the Standard Model fermions.*

The kinetic terms for the gauge fields are given by the Yang-Mills Lagrangian

$$\mathcal{L}_{\mathrm{YM}} = -\frac{1}{4}\left(W^a_{\mu\nu}W^{a\mu\nu} + B_{\mu\nu}B^{\mu\nu}\right), \tag{2.3}$$

$$W^a_{\mu\nu} = \partial_\mu W^a_\nu - \partial_\nu W^a_\mu + g\,\epsilon^{abc}\,W^b_\mu W^c_\nu, \tag{2.4}$$

$$B_{\mu\nu} = \partial_\mu B_\nu - \partial_\nu B_\mu, \tag{2.5}$$

using the symbol ϵ^{abc} for the structure constants of the $\mathrm{SU(2)_I}$ group.

The particles of the Standard Model receive their masses due to the vacuum expectation value of a scalar field doublet, the Higgs field. It is described by the Lagrangian

$$\mathcal{L}_{\mathrm{H}} = \left(D_\mu\phi\right)^\dagger\left(D^\mu\phi\right) - V(\phi), \qquad V(\phi) = -\mu^2\phi^\dagger\phi + \frac{\lambda}{4}\left(\phi^\dagger\phi\right)^2. \tag{2.6}$$

At the minimum of the potential V the Higgs doublet acquires a non-zero vacuum expectation value

$$|\langle 0|\phi|0\rangle|^2 = \frac{2\mu^2}{\lambda} =: \frac{v^2}{2}, \tag{2.7}$$

which generates mass terms for the gauge bosons via the covariant derivatives in (2.6). Expanding the Higgs doublet around its vacuum state it can be written as

$$\phi(x) = \begin{pmatrix} G^+(x) \\ \frac{1}{\sqrt{2}}(v + H(x) + iG^0(x)) \end{pmatrix}, \tag{2.8}$$

introducing the physical Higgs boson H with mass $M_{\mathrm{H}} = \sqrt{2}\mu$ and the massless Goldstone bosons G^0, G^+ and $G^- = (G^+)^*$.

The mass eigenstates of the gauge bosons are mixtures of the fields introduced in (2.2),

$$W^\pm_\mu = \frac{1}{\sqrt{2}}\left(W^1_\mu \mp iW^2_\mu\right), \tag{2.9}$$

$$\begin{pmatrix} Z_\mu \\ A_\mu \end{pmatrix} = \begin{pmatrix} c_{\mathrm{W}} & s_{\mathrm{W}} \\ -s_{\mathrm{W}} & c_{\mathrm{W}} \end{pmatrix}\begin{pmatrix} W^3_\mu \\ B_\mu \end{pmatrix}, \tag{2.10}$$

with the masses $M_\mathrm{W}, M_\mathrm{Z}$ of the charged $W^\pm$ boson and the neutral Z boson given by

$$M_\mathrm{W} = gv/2, \qquad M_\mathrm{Z} = M_\mathrm{W}/c_\mathrm{W}, \tag{2.11}$$

and the weak mixing angle θ_W defined as

$$c_\mathrm{W} = \cos\theta_\mathrm{W} = \frac{g}{\sqrt{g^2+g'^2}} = \frac{M_\mathrm{W}}{M_\mathrm{Z}}, \quad s_\mathrm{W} = \sin\theta_\mathrm{W} = \frac{g'}{\sqrt{g^2+g'^2}} = \sqrt{1-\frac{M_\mathrm{W}}{M_\mathrm{Z}}}. \tag{2.12}$$

The massless photon A_μ is the gauge boson of the unbroken electromagnetic subgroup $\mathrm{U}(1)_\mathrm{em} \subset \mathrm{SU}(2)_\mathrm{W} \times \mathrm{U}(1)_\mathrm{Y}$ with the electromagnetic coupling e given by

$$e = \frac{g'g}{\sqrt{g^2+g'^2}}, \qquad g = \frac{e}{s_\mathrm{W}}, \qquad g' = \frac{e}{c_\mathrm{W}}. \tag{2.13}$$

The charges Q of the fermions with respect to the electromagnetic gauge group are listed in the last column of table 2.1.

In order to generate masses for the fermions, the Higgs doublet is coupled to the fermions via Yukawa interactions,

$$\mathcal{L}_\mathrm{Yuk} = c_\mathrm{l}\overline{L}_\mathrm{L} l_\mathrm{R}\phi + c_\mathrm{u}\overline{Q}_\mathrm{L} q_\mathrm{u,R}\tilde{\phi} + c_\mathrm{d}\overline{Q}_\mathrm{L} q_\mathrm{d,R}\phi + \mathrm{h.c.}, \tag{2.14}$$

with the conjugated Higgs doublet $\tilde{\phi} = \epsilon\phi^*$. Throughout this thesis mixing between the fermion generation is neglected, i.e. the coupling matrices c_f are taken to be diagonal. In principle, (2.14) could include mass-generating terms for the neutrinos. However, as already mentioned, in this work the masses and Yukawa couplings of neutrinos are consistently neglected.

2.2 The minimal supersymmetric extension of the Standard Model

Supersymmetry is the only non-trivial extension of the well-known Poincaré and gauge symmetries which may be applied to an S-matrix within quantum field theory [5]. The generators of the supersymmetry group transform fermionic quantities into bosonic ones and vice versa. In general, the number N of independent supersymmetry operators may be larger than one, however for most phenomenological studies—and for this thesis—only the case $N = 1$ is considered, since higher numbers of N do not allow chiral interactions [20].

In supersymmetric quantum field theories with $N = 1$ [4] each bosonic particle with spin 0 or 1 is accompanied by a fermionic partner of spin 1/2. Apart from the spin, the partners have identical quantum numbers.

2.2.1 Motivation for supersymmetry

In this section some of the most important theoretical drawbacks of the Standard Model shall be addressed and it is explained how supersymmetry may help to overcome these problems.

Non-supersymmetric theories like the Standard Model suffer from the fact that radiative corrections to scalar masses are quadratically dependent on any other scale present in theory. In a Grand Unified Theory additional super-heavy gauge bosons with masses of $M_{\mathrm{GUT}} \sim \mathcal{O}(10^{16}\ \mathrm{GeV})$ are predicted. Any scalar mass would receive loop corrections from these bosons which result in a shift of the scalar mass of

$$\frac{\delta M_{\mathrm{S}}^2}{M_{\mathrm{S}}^2} \sim \alpha \frac{M_{\mathrm{GUT}}^2}{\Lambda_{\mathrm{EW}}^2} \sim \mathcal{O}(10^{27}), \tag{2.15}$$

where the electroweak scale $\Lambda_{\mathrm{EW}} \sim \mathcal{O}(100\ \mathrm{GeV})$ is taken as an rough measure of the masses of all other particles which do not decouple at the high scale. In order to arrange for the mass of the Higgs boson to be less than 1 TeV an enormous amount of finetuning is required. Furthermore at each order of perturbation theory this finetuning has to be performed independently. Since this possibility seems to be very unnatural one usually speaks of the *naturalness problem* of the Higgs boson.

In supersymmetric theories each bosonic particle has a corresponding fermionic partner with equal mass which also yields loop contributions to the scalar mass corrections. Since the leading fermionic contributions enter with a minus sign relative to the bosonic corrections, the two contributions cancel and the remaining dependence on the high scale is merely logarithmic,

$$\frac{\delta M_{\mathrm{S}}^2}{M_{\mathrm{S}}^2} \sim \alpha \log \frac{M_{\mathrm{GUT}}^2}{\Lambda_{\mathrm{EW}}^2} \sim \mathcal{O}(1). \tag{2.16}$$

In reality, of course, supersymmetry cannot be an exact symmetry of nature since no supersymmetric partner to any of the Standard Model particles has been observed yet. Due to some unknown breaking mechanism, the masses of the supersymmetric partners are shifted to some higher scale above the electroweak scale. However, in order to keep the quadratic corrections to scalar masses reasonably small, the supersymmetry breaking scale $\tilde{m}$ is expected to exceed the typical mass scale m of the Standard Model by less than one order of magnitude, so that the rough bound $\tilde{m} \lesssim 1$ TeV is obtained.

Beside the stability of the low-energy sector against radiative corrections, a realistic picture of a Grand Unified Theory would require that the three gauge couplings of the Standard Model unify at some high scale. In order to check this assumption, the measured values of the fine structure constant α, the weak mixing angle $\sin^2\theta_{\mathrm{W}}$ and the strong coupling α_{s} are extrapolated to higher energies using two-loop renormalization group [21] equations. Within the minimal supersymmetric extension of the Standard Model (MSSM), the renormalization group running of the couplings is altered due to supersymmetric loop contributions [22]. In contrast to the Standard Model, it turns out that in the MSSM the three running couplings unify with a remarkable agreement at a scale $M_{\mathrm{GUT}} \approx 2 \times 10^{16}$ GeV in the MSSM under the assumption that the supersymmetry breaking scale is around 1 TeV. Furthermore the numerical agreement does not change significantly for a variation of the breaking scale by one order of magnitude [23].

It is widely expected that at some very high scale like the Plank scale the electroweak and strong gauge interaction would ultimately unify with gravity into one fundamental force. The only non-trivial unification of internal gauge symmetries and the space-time

Names		spin 0	spin $\frac{1}{2}$
squarks, quarks	Q	$\left(\tilde{u}_\mathrm{L}\ \ \tilde{d}_\mathrm{L}\right)$	$\left(u_\mathrm{L}\ \ d_\mathrm{L}\right)$
up-squark, up-quark	U	$\tilde{u}^*_\mathrm{R}$	$u^\dagger_\mathrm{R}$
down-squark, down-quark	D	$\tilde{d}^*_\mathrm{R}$	$d^\dagger_\mathrm{R}$
sleptons, leptons	L	$\left(\tilde{\nu}_\mathrm{L}\ \ \tilde{e}_\mathrm{L}\right)$	$\left(\nu_\mathrm{L}\ \ e_\mathrm{L}\right)$
sneutrino, neutrino	N	$\tilde{\nu}^*_\mathrm{R}$	$\nu^\dagger_\mathrm{R}$
selectron, electron	E	$\tilde{e}^*_\mathrm{R}$	$e^\dagger_\mathrm{R}$
Higgs, higgsinos	H_u	$\left(H^+_\mathrm{u}\ \ H^0_\mathrm{u}\right)$	$\left(\widetilde{H}^+_\mathrm{u}\ \ \widetilde{H}^0_\mathrm{u}\right)$
	H_d	$\left(H^0_\mathrm{d}\ \ H^-_\mathrm{d}\right)$	$\left(\widetilde{H}^0_\mathrm{d}\ \ \widetilde{H}^-_\mathrm{d}\right)$

Table 2.2: *Chiral supermultiplets in the MSSM. The leptonic and quark fields exist in three generation of which the first generation is shown here as an example.*

symmetry can be achieved by introducing supersymmetry. On the other hand, the requirement of local supersymmetry naturally leads to the construction of General Relativity and is therefore usually called supergravity [24]. It is known that supergravity models cannot be considered as a "Theory of Everything", since they are non-renormalizable (see e.g. [25]). There is the hope that these problems will eventually be resolved within the framework of superstrings, whereof supergravity is a low-energy effective theory. Nevertheless, supergravity models are important for the low-energy sector since they provide a scenario for the breaking of supersymmetry.

In R-parity conserving models (see page 11), the lightest supersymmetric particle (LSP) cannot decay into any of the Standard Model particles and is thus stable. When being neutral it might therefore provide an ideal candidate for non-baryonic dark matter [26], which forms the dominant contribution of all mass in the universe.

2.2.2 The Lagrangian of the MSSM

The Minimal Supersymmetric Standard Model (MSSM) introduces the minimal particle content which is needed to extend the Standard Model into a supersymmetric theory. Each of the fermions is embedded into a chiral multiplet which in addition contains a complex scalar field. It is important to note that the left- and right-handed components of a Dirac fermion reside in different superfields. Correspondingly each scalar field of the Standard Model is accompanied by a fermionic partner. The gauge vector fields together with a fermionic partner compose a vector multiplet. The general form of a vector multiplet is quite involved, but by exploiting the invariance under supersymmetric gauge transformations it can be restricted to a special gauge, such as the Wess-Zumino gauge [4]. In addition to the aforementioned components each super-multiplet contains an additional auxiliary field in order to close the supersymmetry algebra. However these

Names		spin $\frac{1}{2}$	spin 1
bino, B_μ boson	V'	$\widetilde{B}$	B_μ
winos, W^a_μ bosons	V^a	$\widetilde{W}^a$	W^a_μ
gluinos, gluons	$V^a_{\rm s}$	$\tilde{g}^a$	G^a_μ

Table 2.3: *Vector supermultiplets in the MSSM.*

auxiliary fields have no dynamical degrees of freedoms and can be directly integrated out.

Since a superfield contains bosonic, commuting and fermionic, anti-commuting degrees of freedom, it is a function not only of the usual Minkowski coordinates x^μ, but also of anti-commuting, spinor-like *Grassmann* variables $\theta, \bar{\theta}$.

The particle content of the MSSM is listed in Tables 2.2 and 2.3. In contrast to the Standard Model, two Higgs doublets $H_{\rm u}$ and $H_{\rm d}$ are required in the MSSM in order to give masses to both up- and down-type fermions. The reason for this is that a Yukawa coupling involving a conjugated Higgs field like $\tilde{\phi}$ in (2.14) is forbidden in supersymmetry. Furthermore, since the corresponding higgsinos contribute to the axial anomaly, two Higgs doublets are needed to let the anomaly vanish.

The exactly supersymmetric part of the Lagrangian of the electroweak MSSM reads

$$\begin{aligned}
\mathcal{L}_{\rm susy} = & \int d^2\theta \left[\frac{1}{16g^2} W^{a\alpha} W^a_\alpha + \frac{1}{16g'^2} W'^\alpha W'_\alpha + \text{h.c.}\right] \\
& + \int d^2\theta\, d^2\bar{\theta} \Big[\overline{Q}\, e^{g'YV' + 2gI^aV^a} Q + \overline{U}\, e^{g'YV' + 2gI^aV^a} U + \overline{D}\, e^{g'YV' + 2gI^aV^a} D \\
& \qquad + \overline{L}\, e^{g'YV' + 2gI^aV^a} L + \overline{E}\, e^{g'YV' + 2gI^aV^a} E \\
& \qquad + \overline{H}_{\rm u}\, e^{g'YV' + 2gI^aV^a} H_{\rm u} + \overline{H}_{\rm d}\, e^{g'YV' + 2gI^aV^a} H_{\rm d} \Big] \\
& + \int d^2\theta \Big[\lambda_{\rm u} H_{\rm u} Q U + \lambda_{\rm d} H_{\rm d} Q D + \lambda_{\rm e} H_{\rm d} L E - \mu H_{\rm u} H_{\rm d} + \text{h.c.}\Big].
\end{aligned} \tag{2.17}$$

The first four lines of (2.17) comprise the most general supersymmetric Lagrangian for the given gauge group $\mathrm{SU(2)_I}\times\ \mathrm{U(1)_Y}$ and the chiral superfields in Table 2.2. The first line contains the kinetic terms for the gauge bosons and gauginos in terms of the superfield tensor $W'_\alpha = \overline{D}_{\dot{\alpha}} \overline{D}^{\dot{\alpha}}\, e^{-g'YV'} D_\alpha\, e^{g'YV'}$. Here $D_\alpha = \partial/\partial\theta^\alpha - i\sigma^\mu_{\alpha\dot{\beta}} \bar{\theta}^{\dot{\beta}} \partial_\mu$ and $\overline{D}_{\dot{\alpha}} = -\partial/\partial\bar{\theta}^{\dot{\alpha}} + i\theta^\beta \sigma^\mu_{\beta\dot{\alpha}} \partial_\mu$ are supersymmetry-covariant derivatives with Weyl-spinor indices α, $\dot{\alpha}$ and σ denotes the usual Pauli matrices. The following three lines comprise the kinetic and gauge interaction terms for the quarks, leptons and their scalar partners, using the common symbols Y and I^a for the U(1) and SU(2) operators, respectively. As before, the contribution from right-handed neutrinos and their supersymmetric partners, the R-sneutrinos, is neglected.

The interaction terms in the last line are called the superpotential and contain the Yukawa couplings which generate masses for the quarks and leptons. As before, Yukawa couplings for the neutrinos are neglected. The superpotential of the MSSM incorporates all possible terms which preserve lepton and baryon number. While both are conserved

quantities in the Standard Model, in supersymmetric theories they could easily be broken by additional terms in the superpotential. However, in order to avoid very rapid proton decay, certain combinations of these additional couplings are constrained to be almost zero. Therefore the baryon and lepton number violating terms are forbidden in the MSSM by imposing an additional symmetry called R-parity. The eigenvalues of the R-parity are $+1$ for Standard Model particles and -1 for their supersymmetric partners ("sparticles"). As a consequence, within the MSSM, sparticles can only be produced in pairs and the lightest supersymmetric particle (LSP) is stable.

Since no supersymmetric partner of any of the Standard Model particles has yet been observed, supersymmetry cannot be realized exactly in the low-energy regime. Unfortunately, the construction of a realistic breaking mechanism cannot be achieved within the MSSM but requires the introduction of additional fields and interactions at high mass scales. Since the nature of this "hidden sector" cannot be determined unequivocally, usually supersymmetry breaking is introduced into the MSSM Lagrangian by adding explicit breaking terms. The structure of the breaking terms is constrained by non-renormalization theorems [6] which ensure that no quadratic dependencies on high scales like in (2.15) are present in the theory. This is called *soft breaking* of supersymmetry.

The most general form of the soft-breaking Lagrangian is given by

$$\begin{aligned}\mathcal{L}_{\text{soft}} = &-\frac{1}{2}\big(M_1\widetilde{B}\widetilde{B} + M_2\widetilde{W}^a\widetilde{W}_a + M_3\tilde{g}^a\tilde{g}_a + \text{h.c.}\big)\\ &- m_{\text{H}_\text{u}}^2|H_\text{u}|^2 - m_{\text{H}_\text{d}}^2|H_\text{d}|^2 - \big(b\,H_\text{u}H_\text{d} + \text{h.c.}\big)\\ &- m_{\tilde{\text{q}}_\text{L}}^2|\tilde{q}_\text{L}|^2 - m_{\tilde{\text{u}}_\text{R}}^2|\tilde{u}_\text{R}|^2 - m_{\tilde{\text{d}}_\text{R}}^2|\tilde{d}_\text{R}|^2 - m_{\tilde{\text{l}}_\text{L}}^2|\tilde{l}_\text{L}|^2 - m_{\tilde{\text{e}}_\text{R}}^2|\tilde{e}_\text{R}|^2\\ &- \big(\lambda_\text{u}A_\text{u}H_\text{u}\tilde{q}_\text{L}\tilde{u}_\text{R}^* + \lambda_\text{d}A_\text{d}H_\text{d}\tilde{q}_\text{L}\tilde{d}_\text{R}^* + \lambda_\text{e}A_\text{e}H_\text{d}\tilde{l}_\text{L}\tilde{e}_\text{R}^* + \text{h.c.}\big).\end{aligned} \tag{2.18}$$

It consists of mass terms for the gauginos (bino, wino and gluino), bilinear interactions for the Higgs scalar doublets H_u and H_d, mass terms for the scalar fermions and trilinear scalar interactions. In principle, there also exist soft-breaking terms for right-chiral sneutrinos $\tilde{\nu}_\text{R}$. However, since the mixing between left- and right-chiral components of the neutrinos and sneutrinos is neglected throughout this thesis, the soft-breaking term for R-sneutrinos is of no importance here and has been dropped in (2.18). The sfermion parameters $m^2_{\tilde{\text{q}}_\text{L},\tilde{\text{u}}_\text{R},\tilde{\text{d}}_\text{R},\tilde{\text{l}}_\text{L},\tilde{\text{e}}_\text{R}}$ and $A_{\text{u,d,e}}$ are 3×3 matrices in generation space. In general these parameters can lead to large flavour-changing neutral currents (FCNC) and CP-violating effects, which can be evaded by taking the matrices diagonal [27], as in mSUGRA or GMSB, see section 2.3.

2.2.3 The mass spectrum of the MSSM

Nearly all of the mass eigenstates of the new MSSM particles are mixtures of the interaction eigenstates given in Tables 2.2, 2.3.

The Higgs sector of the MSSM (for a review see [28]) consists of two Higgs doublets H_u and H_d which both acquire non-zero vacuum expectation values (vev) v_u and v_d in the minimum of the scalar potential. The ratio of the two vev's is written as

$$\tan\beta \equiv v_\text{u}/v_\text{d}. \tag{2.19}$$

Three of the eight scalar degrees of freedom form the Goldstone bosons $G^0, G^\pm$. The remaining five physical mass eigenstates can be divided into two CP-even neutral scalars h^0 and H^0, one CP-odd neutral scalar A^0 and a charged scalar with its conjugate $H^\pm$. In terms of the gauge eigenstates they are given by

$$\begin{pmatrix} G^0 \\ A^0 \end{pmatrix} = \sqrt{2} \begin{pmatrix} \sin\beta & -\cos\beta \\ \cos\beta & \sin\beta \end{pmatrix} \begin{pmatrix} \Im m\, H_\mathrm{u}^0 \\ \Im m\, H_\mathrm{d}^0 \end{pmatrix}, \tag{2.20}$$

$$\begin{pmatrix} G^+ \\ H^+ \end{pmatrix} = \begin{pmatrix} \sin\beta & -\cos\beta \\ \cos\beta & \sin\beta \end{pmatrix} \begin{pmatrix} H_\mathrm{u}^+ \\ H_\mathrm{d}^{-*} \end{pmatrix}, \tag{2.21}$$

$$\begin{pmatrix} h^0 \\ H^0 \end{pmatrix} = \sqrt{2} \begin{pmatrix} \cos\alpha & -\sin\alpha \\ \sin\alpha & \cos\alpha \end{pmatrix} \begin{pmatrix} \Re e\, H_\mathrm{u}^0 - v_\mathrm{u} \\ \Re e\, H_\mathrm{d}^0 - v_\mathrm{d} \end{pmatrix}. \tag{2.22}$$

By taking the mass of the CP-odd scalar A^0 as input parameter, the other masses can be expressed in the form

$$M_{\mathrm{H}^\pm}^2 = M_{\mathrm{A}^0}^2 + M_\mathrm{W}^2, \tag{2.23}$$

$$M_{\mathrm{h}^0,\mathrm{H}^0}^2 = \frac{1}{2}\left[M_{\mathrm{A}^0}^2 + M_\mathrm{Z}^2 \mp \sqrt{\left(M_{\mathrm{A}^0}^2 + M_\mathrm{Z}^2\right)^2 - 4 M_{\mathrm{A}^0}^2 M_\mathrm{Z}^2 \cos^2 2\beta} \right]. \tag{2.24}$$

In this way, the Lagrangian parameters $m_{\mathrm{H_u}}^2, m_{\mathrm{H_d}}^2$ and b are rephrased in terms of $\tan\beta, M_{\mathrm{A}^0}$ and M_Z. The mixing angle α is given by

$$\tan 2\alpha = \tan 2\beta \, \frac{M_{\mathrm{A}^0}^2 + M_\mathrm{Z}^2}{M_{\mathrm{A}^0}^2 - M_\mathrm{Z}^2}. \tag{2.25}$$

It should be noted that these tree level relations are substantially modified by radiative corrections [29–31]. In particular, the bound $M_{\mathrm{h}^0}^2 < |\cos 2\beta| M_\mathrm{Z}$, which follows from (2.24), gets weakened, yielding an upper bound of ∼135 GeV including dominant two-loop corrections.

In the sfermion sector, mixing occurs between the scalar partners of left- and right-handed fermions, in addition to the well-known CKM mixing[1]. The mass term for a given flavour species f reads

$$\mathcal{L}_{\mathrm{m}_{\tilde{\mathrm{f}}}} = -\left(\tilde{f}_\mathrm{L}^*,\ \ \tilde{f}_\mathrm{R}^*\right) M_{\tilde{\mathrm{f}}}^2 \begin{pmatrix} \tilde{f}_\mathrm{L} \\ \tilde{f}_\mathrm{R} \end{pmatrix} \tag{2.26}$$

with

$$M_{\tilde{\mathrm{f}}}^2 = \begin{pmatrix} m_\mathrm{f}^2 + m_{\tilde{\mathrm{F}}_\mathrm{L}}^2 + M_\mathrm{Z}^2 \cos 2\beta \, (I_\mathrm{f}^3 - Q_\mathrm{f} s_\mathrm{W}^2) & m_\mathrm{f}\left(A_\mathrm{f} - \mu(\cot\beta)^{2I_\mathrm{f}^3}\right) \\ m_\mathrm{f}\left(A_\mathrm{f} - \mu(\cot\beta)^{2I_\mathrm{f}^3}\right) & m_\mathrm{f}^2 + m_{\tilde{\mathrm{f}}_\mathrm{R}}^2 + M_\mathrm{Z}^2 \cos 2\beta \, Q_\mathrm{f} s_\mathrm{W}^2 \end{pmatrix}, \tag{2.27}$$

where I_f^3 and Q_f denote the third component of the weak isospin and the electric charge of the fermion f. Thus $(\cot\beta)^{2I_\mathrm{f}^3}$ is $\cot\beta$ for up-type fermions and $\tan\beta$ for down-type

[1] For sneutrinos in the MSSM, only the partners of the left-chiral neutrinos are considered, so that the mass is simply given by $m_{\tilde{\nu}}^2 = m_{\tilde{\mathrm{l}}_\mathrm{L}}^2 + M_\mathrm{Z}^2/2 \cos 2\beta$.

fermions. The quantities $m_{\tilde{\mathrm{F}}_\mathrm{L}} \in \{m_{\tilde{\mathrm{q}}_\mathrm{L}}, m_{\tilde{\mathrm{l}}_\mathrm{L}}\}$ and $m_{\tilde{\mathrm{f}}_\mathrm{R}} \in \{m_{\tilde{\mathrm{u}}_\mathrm{R}}, m_{\tilde{\mathrm{d}}_\mathrm{R}}, m_{\tilde{\mathrm{e}}_\mathrm{R}}\}$ are the corresponding sfermion soft-breaking masses in (2.18).

Considering that the soft-breaking parameters A_f are of the same order as the soft-breaking masses of the MSSM and thus should not exceed a value of a few TeV, the off-diagonal entries in (2.27) are very small for first and second generation sfermions. This assertion is supported by the requirement that the global minimum of the scalar potential, i.e. the vacuum state, does not break colour and charge invariance. For the trilinear couplings A_l of the sleptons this leads to the necessary upper bound [32]

$$A_\mathrm{l} < 3(m^2_{\tilde{\mathrm{l}}_\mathrm{L}} + m^2_{\tilde{\mathrm{l}}_\mathrm{R}} + m^2_{\mathrm{H_d}} + \mu^2). \tag{2.28}$$

In principle, this condition does not place any stringent bound on A_l for large $m^2_{\mathrm{H_d}}$, which can be the case for large values of $\tan\beta$ but would require an undesirable amount of finetuning. After all, if $A_\mathrm{l} \lesssim \mathcal{O}(1\ \mathrm{TeV})$, mixing effects for the smuons are of order 10^{-5} or less, for selectrons even below 10^{-9}. Therefore in this thesis mixing is generally neglected for the first two generations of sfermions. Mixing effects may be important in the stop sector and, in the case of large $\tan\beta$, also for sbottoms and staus.

The higgsinos and electroweak gauginos mix with each other because of the effects of electroweak symmetry breaking. The mixed states of the charged higgsinos $\widetilde{H}^\pm_\mathrm{u,d}$ and winos $\widetilde{W}^\pm = (\widetilde{W}^1 \pm i\widetilde{W}^2)/\sqrt{2}$ are called charginos $\tilde{\chi}^\pm_i$ $(i = 1, 2)$, while the neutral higgsinos $\widetilde{H}^0_\mathrm{u,d}$ and gauginos $\widetilde{B}, \widetilde{W}^0$ form four mass eigenstates called neutralinos $\tilde{\chi}^0_i$ $(i = 1, 2, 3, 4)$. The mass eigenstates are conventionally ordered in ascending order, $m^2_{\tilde{\chi}^\pm_1} < m^2_{\tilde{\chi}^\pm_2}$ and $m^2_{\tilde{\chi}^0_1} < m^2_{\tilde{\chi}^0_2} < m^2_{\tilde{\chi}^0_3} < m^2_{\tilde{\chi}^0_4}$.

For the charginos the mass term reads

$$\mathcal{L}_{\mathrm{m}_{\tilde{\chi}^\pm}} = -\big(\widetilde{W}^-, \widetilde{H}^-_\mathrm{d}\big)\, X \begin{pmatrix} \widetilde{W}^+ \\ \widetilde{H}^+_\mathrm{u} \end{pmatrix} + \mathrm{h.c.} \tag{2.29}$$

where $\widetilde{W}^\pm, \widetilde{H}^\pm_\mathrm{u,d}$ are the Weyl spinors of the charged winos and higgsinos. The mass matrix

$$X = \begin{pmatrix} M_2 & \sqrt{2}M_\mathrm{W}\sin\beta \\ \sqrt{2}M_\mathrm{W}\cos\beta & \mu \end{pmatrix} \tag{2.30}$$

can be diagonalized by two unitary matrices U and V according to

$$U^* X V^{-1} = \begin{pmatrix} m_{\tilde{\chi}^\pm_1} & 0 \\ 0 & m_{\tilde{\chi}^\pm_2} \end{pmatrix}, \qquad \begin{pmatrix} \chi^-_1 \\ \chi^-_2 \end{pmatrix} = U \begin{pmatrix} \widetilde{W}^- \\ \widetilde{H}^-_\mathrm{d} \end{pmatrix}, \qquad \begin{pmatrix} \chi^+_1 \\ \chi^+_2 \end{pmatrix} = V \begin{pmatrix} \widetilde{W}^+ \\ \widetilde{H}^+_\mathrm{u} \end{pmatrix}, \tag{2.31}$$

yielding the mass eigenstates $\chi^\pm_i$. In the chiral representation, the Dirac spinors $\tilde{\chi}^\pm_i$ of the charginos are constructed from the Weyl spinors as follows,

$$\tilde{\chi}^-_i = \begin{pmatrix} \chi^-_i \\ \hline \chi^+_i \end{pmatrix}, \qquad\qquad \tilde{\chi}^+_i = \begin{pmatrix} \chi^+_i \\ \hline \chi^-_i \end{pmatrix}. \tag{2.32}$$

The neutralino mass term in the gauge eigenbasis is given by

$$\mathcal{L}_{\mathrm{m}_{\tilde{\chi}^0}} = -\frac{1}{2}\psi^{0\top}\, Y\, \psi^0 + \mathrm{h.c.}, \qquad \psi^0 = \left(\widetilde{B}, \widetilde{W}^0, \widetilde{H}^0_{\mathrm{d}}, \widetilde{H}^0_{\mathrm{u}}\right)^\top, \tag{2.33}$$

with the symmetric mass matrix

$$Y = \begin{pmatrix} M_1 & 0 & -M_{\mathrm{Z}}\, s_{\mathrm{W}}\, c_\beta & M_{\mathrm{Z}}\, s_{\mathrm{W}}\, s_\beta \\ 0 & M_2 & M_{\mathrm{Z}}\, c_{\mathrm{W}}\, c_\beta & -M_{\mathrm{Z}}\, c_{\mathrm{W}}\, s_\beta \\ -M_{\mathrm{Z}}\, s_{\mathrm{W}}\, c_\beta & M_{\mathrm{Z}}\, c_{\mathrm{W}}\, c_\beta & 0 & -\mu \\ M_{\mathrm{Z}}\, s_{\mathrm{W}}\, s_\beta & -M_{\mathrm{Z}}\, c_{\mathrm{W}}\, s_\beta & -\mu & 0 \end{pmatrix}, \tag{2.34}$$

where the abbreviations $s_\beta = \sin\beta$ and $c_\beta = \cos\beta$ have been introduced. The transition to the mass eigenbasis is performed by the unitary mixing matrix N,

$$N^* Y N^{-1} = \mathrm{diag}\big(m^2_{\tilde{\chi}^0_1}, m^2_{\tilde{\chi}^0_2}, m^2_{\tilde{\chi}^0_3}, m^2_{\tilde{\chi}^0_4}\big), \qquad \chi^0_i = N_{ij}\psi^0_j. \tag{2.35}$$

The Majorana spinors $\tilde{\chi}^0_i$ of the physical neutralinos are composed of the Weyl spinors as follows,

$$\tilde{\chi}^0_i = \begin{pmatrix} \chi^0_i \\ \overline{\chi^0_i} \end{pmatrix}. \tag{2.36}$$

In practice, there are two possibilities to specify the mixing matrix N. By choosing N to have only real entries, some of the mass parameters in (2.35) may turn out to be negative. On the other hand, all mass parameters can be made real and positive if N is allowed to be an complex SU(4) matrix. Both methods have been applied for the calculations in chapter 4 and it was checked that they agree numerically.

The Feynman rules for the complete MSSM are collected in [33, 34]. For this thesis the generation of Feynman diagram amplitudes is performed with the computer algebra package *FeynArts* [35]. Since the neutralinos are Majorana fermions, fermion-number-violating interactions are possible within the MSSM. In *FeynArts* they are handled using the Dirac spinor techniques of Ref. [36]. Recently the Feynman rules for the MSSM have been implemented in a comprehensive model file for *FeynArts* [37].

2.3 Supersymmetry breaking schemes

As mentioned in the previous section it is obvious that supersymmetry cannot be an exact symmetry of nature, however it is far from obvious what can be accounted for as the source of supersymmetry breaking. Furthermore, it is impossible to construct a realistic breaking scenario within the phenomenologically accessible particle content of the MSSM, because of the existence of mass sum rules [38]. Therefore, the origin of supersymmetry breaking is usually transferred to a "hidden sector" of particles which have no direct coupling to the MSSM particles. While this opens up a variety of possibilities to construct viable breaking mechanisms, more important from a phenomenological point of view is the question, how the supersymmetry breaking is mediated from the hidden to the visible sector. There are three main proposals for the mediating interactions.

2.3.1 Gravity-mediated supersymmetry breaking

Within the framework of supersymmetry, gravity can be introduced in a very elegant way by requiring that the Lagrangian is not only invariant under global supersymmetry but also under the local variation of supersymmetry. In analogy to gauge theories this requires the existence of an additional degree of freedom, which in this case is a fermion with spin 3/2 and odd R-parity. It can be identified as the supersymmetric partner of the spin-2 graviton. Thus the resulting locally supersymmetric theory unifies the space-time symmetries of general relativity with supersymmetry transformations and is therefore called supergravity [24, 39].

In models of gravity-mediated supersymmetry breaking the hidden sector of the theory communicates with the MSSM particles through gravitational interactions [25]. Since gravity is flavour-blind, the breaking terms can be realized in a minimal version [40], introducing a common scalar mass parameter m_0 and trilinear coupling A_0, a universal gaugino mass parameter $M_{1/2}$ and the bilinear Higgs parameter b. This reduced set of breaking parameters is called *minimal supergravity* (mSUGRA) and can be accounted for by a global U(N) symmetry. The framework of mSUGRA has the virtue of being highly predictive, since the soft-breaking parameters of the MSSM in (2.18) can be expressed in terms of just four parameters,

$$m^2_{\tilde{\mathrm{q}}_\mathrm{L}} = m^2_{\tilde{\mathrm{u}}_\mathrm{R}} = m^2_{\tilde{\mathrm{d}}_\mathrm{R}} = m^2_{\tilde{\mathrm{l}}_\mathrm{L}} = m^2_{\tilde{\mathrm{e}}_\mathrm{R}} = m^2_{\mathrm{H_u}} = m^2_{\mathrm{H_d}} = m_0^2, \tag{2.37}$$

$$A_\mathrm{u} = A_\mathrm{d} = A_\mathrm{e} = A_0, \tag{2.38}$$

$$M_1 = M_2 = M_3 = M_{1/2}, \tag{2.39}$$

and the bilinear parameter b. Furthermore, also the superpotential parameter μ—up to its sign—can be constrained by the requirement of electroweak symmetry breaking. b is usually re-expressed in terms of $\tan\beta$. While eqs. (2.37)–(2.39) can be assumed to hold at an energy scale around the Planck scale or GUT scale, the breaking parameters receive important radiative corrections at other scales, thereby leading to a more complicated spectrum at the weak scale. This scale dependence of the soft breaking parameters can be determined with renormalization group studies [41], so that the low-energy spectrum can be predicted in terms of the four universal mSUGRA parameters.

An important characteristic of the weak scale mSUGRA spectrum is a neutralino LSP, $\tilde{\chi}^0_1$, which is an almost pure bino and has only small admixtures of wino and higgsino components. The second lightest neutralino, $\tilde{\chi}^0_2$, typically has a dominant wino component. Furthermore, the scalar leptons are generally considerably lighter than the scalar squarks.

2.3.2 Gauge-mediated supersymmetry breaking

In the concept of gauge-mediated supersymmetry breaking (GMSB) [42] the breaking of supersymmetry is transmitted to the visible sector by the ordinary gauge interactions of the MSSM. For this purpose, additional chiral supermultiplets, called *messengers*, are introduced which are subject to the gauge interaction and also couple to the hidden source of symmetry breaking. The messengers impose masses on the MSSM gauginos and scalars through radiative corrections.

Since the gauge interactions are significantly stronger than gravitational forces, the typical scale for supersymmetry breaking and the messenger particles in GMSB will be significantly lower than in mSUGRA, around 100 TeV. However, as a consequence, the messengers then would affect the renormalization group running of the gauge couplings and might threaten their apparent unification at the GUT scale. To avoid this problem, the messengers are often considered to exist in multiplets of the SU(5) global symmetry that contains the Standard Model gauge group. In this case the sparticle spectrum depends on just five parameters,

$$\sqrt{\langle F \rangle},\ M_{\text{mess}},\ N_{\text{mess}},\ \Lambda,\ \tan\beta, \tag{2.40}$$

where $\langle F \rangle$ denotes the vev of a hidden auxiliary field that breaks supersymmetry, M_{mess} is the messenger mass scale, N_{mess} is an index that depends on the number of messenger fields and their gauge representation, and Λ is a universal soft breaking scale. As in mSUGRA, the bilinear Higgs term is absorbed in favour of $\tan\beta$ and the absolute value of μ is fixed by the requirement of electroweak symmetry breaking (the sign of μ still needs to be specified). The soft-breaking masses of the gauginos and scalars are then given by

$$M_i = N_{\text{mess}} \frac{\alpha_i}{4\pi} g \frac{\Lambda^2}{M_{\text{mess}}}, \qquad (i = 1, 2, 3), \tag{2.41}$$

$$m_\phi^2 = 2 N_{\text{mess}} f \frac{\Lambda^3}{M_{\text{mess}}} \sum_i \left(\frac{\alpha_i}{4\pi}\right)^2 C_i^\phi, \tag{2.42}$$

with C_i^ϕ being the quadratic Casimir invariant for the gauge group i of the scalar ϕ. g and f are loop functions of the diagrams which contribute to the radiative mass generation [43]. The trilinear couplings A_j are almost zero at the messenger scale since they are suppressed by one loop order. However, they acquire non-vanishing values from the evolution down to the weak scale.

Since the masses of the sfermions only depend on their gauge quantum number, this automatically leads to degeneracy between the three generations, thereby naturally suppressing FCNC effects. Another important consequence of GMSB is the rôle of the gravitino—which does not have phenomenological consequences in mSUGRA—as the LSP. Sleptons are typically considerably lighter than squarks, and it may easily be that the next-to-lightest supersymmetric particle is a stau instead of a neutralino.

2.3.3 Anomaly-mediated supersymmetry breaking

In general, soft supersymmetry breaking terms receive contributions from the super-Weyl anomaly via loop effects. If the effects of gravity and gauge meditation are somehow suppressed, the anomaly mediated supersymmetry breaking (AMSB) can be the dominant mechanism for the generation of soft breaking terms. This idea was invented and is mostly discussed in the context of brane models [44]. The super-Weyl anomaly is connected with the violation of scale invariance. Therefore the anomaly-mediated contributions to supersymmetry breaking can be written in a form that does not depend on the energy

scale and need not be extrapolated with renormalization group equations,

$$M_i = \frac{\beta_i}{g_i}\, m_{3/2}, \tag{2.43}$$

$$m_\phi^2 = m_0^2 - \frac{1}{4} m_{3/2} \left(\sum_i \frac{\partial \gamma_\phi}{\partial g_i} \beta_i + \frac{\partial \gamma_\phi}{\partial \lambda} \beta_\lambda \right), \tag{2.44}$$

$$A_\lambda = -\frac{\beta_\lambda}{\lambda}\, m_{3/2}. \tag{2.45}$$

Here $g_i, i = 1, 2, 3$ are the gauge couplings and λ refers to one of the Yukawa couplings in the last line of (2.17). $\beta_{i,\lambda}$ denotes the relevant β-function and γ_ϕ is the anomalous dimension of the chiral superfield ϕ. All anomaly-mediated soft breaking terms only depend on the single parameter, the $m_{3/2}$ gravitino mass. However, in order to avoid negative (tachyonic) squared scalar masses, an additional contribution m_0 to the scalar masses has to be introduced, which must originate from some other mediation mechanism. In the minimal form, as in (2.44), this scalar parameter is assumed to be universal. As for mSUGRA and GMSB, $\tan\beta$ and the sign of μ also have to be specified as input parameters.

A direct consequence of (2.43) is the prediction of the ratios of the gaugino mass parameters $|M_1| : |M_2| : |M_3| \approx 2.8 : 1 : 7.1$. Accordingly, the LSP is the lightest neutralino $\tilde{\chi}_1^0$ with a dominant wino component, in contrast to GMSB and mSUGRA where $\tilde{\chi}_1^0$ is bino-like. The next-to-lightest supersymmetric particle is the lightest chargino $\tilde{\chi}_1^\pm$ which is a almost pure wino and very close in mass to the LSP. While in most scenarios the sleptons are lighter than the squarks, this is not a necessary feature of AMSB.

2.3.4 Reconstruction of supersymmetric theories

Even after detection of supersymmetric particles, it will be a difficult task to disentangle the mechanism that governs the spectrum of supersymmetry breaking. Although the models presented in the last sections differ by some distinct features, it is not possible to identify a particular observable that could be interpreted as an unambiguous signal of a specific breaking scheme.

Since in most models the breaking source is related to physics at some high energy scale, one could try to reconstruct the parameter spectrum at this scale by renormalization group evolution [13]. This bottom-up approach has the advantage that no assumption about the high-scale structure has to be made[2].

However, since this direct reconstruction depends on all parameters of the MSSM independently, it is in practice much more involved. In particular, the soft-breaking parameters at the weak scale have to be measured very precisely. One can see from Fig. 2.1 that in the process of renormalization group evolution to the high scale the error bands are significantly widened. For a stable extrapolation it is therefore essential to have precision data available.

[2]In so-called top-down approaches, a given model is assumed at the high scale and, after evolution down to the weak scale, its consistency with the data has to be checked.

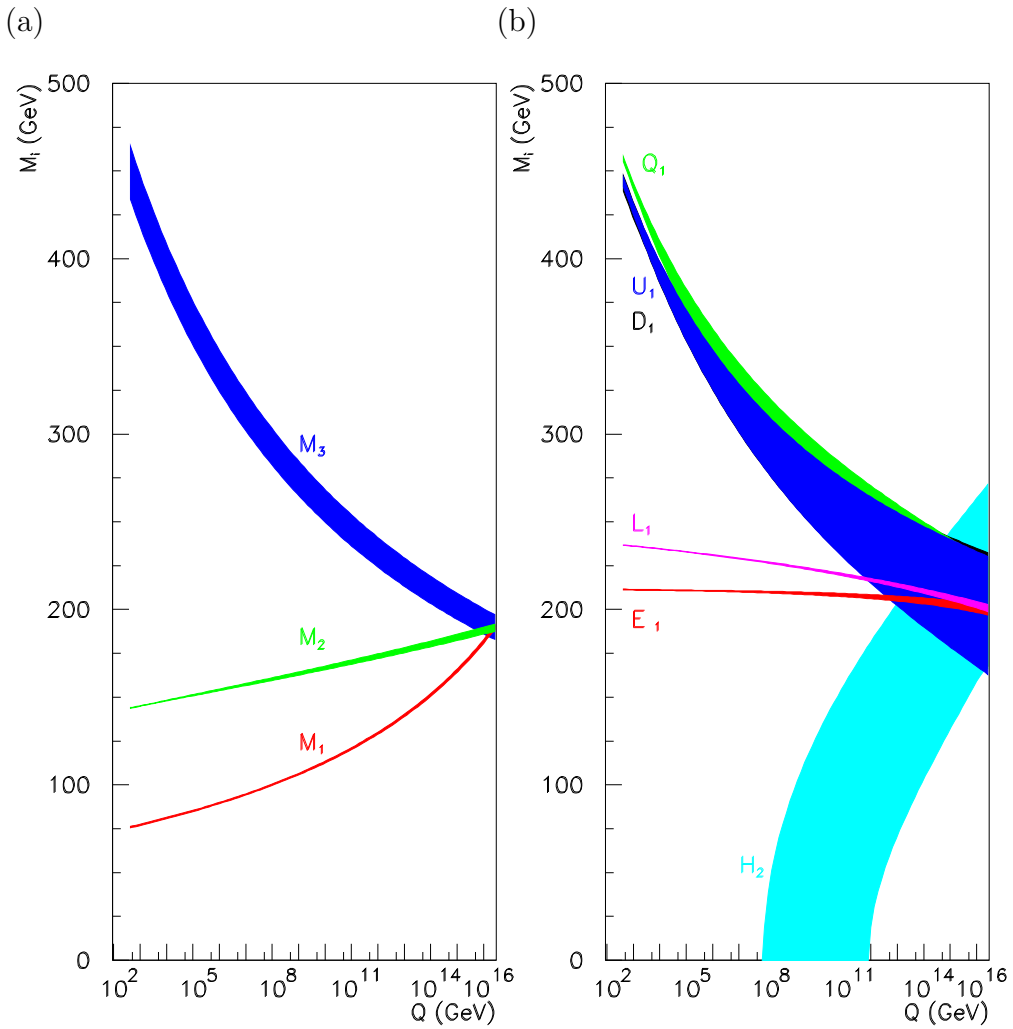

Figure 2.1: *Evolution of gaugino (a) and sfermion (b) parameters in the bottom-up approach for a exemplary mSUGRA point ($m_0 = 200$ GeV, $M_{1/2} = 190$ GeV, $A_0 = 550$ GeV, $\tan\beta = 30$, $\mu < 0$). The widths of the bands indicate 95% confidence level. Figure taken from [13].*

The ideal tool for this purpose is a high-energy e^+e^- linear collider[3]. Several proposals for such a machine have been developed by different institutions in the world [7–9]. Concerning their physics prospects [10–12], the high luminosity of such a linear collider would allow one to measure the masses and couplings of Standard Model and supersymmetric particles with unparallelled precision. On the other hand, the expected experimental performance would require some effort from the theoretical side in order to match the experimental accuracy.

[3]For certain purposes also the e^-e^-, $e^-\gamma$ and $\gamma\gamma$ options are considered.

Chapter 3

Phenomenology of sleptons at linear colliders

In supersymmetric theories with R-parity conservation, such as the MSSM, scalar leptons can be produced in pairs. The focus of this thesis is on the scalar partners of the first two generation leptons, i.e. smuons and selectrons. Since mixing amongst smuons and selectrons is neglected (see section 2.2.3), the partners of the left- and right-chiral leptons, $\tilde{l}_{\rm L}$ and $\tilde{l}_{\rm R}$, are also the mass eigenstates of the sleptons. Many authors have studied the production of smuons [45, 46], selectrons [45, 47–49] and their decay [48, 50] at the Born level.

Scalar muons are produced via s-channel photon and Z-boson exchange in e^+e^- annihilation, see Fig. 3.1 (a),

$$e^+\,e^- \to \tilde{\mu}_i^+\,\tilde{\mu}_i^- \qquad (i = {\rm L/R}). \tag{3.1}$$

Due to conservation of angular momentum, the smuons are produced in an S-wave, so that near threshold, the cross-section rises $\sim \beta^3$, where

$$\beta = \sqrt{1 - \frac{4m^2_{\tilde{\mu}_i}}{s}} \tag{3.2}$$

denotes the smuon velocity. The Born cross-section for the production of on-shell smuons reads

$$\begin{aligned}\sigma[e^+\,e^- \to \tilde{\mu}_i^+\,\tilde{\mu}_i^-] = \frac{\pi\alpha^2}{3s}\beta^3\Bigg[1 - g_i\,\frac{1-4s^2_{\rm W}}{2s_{\rm W}c_{\rm W}}\,\frac{s}{s-M^2_{\rm Z}} \\ + g_i^2\,\frac{1+(1-4s^2_{\rm W})^2}{16s^2_{\rm W}c^2_{\rm W}}\left(\frac{s}{s-M^2_{\rm Z}}\right)^2\Bigg].\end{aligned} \tag{3.3}$$

Here

$$g_{\rm L} = \frac{-1+2s^2_{\rm W}}{2s_{\rm W}c_{\rm W}}, \qquad g_{\rm R} = \frac{s_{\rm W}}{c_{\rm W}} \tag{3.4}$$

denote the couplings of the Z-boson to left- and right-handed muons, respectively. One can incorporate some of the leading QED corrections by evaluating the fine structure

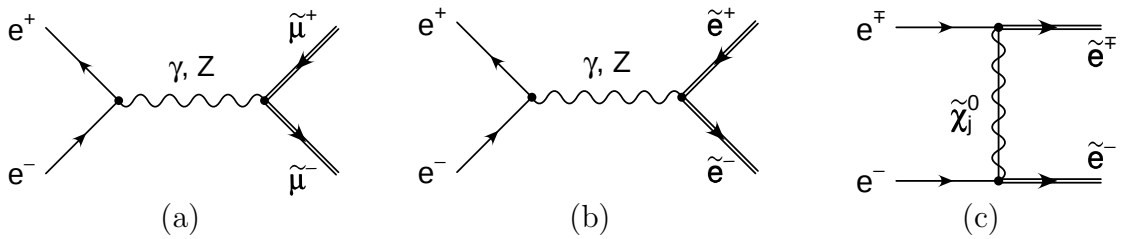

Figure 3.1: *Leading order diagrams for the pair production of smuons and selectrons at in e^+e^- or e^-e^- scattering.*

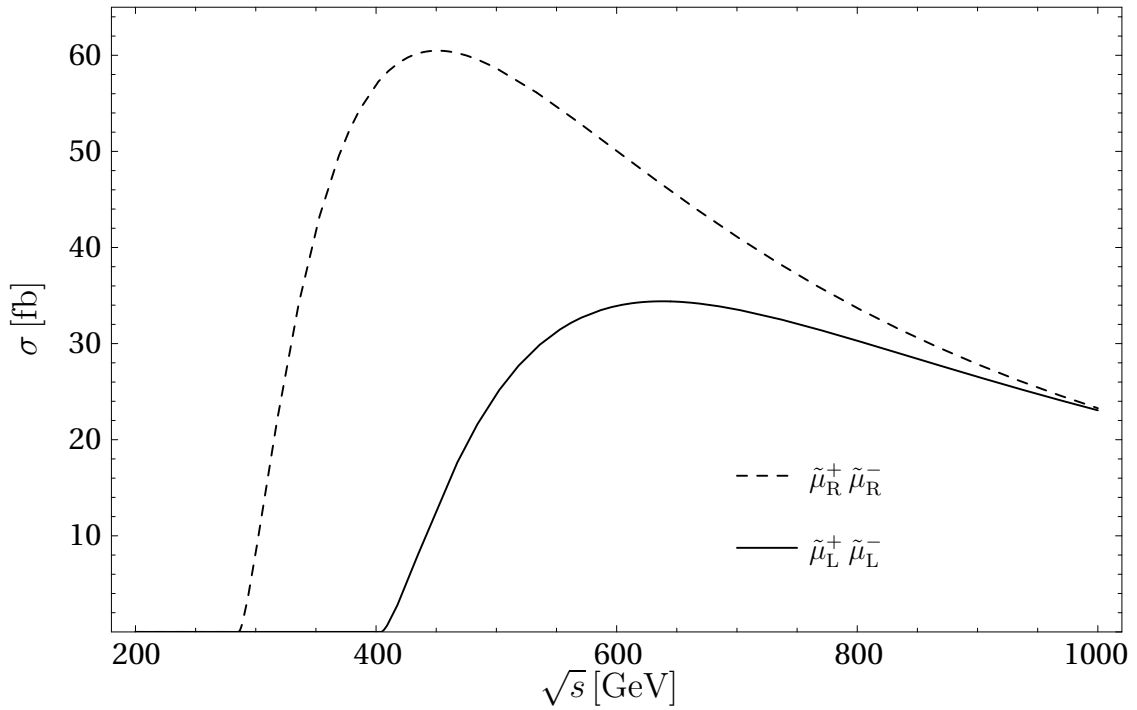

Figure 3.2: *Born cross-sections for right- and left-chiral smuon pair production in e^+e^- annihilation. Values for SPS1 scenario.*

constant α at the scale $\sqrt{s}$. In the continuum, the cross-sections typically take on values of $20 - 50$ fb for smuon masses around 200 GeV, see Fig. 3.2.

In the following chapters, the use of polarized initial beams will be frequently discussed. Therefore the polarized cross-sections for smuon pair production are also given here,

$$\sigma[e^+_{\rm R}\, e^-_{\rm L} \to \tilde{\mu}^+_i\, \tilde{\mu}^-_i] = \frac{2\pi\alpha^2}{3s}\beta^3 \left[1 + g_i\, g_{\rm L} \frac{s}{s - M_Z^2}\right]^2, \tag{3.5}$$

$$\sigma[e^+_{\rm L}\, e^-_{\rm R} \to \tilde{\mu}^+_i\, \tilde{\mu}^-_i] = \frac{2\pi\alpha^2}{3s}\beta^3 \left[1 + g_i\, g_{\rm R} \frac{s}{s - M_Z^2}\right]^2. \tag{3.6}$$

The other polarization combinations vanish.

Scalar electrons, in addition to the s-channel γ, Z exchange, Fig. 3.1 (b), are also produced via exchange of neutralinos $\tilde{\chi}^0_j$ in the t-channel, Fig. 3.1 (c). As a consequence,

Process	exchange particles	orbital wave	threshold excitation
$e^+_{\rm L}e^-_{\rm R} \to \tilde{e}^+_{\rm R}\tilde{e}^-_{\rm R}$	$\gamma, Z, \tilde{\chi}^0$	P-wave	$\propto \beta^3$
$e^+_{\rm R}e^-_{\rm L} \to \tilde{e}^+_{\rm R}\tilde{e}^-_{\rm R}$	γ, Z	P-wave	$\propto \beta^3$
$e^+_{\rm L}e^-_{\rm L} \to \tilde{e}^+_{\rm R}\tilde{e}^-_{\rm L}$	$\tilde{\chi}^0$	S-wave	$\propto \beta$
$e^+_{\rm R}e^-_{\rm R} \to \tilde{e}^+_{\rm L}\tilde{e}^-_{\rm R}$	$\tilde{\chi}^0$	S-wave	$\propto \beta$
$e^+_{\rm L}e^-_{\rm R} \to \tilde{e}^+_{\rm L}\tilde{e}^-_{\rm L}$	γ, Z	P-wave	$\propto \beta^3$
$e^+_{\rm R}e^-_{\rm L} \to \tilde{e}^+_{\rm L}\tilde{e}^-_{\rm L}$	$\gamma, Z, \tilde{\chi}^0$	P-wave	$\propto \beta^3$
$e^-_{\rm R}e^-_{\rm R} \to \tilde{e}^-_{\rm R}\tilde{e}^-_{\rm R}$	$\tilde{\chi}^0$	S-wave	$\propto \beta$
$e^-_{\rm L}e^-_{\rm R} \to \tilde{e}^-_{\rm L}\tilde{e}^-_{\rm R}$	$\tilde{\chi}^0$	P-wave	$\propto \beta^3$
$e^-_{\rm L}e^-_{\rm L} \to \tilde{e}^-_{\rm L}\tilde{e}^-_{\rm L}$	$\tilde{\chi}^0$	S-wave	$\propto \beta$

Table 3.1: *Classification of selectron production modes in terms of the exchanged particles, the orbital angular momentum of the final state wave function and the rise of the excitation curve near threshold. The dependence on the beam polarization is also given.*

in contrast to the smuon case, selectrons can also be generated in mixed pairs $\tilde{e}_{\rm R}\tilde{e}_{\rm L}$. Furthermore they can be produced in e^-e^- scattering, where only the neutralino exchange contributes. The different production modes can be classified according to Tab. 3.1.

The formulae for the corresponding polarized Born cross-sections read:

$$\begin{aligned}\sigma[e^+_{-i}\, e^-_i \to \tilde{e}^+_i\, \tilde{e}^-_i] = {} & \frac{2\pi\alpha^2}{3s}\beta^3\left[1 + g_i^2\frac{s}{s-M_{\rm Z}^2}\right]^2 \\ & + \frac{16\pi\alpha^2}{s}\sum_{j=1}^{4}\sum_{k=1}^{4}|X_{ij}|^2\,|X_{ik}|^2\,h^{jk} \\ & + \frac{8\pi\alpha^2}{s}\sum_{j=1}^{4}|X_{ij}|^2\left[1 + g_i\,\frac{s}{s-M_{\rm Z}^2}\right]f^j \qquad (i = {\rm L/R}, -i = {\rm R/L}),\end{aligned} \tag{3.7}$$

$$\sigma[e^+_i\, e^-_{-i} \to \tilde{e}^+_i\, \tilde{e}^-_i] = \frac{2\pi\alpha^2}{3s}\beta^3\left[1 + g_i\, g_{-i}\frac{s}{s-M_{\rm Z}^2}\right]^2 \qquad (i = {\rm L/R}, -i = {\rm R/L}), \tag{3.8}$$

$$\sigma[e^+_{\rm L}\, e^-_{\rm L} \to \tilde{e}^+_{\rm R}\, \tilde{e}^-_{\rm L}] = \frac{16\pi\alpha^2}{s}\sum_{j=1}^{4}\sum_{k=1}^{4}X_{{\rm L}j}\,X^*_{{\rm R}j}\,X_{{\rm R}k}\,X^*_{{\rm L}k}\,H^{jk}, \tag{3.9}$$

$$\sigma[e^+_{\rm R}\, e^-_{\rm R} \to \tilde{e}^+_{\rm L}\, \tilde{e}^-_{\rm R}] = \sigma[e^+_{\rm L}\, e^-_{\rm L} \to \tilde{e}^+_{\rm R}\, \tilde{e}^-_{\rm L}],$$

$$\sigma[e^-_i\, e^-_i \to \tilde{e}^-_i\, \tilde{e}^-_i] = \frac{16\pi\alpha^2}{s}\sum_{j=1}^{4}\sum_{k=1}^{4}X^2_{ij}\,X^{*2}_{ik}\left[G^{jk}_+ + H^{jk}\right] \qquad (i = {\rm L/R}), \tag{3.10}$$

$$\sigma[e^-_{\rm L}\, e^-_{\rm R} \to \tilde{e}^-_{\rm L}\, \tilde{e}^-_{\rm R}] = \frac{16\pi\alpha^2}{s}\sum_{j=1}^{4}\sum_{k=1}^{4}X^*_{{\rm L}j}\,X^*_{{\rm R}j}\,X_{{\rm L}k}\,X_{{\rm R}k}\,h^{jk}, \tag{3.11}$$

with

$$f^j = \Delta_j\beta - \frac{\Delta_j^2-\beta^2}{2}\,\ln\frac{\Delta_j+\beta}{\Delta_j-\beta}, \tag{3.12}$$

$$h^{jk} = \begin{cases} -2\beta + \Delta_j \ln\dfrac{\Delta_j+\beta}{\Delta_j-\beta} & j=k \\ \dfrac{f^k-f^j}{\Delta_j-\Delta_k} & j\neq k \end{cases}, \tag{3.13}$$

$$G_\pm^{jk} = \frac{2}{s}\,\frac{m_{\tilde\chi_j^0} m_{\tilde\chi_k^0}}{\Delta_j\pm\Delta_k}\left[\ln\frac{\Delta_k+\beta}{\Delta_k-\beta} \pm \ln\frac{\Delta_j+\beta}{\Delta_j-\beta}\right], \tag{3.14}$$

$$H^{jk} = \begin{cases} \dfrac{4\beta}{s}\,\dfrac{m^2_{\tilde\chi_j^0}}{\Delta_j^2-\beta^2} & j=k \\ G_-^{ij} & j\neq k \end{cases}, \tag{3.15}$$

where for the case of diagonal selectron pairs, $\tilde e_\mathrm{R}\tilde e_\mathrm{R}$ and $\tilde e_\mathrm{L}\tilde e_\mathrm{L}$,

$$\Delta_j = \frac{2}{s}(m^2_{\tilde e_i} - m^2_{\tilde\chi_j^0}) - 1 \quad\text{and}\quad \beta = \sqrt{1-4m^2_{\tilde e_i}/s}, \tag{3.16}$$

while for mixed pairs

$$\Delta_j = \frac{1}{s}(m^2_{\tilde e_\mathrm{L}} + m^2_{\tilde e_\mathrm{R}} - 2m^2_{\tilde\chi_j^0}) - 1 \quad\text{and}\quad \beta = \frac{1}{s}\sqrt{(s-m^2_{\tilde e_\mathrm{L}} - m^2_{\tilde e_\mathrm{R}})^2 - 4m^2_{\tilde e_\mathrm{L}} m^2_{\tilde e_\mathrm{R}})^2}. \tag{3.17}$$

The symbol $X_{ij} = \big((c_\mathrm{W}+g_i s_\mathrm{W})N_{j1} + (s_\mathrm{W}-g_i c_\mathrm{W})N_{j2}\big)/\sqrt{2}$ accounts for the neutralino mixing.

As a result of the additional t-channel contribution, the cross-section for selectron production is about one order of magnitude larger than for smuons. The Born cross-sections for the different collider modes and selectron chiralities are shown in Fig. 3.3 and Fig. 3.4.

The e^-e^- mode is of particular interest for selectron production. On one hand, diagonal selectrons pairs, $\tilde e_\mathrm{R}\tilde e_\mathrm{R}$ and $\tilde e_\mathrm{L}\tilde e_\mathrm{L}$, are produced in an S-wave, which is only possible for mixed pairs in e^+e^- collisions. This is especially favourable for precision measurements in threshold scans due to the steep rise $\propto\beta$. Furthermore, in the e^-e^- mode there is only very little background from Standard Model and supersymmetric processes.

The decays of the right-chiral sleptons $\tilde\mu_\mathrm{R}$ and $\tilde e_\mathrm{R}$ predominantly proceed into neutralinos if the bino mass M_1 is lighter than the R-slepton masses[1]. For the left-chiral sleptons $\tilde\mu_\mathrm{L}$ and $\tilde e_\mathrm{L}$, also additional chargino decays play a rôle. The tree-level decay widths are

[1] If this is not the case, there can be sizeable branching fractions of three-particle decays into staus. Since in this case the width of the R-sleptons is generally very small, such scenarios are not considered in the following.

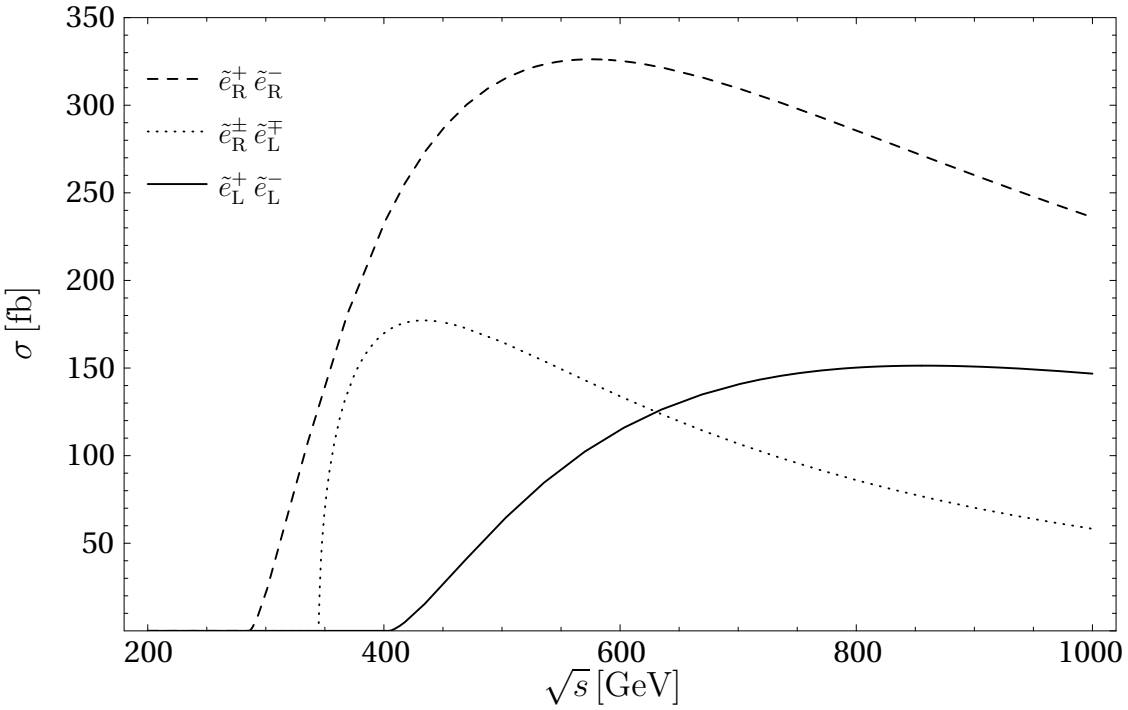

Figure 3.3: *Born cross-sections for selectron pair production in e^+e^- annihilation. Values for SPS1 scenario.*

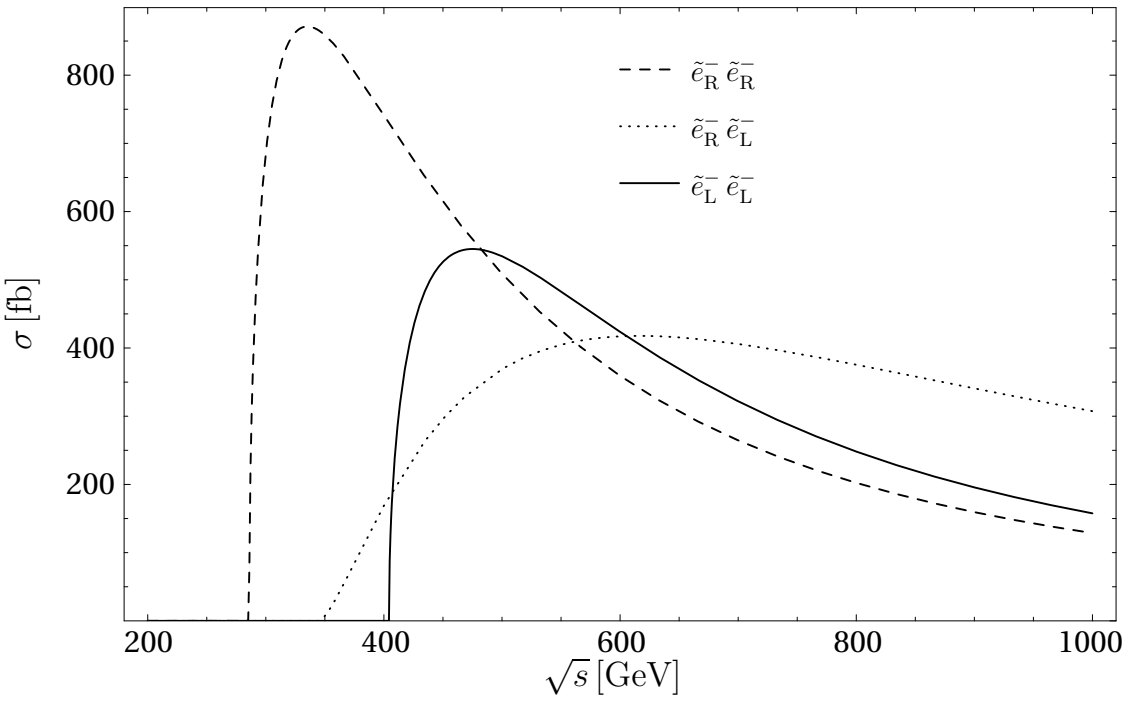

Figure 3.4: *Born cross-sections for selectron pair production in e^-e^- scattering. Values for SPS1 scenario.*

given by

$$\Gamma[\tilde{l}_i^- \to l^- \tilde{\chi}_j^0] = \alpha\,|X_{ij}|^2\, m_{\tilde{l}_i}\left(1 - \frac{m^2_{\tilde{\chi}_j^0}}{m^2_{\tilde{l}_i}}\right)^2 \qquad (i = \mathrm{L/R}), \tag{3.18}$$

$$\Gamma[\tilde{l}_i^- \to \nu_l\, \tilde{\chi}_k^-] = \frac{\alpha}{4}|U_{k1}|^2\, m_{\tilde{l}_\mathrm{L}}\left(1 - \frac{m^2_{\tilde{\chi}_j^\pm}}{m^2_{\tilde{l}_\mathrm{L}}}\right)^2. \tag{3.19}$$

For slepton masses in the range of about 200 GeV, the widths are roughly of the order $300 - 1000$ MeV.

In many scenarios, the decay of right-chiral sleptons into a lepton and a neutralino LSP is one of the dominant decay channels. In this case the pair production of sleptons yields a very simple detector signature consisting of just two charged leptons plus missing energy. Therefore this is one of the most outstanding processes for detection of supersymmetry at a linear collider and allows precision measurements at the per-cent or even per-mille level. The decay modes into heavier neutralinos or charginos result in additional leptons or light-quark jets in the final state, which can also be easily handled in experiment.

Detailed studies [49, 51] indicate that it is also possible to obtain information about scalar leptons below the kinematical threshold for pair production, however, in this case the reachable precision is much reduced.

Chapter 4

Predictions for off-shell slepton pair production

4.1 Finite width effects and gauge invariance

One of the specific capabilities of a linear collider with high luminosity is the precise measurement of sparticle masses in threshold scans. As will be discussed in section 6.1, the masses of right-chiral selectrons and smuon could be determined with an accuracy of $\mathcal{O}(100$ MeV) or even below. This experimental error is significantly smaller than the widths of the sleptons, which in mSUGRA and GMSB scenarios is typically of the order of $\mathcal{O}(1$ GeV). Thus the investigation of width effects is mandatory for this purpose.

Several problems arising in this context are quite similar to the case of W boson pair production in e^+e^- annihilation in the Standard Model [53–55]. In this section the production of right-chiral smuons will be studied as an example. Since smuons are unstable particles they can be produced off-shell. The dominant decay mode of right-chiral smuons in the MSSM is the decay into the lightest neutralino $\tilde{\chi}_1^0$,

$$\tilde{\mu}_{\mathrm{R}}^- \to \mu^- \tilde{\chi}_1^0. \tag{4.1}$$

Thus the pair production of smuons in this channel is described by the diagram in Fig. 4.1 (a). However from this doubly resonant diagram alone one would obtain a gauge-dependent amplitude. This can be made explicit by considering an axial gauge fixing for the s-channel bosons[1] [53]. The introduction of the gauge fixing term $\mathcal{L}_{\mathrm{gf}} = -\frac{1}{2}(n_\gamma^\mu A_\mu)^2$ for the photon field A_μ yields an additional contribution to the matrix element,

$$\mathcal{M}_{\mathrm{dblres}}|_{\text{axial gauge}} - \mathcal{M}_{\mathrm{dblres}}|_{\text{cov. gauge}} = e^2 \bar{v}_e \not{n} u_e \, \frac{\mathcal{M}_{\mathrm{dec}}}{s(n\cdot(k_+ + k_-))} \left[\frac{1}{k_-^2 - m_{\tilde{\mu}}^2} - \frac{1}{k_+^2 - m_{\tilde{\mu}}^2} \right], \tag{4.2}$$

where $\mathcal{M}_{\mathrm{dec}}$ is the matrix element for the decay amplitude, $k_\pm$ and $m_{\tilde{\mu}}$ are the momenta and masses of the smuons, respectively, and $\bar{v}_e, u_e$ denote the spinors of the initial e^+e^- system.

[1] The gauge parameter dependence in a covariant R_ξ gauge is cancelled by the conserved incoming current.

It can be seen that the additional term in (4.2) depends on the axial gauge vector n and can therefore be made arbitrarily large. The reason for the gauge dependence originates from the fact that by just considering the diagram in Fig. 4.1 (a), a subset of the full gauge-independent process $e^+e^- \to \mu^+\mu^- \tilde{\chi}_1^0 \tilde{\chi}_1^0$ is singled out. This can be cured by adding the singly resonant diagrams contributing to the same final state in Fig. 4.1 (b), which exactly cancel the singly resonant gauge-dependent terms in (4.2).

The diagrams in Fig. 4.1 together form a gauge-invariant subset of the full process $e^+e^- \to \mu^+\mu^- \tilde{\chi}_1^0 \tilde{\chi}_1^0$. Nevertheless, this does not solve the gauge-invariance problem completely. The introduction of finite widths in the resonant propagators of unstable particles follows from a Dyson resummation of self-energy graphs. However, this procedure selects a very limited part of the higher order diagrams, so that in general gauge invariance is not preserved. With the techniques available today, it is not feasible to perform a complete higher order calculation to the full process. Therefore a consistent and practical scheme for the calculation of gauge-invariant cross-sections is needed.

One possibility is the *pole scheme* [56], which systematically decomposes the complete amplitude, consisting of doubly resonant diagrams R_{dblres}, singly-resonant diagrams $R_{\mathrm{sglres},\pm}$ and non-resonant diagrams R_{nonres}, according to its analytical pole structure:

$$
\begin{aligned}
\mathcal{M} &= \frac{R_{\mathrm{dblres}}(k_+^2,k_-^2)}{(k_-^2-m_i^2)(k_+^2-m_i^2)} + \frac{R_{\mathrm{sglres},-}(k_+^2,k_-^2)}{k_-^2-m_i^2} + \frac{R_{\mathrm{sglres},+}(k_+^2,k_-^2)}{k_+^2-m_i^2} + R_{\mathrm{nonres}}(k_+^2,k_-^2) \\
&= \frac{R_{\mathrm{dblres}}(m_i^2,m_i^2)}{(k_-^2-m_i^2)(k_+^2-m_i^2)} \\
&\quad + \frac{1}{k_-^2-m_i^2}\left[\frac{R_{\mathrm{dblres}}(k_+^2,m_i^2)-R_{\mathrm{dblres}}(m_i^2,m_i^2)}{k_+^2-m_i^2} + R_{\mathrm{sglres},-}(k_+^2,m_i^2)\right] \\
&\quad + \frac{1}{k_+^2-m_i^2}\left[\frac{R_{\mathrm{dblres}}(m_i^2,k_-^2)-R_{\mathrm{dblres}}(m_i^2,m_i^2)}{k_-^2-m_i^2} + R_{\mathrm{sglres},+}(m_i^2,k_-^2)\right] \\
&\quad + \left[\frac{R_{\mathrm{dblres}}(k_+^2,k_-^2)-R_{\mathrm{dblres}}(k_+^2,m_i^2)-R_{\mathrm{dblres}}(m_i^2,k_-^2)+R_{\mathrm{dblres}}(m_i^2,m_i^2)}{(k_-^2-m_i^2)(k_+^2-m_i^2)}\right. \\
&\qquad + \frac{R_{\mathrm{sglres},-}(k_+^2,k_-^2)-R_{\mathrm{sglres},-}(k_+^2,m_i^2)}{k_-^2-m_i^2} \\
&\qquad \left. + \frac{R_{\mathrm{sglres},+}(k_+^2,k_-^2)-R_{\mathrm{sglres},+}(m_i^2,k_-^2)}{k_+^2-m_i^2} + R_{\mathrm{nonres}}(k_+^2,k_-^2)\right].
\end{aligned}
\tag{4.3}
$$

Thus the matrix element is decomposed as a Laurent series into gauge-invariant double-pole terms, single-pole terms and non-resonant terms. Introducing now a finite width in the pole factors only but not in the residues does not destroy gauge invariance. The double-pole term in the second line of (4.3) provides a good approximation of the full result in the continuum region, as has been successfully used for calculating radiative corrections to W pair production [57]. Near threshold, it is necessary to include also the other terms in order to get a realistic result, which is technically very involved.

A technically more convenient approach to introduce finite widths is sometimes called the *complex-mass scheme*. Here, the mass m_i^2 of a possibly resonant particle is systematically replaced by a complex mass $m_i^2 - i\,m_i\,\Gamma_i$ [55]. This replacement has to be performed not only in the resonant propagators but for all mixing matrices and other quantities

(a) Double resonance diagram

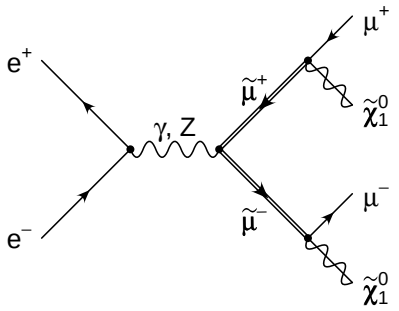

(b) Single resonance diagrams

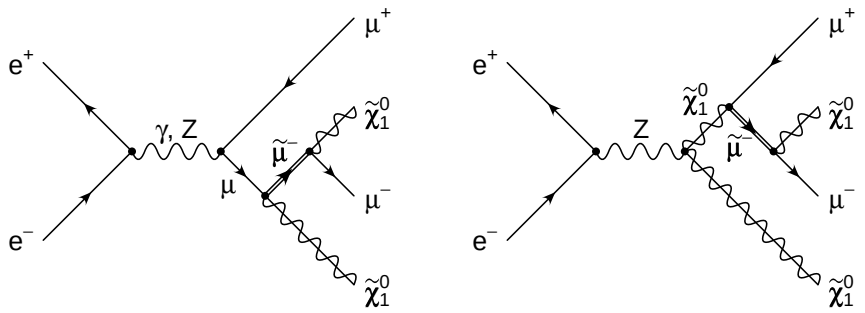

Figure 4.1: *The doubly and singly resonant contributions to the process* $e^+e^- \to \mu^+\mu^-\tilde{\chi}_1^0\tilde{\chi}_1^0$.

which depend on the particular mass. Since this is a pure parameter transformation the gauge-invariance is not touched. Furthermore it provides a realistic description of the cross-section near threshold.

The main drawback of this scheme is that the hermicity of the Lagrangian is destroyed by the introduction of complex parameters, thereby violating unitarity. This fact illustrates that the complex quantities do not have any physical motivation but rather serve as a technical parametrization of the finite width effects. Up to now, no systematic study has been undertaken as to quantitatively estimate the magnitude of the unitarity violation effects. However it is believed that they are of minor significance in comparison with the gauge violation effects, so that the complex mass scheme is expected to provide a reliable approximation of the threshold cross-section. Therefore this scheme is used in the following.

4.2 Leading radiative corrections

4.2.1 Initial-state radiation

The virtual and real corrections to a process in e^+e^- annihilation reveal the presence of large logarithmic QED effects proportional to

$$\frac{\alpha}{\pi}L = \frac{\alpha}{\pi}\log\frac{Q^2}{m_e^2}, \tag{4.4}$$

where $Q^2 \gg m_\mathrm{e}^2$ is a typical scale of the hard scattering process. They originate from the emission of photons in the direction of the incoming particles when the momentum of the latter is kept fixed, i.e. it is treated exclusively [58]. This can be seen by considering the propagator D of the incoming fermion after photon emission, $e^\pm(p) \to \gamma(k) + e^\pm(p-k)$,

$$D = \frac{1}{(p-k)^2 - m_\mathrm{e}^2} \overset{p_0 \gg m_\mathrm{e}}{\approx} \frac{1}{-2p_0k_0[1-(1-\frac{1}{2}m_\mathrm{e}^2/p_0^2)\cos\theta]}, \tag{4.5}$$

where θ is the angle of the photon momentum k with respect to the incoming momentum p. In a massless theory this would give rise to collinear divergences, since in the limit $m_\mathrm{e} \to 0$ the propagator D exhibits a pole at $\cos\theta = 1$. For electroweak processes, the masses of the electron or positron provide a natural cutoff, yielding logarithmic terms of the form $\log(p_0^2/m_\mathrm{e}^2)$, which can be large due to the difference between the involved scales p_0 and m_e.

In the case that some of the final state charged particles are light they also give rise to large collinear logarithms. However, in realistic experimental situations, the collinear photon emission from a final state charged lepton cannot be resolved in the detector. Therefore it is sufficient for leading order predictions to only take into account initial-state radiation and the hard scattering amplitude, while final-state photon radiation does not produce any large observable effects.

Since the large initial-state QED logarithms are universal and process-independent they can be resummed to higher orders. A widely used technique for the calculation of the collinear logarithms is the structure-function method [59]. In addition, it also allows the inclusion of soft-photon effects by means of exponentiation.

According to the mass-factorization theorem, the complete cross-section $\sigma_{e^+e^-\to X+n\gamma}$ is linked to the hard scattering cross-section $\hat{\sigma}_{ij\to X}$, which is free of large collinear logarithms, as follows,

$$\frac{\mathrm{d}\sigma_{e^+e^-\to X+n\gamma}}{\mathrm{d}\theta_k}(s) = \int_0^1 \mathrm{d}x_+ \int_0^1 \mathrm{d}x_- \, \Gamma_{ie^+}(x_+, Q^2)\, \Gamma_{je^-}(x_-, Q^2)\, \frac{\mathrm{d}\hat{\sigma}_{ij\to X}}{\mathrm{d}\theta_k}(\hat{s}, Q^2), \tag{4.6}$$

where $\hat{s} = x_+x_-s$ and θ_k denotes an arbitrary set of dimensionless invariant kinematical variables. The structure functions (or splitting functions) $\Gamma_{ik}(x, Q^2)$ are equivalent to the probability of finding a particle i with momentum fraction x in the initial particle k at the scale Q^2. Both the structure functions and the hard scattering cross-section depend on the factorization scale Q^2.

In general, the structure functions contain also non-diagonal entries. For example, $\Gamma_{\gamma e}$ describes the emission of a hard photon, which triggers the hard scattering process, from the incoming electron, with the latter then escaping undetected in the beam pipe. Nevertheless, the most important contributions to the QED initial-state radiation arise from pure photon radiation. This is in particular the case when soft contributions are dominant, as for the production of particles near threshold. Therefore, in this work only the diagonal structure function Γ_{ee} is considered.

In the leading-log (LL) approximation only terms proportional to $(\alpha L/\pi)^n$ are taken into account. Since all large collinear logarithms are contained in the structure functions, this automatically means that the hard scattering cross-section $\hat{\sigma}$ coincides with the Born

cross-section. In addition it can be supplemented by leading corrections which are not of LL order, as e.g. the Coulomb correction (see next section).

The relevant structure function has been calculated up to order $\mathcal{O}(\alpha^3 L^3)$. Including soft photon exponentiation, it reads [60, 61]

$$\begin{aligned}\Gamma_{ee}^{\mathrm{LL,exp}}(\alpha,x,Q^2) = {}& \frac{\zeta_\alpha\,(1-x)^{\zeta_\alpha-1}}{\Gamma(1+\zeta_\alpha)}\,e^{-\gamma_\mathrm{E}\zeta_\alpha+3\alpha L/4\pi} - \frac{\alpha}{2\pi}L\,(1+x)\\ &- \frac{1}{2}\left(\frac{\alpha}{2\pi}\right)^2 L^2\left[\frac{1+3x^2}{1-x}\log(x)+4(1+x)\,\log(1-x)+5+x\right]\\ &- \frac{1}{6}\left(\frac{\alpha}{2\pi}\right)^3 L^3\Bigg\{(1+x)\left[6\,\mathrm{Li}_2(x)+12\,\log^2(1-x)-3\pi^2\right]\\ &+\frac{1}{1-x}\left[\frac{3}{2}(1+8x+3x^2)\log(x)+6(x+5)(1-x)\log(1-x)\right.\\ &\left.\left.+\,12(1+x^2)\log(x)\log(1-x)-\frac{1}{2}(1+7x^2)\log^2(x)+\frac{1}{4}(39-24x-15x^2)\right]\right\},\end{aligned} \tag{4.7}$$

with

$$\zeta_\alpha = \frac{\alpha}{\pi}(L-1). \tag{4.8}$$

Here Li_2 represents the dilogarithm, $\Gamma(y)$ is the Gamma function and γ_E the Euler constant. In (4.7) some non-leading terms are taken into account by considering that the residue of the soft-photon pole is proportional to $L-1$ rather than L.The total scattering cross-section can then be written as

$$\sigma_{\mathrm{LL,exp}}(s,Q^2) = \int_{E_\mathrm{thrs}^2/s}^1 \mathrm{d}z\;\Gamma_{ee}^{\mathrm{LL,exp}}(2\alpha,z,Q^2)\;\hat{\sigma}_0(zs), \tag{4.9}$$

where $\hat{\sigma}_0(zs)$ denotes the Born cross-section, possibly including some leading radiative corrections, at the reduced centre-of-mass energy $\sqrt{zs}$. E_thrs is the minimal energy necessary for the production of the final state particles.

In the prediction of the total cross-section in terms of (4.9), the scale Q^2 remains a free parameter. Order by order in perturbation theory, the cross-sections are independent of Q^2. However, since the introduction of collinear logarithms in (4.9) is not matched by including the remaining non-logarithmic QED corrections of the same order, the result depends on the choice of the scale Q^2 (for a discussion, see Ref. [53]). One possible choice $Q^2 = s(1-\beta)/(1+\beta)$ is motivated by the high-energy behaviour of the soft and virtual $\mathcal{O}(\alpha)$ QED contributions. Near threshold, the limited phase space implies that $Q^2 = s$ is a reasonable choice. Therefore, in the following, the second choice has been employed.

Besides corrections from soft and collinear photon radiation, the *beamstrahlung* needs to be taken into account in the initial state. It arises due to electromagnetic interactions between the two overlapping incoming electron/positron beams and results in a spread of the beam energy spectra. Beamstrahlung effects grow especially important for colliders with high luminosity, as envisaged for future linear collider projects [7–9].

Measurements of the cross-section near threshold are strongly influenced by beamstrahlung effects since they depend on the energy of the colliding particles. Therefore a

precise prediction of the beamstrahlung spectra is of utmost importance. In this thesis the program *Kιρκη* (*Circe*) [62] is used, which incorporates simple parametrizations of detailed simulations performed with the program *Guinea-Pig* [63]. For the given examples, TESLA accelerator design parameters are taken.

The change of the observable cross-section due to beamstrahlung effects can be described by a convolution similar to (4.6),

$$\frac{\mathrm{d}\sigma_{\mathrm{beamstr}}}{\mathrm{d}\Omega}(s) = \int_0^1 \mathrm{d}\xi_+ \int_0^1 \mathrm{d}\xi_- \, D_{e^+e^-}(\xi_+, \xi_-; s)\, J(\Omega, \Omega') \, \frac{\mathrm{d}\sigma_{e^+e^-\to X+n\gamma}}{\mathrm{d}\Omega'}(\xi_+\xi_- s). \tag{4.10}$$

The function D gives the energy distribution of the particles inside the beams at the interaction point in terms of the fractions $\xi_\pm$ of the design centre-of-mass energy $\sqrt{s}$. Here $\sigma_{e^+e^-\to X+n\gamma}$ is the cross-section for a single colliding e^+e^- pair (i.e. disregarding the surrounding beam) including initial-state radiation as discussed above.

4.2.2 Coulomb rescattering effects

Another source of large corrections to the cross section for pair production processes near threshold is the Coulomb interaction due to photon exchange between slowly moving final-state charged particles. When the produced particles are stable, the Coulomb rescattering effects are described by the well-known universal factor [64]

$$\sigma_{\mathrm{Coul}}^{\mathrm{on-shell}} = \sigma_{\mathrm{Born}} \frac{\alpha\pi}{2\beta}, \tag{4.11}$$

with β denoting the velocity of the produced particles. This result is independent of the spin and angular momentum of the involved particles. Since the relative factor in (4.11) grows infinitely large for $\beta \to 0$, it is often also considered as the *Coulomb singularity*.

For production of unstable particles the Coulomb singularity is partially screened by off-shellness and finite width effects. This has been studied for the case of W pairs [65–67], which are produced in an S-wave. In general, however, one has to consider higher orbital angular momenta. For the case of smuon production, conservation of angular momentum requires the smuons to be produced in a P-wave.

In the following the Coulomb correction shall be examined for the general case of production of particles $X^\pm$ with arbitrary integer spin j_X via the s-channel exchange of an intermediate state Y with spin j_Y, cf. Fig. 4.2 (a). A t-channel contribution in the limit of vanishing velocity near threshold can be re-expressed as a scalar s-channel diagram.

In order to determine the leading Coulomb rescattering effects it is only necessary to consider the first term of an expansion in β. Since the production amplitude rises proportional to β^l near threshold, the leading contribution is generated by the configuration of minimal orbital angular momentum l. For $2j_\mathrm{X} < j_\mathrm{Y}$, l is given by $l = j_\mathrm{Y} - 2j_\mathrm{X}$, and 0/1 for even/odd j_Y otherwise.

If the bosons X, Y are assumed to be scalar or gauge particles, their polarizations can be constrained by requiring transversality and tracelessness. Furthermore by exploiting Bose symmetry, the leading contribution in β to the Born production vertex is determined

Figure 4.2: *Born contribution (a) and electromagnetic loop correction (b) to the process* $(e^+e^- \to) Y \to X^+X^-$ *with arbitrary integer spins.*

to be of the form

$$\mathcal{M}_{\rm Born} = ie\,C \prod_{i=2m+1}^{j_{\rm Y}} (p_- - p_+)_{\lambda_i} \prod_{j=1}^{m} g_{\lambda_j\mu_j} g_{\lambda_{m+j}\nu_j} \prod_{k=m+1}^{j_{\rm X}} g_{\mu_k\nu_k}\,. \tag{4.12}$$

The symbol $m = m_{\rm X}$ denotes the quantum number of the component of $j_{\rm X}$ in direction of $j_{\rm Y}$, given by $m = \frac{1}{2}(j_{\rm Y} - l)$, while $p_\pm$ are the momenta of the produced particles.

The Coulomb interaction can be obtained from the photon exchange diagram Fig. 4.2 (b). By exploiting the fact that the photonic vertices in the diagram are restricted by electromagnetic gauge invariance, the amplitude for the leading order in β is then given by

$$\begin{aligned}\mathcal{M}_{\rm Born} = e^3\,Q_{\rm X}^2 \int \frac{{\rm d}^4q}{(2\pi)^4} \frac{(q-2p_-)\cdot(q+2p_+)}{q^2[(q+p_+)^2 - M_{\rm X}^2][(q-p_-)^2 - M_{\rm X}^2]} \\ \times \prod_{i=2m+1}^{j_{\rm Y}} (p_- - p_+ - 2q)_{\lambda_i} \prod_{j=1}^{m} g_{\lambda_j\mu_j} g_{\lambda_{m+j}\nu_j} \prod_{k=m+1}^{j_{\rm X}} g_{\mu_k\nu_k}.\end{aligned} \tag{4.13}$$

After some algebra one obtains

$$\sigma_{\rm Coul}^{\rm off-shell} = -\sigma_{\rm Born}\,\frac{\alpha s}{2\pi} Q_{\rm X}^2\,C_0\;\; \Re e\left(\frac{2p_+p_- - 2M_{\rm X}^2}{2p_+p_- - p_+^2 - p_-^2}\right)^l, \tag{4.14}$$

where the Coulomb part of the scalar triangle function C_0 can be evaluated according to [67, 68]. The final result then reads

$$\sigma_{\rm Coul}^{\rm off-shell} = \sigma_{\rm Born}\,\frac{\alpha\pi}{2\beta}\,Q_{\rm X}^2 \left[1 - \frac{2}{\pi}\arctan\frac{|\beta_{\rm M}|^2 - \beta^2}{2\beta\,\Im m\,\beta_{\rm M}}\right] \Re e\,\mathcal{C}_l, \tag{4.15}$$

$$\mathcal{C}_l = \left(\frac{\beta^2 + \beta_{\rm M}^2}{2\beta^2}\right)^l. \tag{4.16}$$

Here the generalized velocities

$$\beta = \frac{1}{s}\lambda^{1/2}(s, p_+^2, p_-^2) \equiv \frac{1}{s}\sqrt{(s - p_+^2 - p_-^2)^2 - 4p_+^2p_-^2}, \tag{4.17}$$

$$\beta_{\rm M} = \sqrt{1 - 4M_{\rm X}^2/s} \tag{4.18}$$

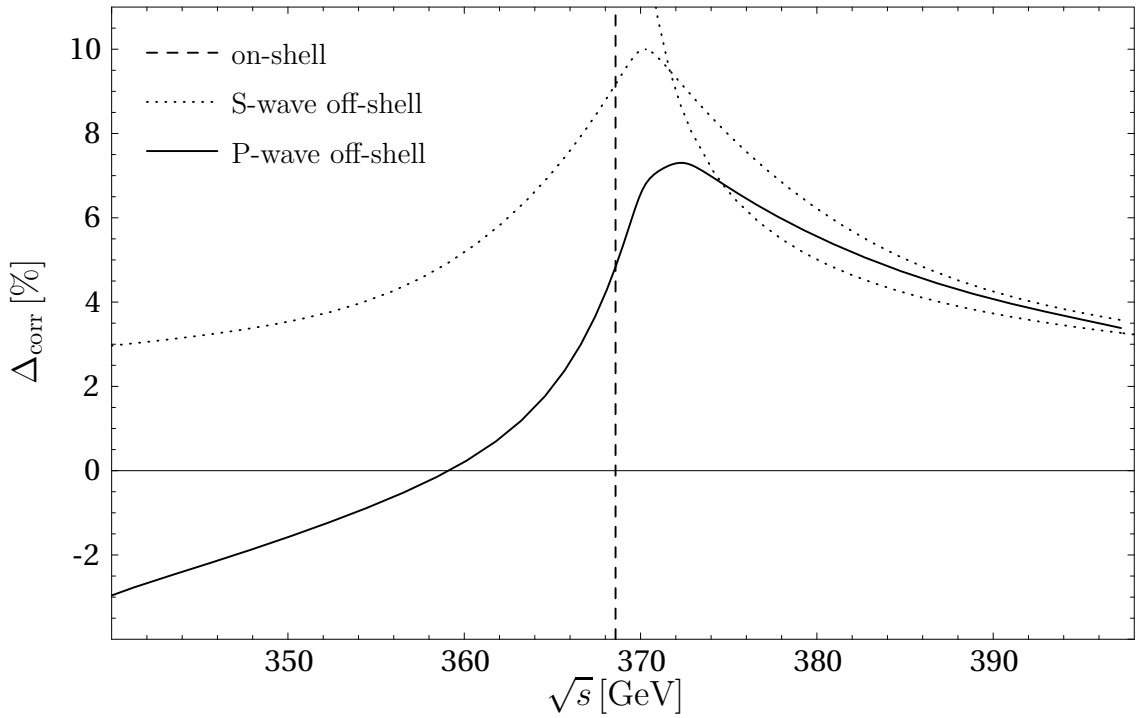

Figure 4.3: *Correction factor Δ_{corr} due to Coulomb rescattering relative to the Born cross-section for on-shell and off-shell S- and P-wave production.*

have been introduced, where $M_{\rm X}^2 = m_{\rm X}^2 - im_{\rm X}\Gamma_{\rm X}$ denotes the complex pole mass of the produced particles. The well-known damping of the Coulomb singularity for S-waves is given by the term in square brackets in (4.15). It is even enhanced for waves of higher orbital angular momentum l, due to the additional coefficient $\mathcal{C}_l$, as can be seen in Fig. 4.3.

Finally, in order to also cover the possibility of selectron production in mixed pairs, $\tilde{e}_{\rm R}^{\pm}\tilde{e}_{\rm L}^{\mp}$, the Coulomb correction has to be evaluated for the case that the two produced particles have different masses. The result for this situation is given by (4.15) with the replacement

$$\beta_{\rm M} = \frac{1}{s}\lambda^{1/2}(s, M_+^2, M_-^2). \tag{4.19}$$

Here $M_\pm^2 = m_\pm^2 - im_\pm\Gamma_\pm$ are the complex pole masses of the two produced particles.

4.3 The Monte Carlo program

The findings of the previous sections have been implemented into a Monte Carlo program in order to facilitate reliable predictions of threshold excitation curves.

As explained in section 4.1, for a consistent and gauge-invariant treatment of finite widths in the pair production of scalar leptons, it is necessary to consider the full $2 \to 4$ process including production and decay of the sleptons. Taking into account all contributions with the same final state, i.e. including backgrounds, this can easily amount to several hundred diagrams at tree-level. Therefore it is virtually impossible to perform the

calculation in the traditional way by taking the square of the amplitude and summing over the polarization states of the external particles. In particular, an amplitude consisting of n diagrams would result in a squared matrix element which is the sum of $n(n+1)/2$ terms.

This problem can be circumvented by calculating the amplitudes for specific polarization states (for example in the helicity basis). Each helicity amplitude can be calculated numerically and results in a complex number, then the square of the amplitudes and the summation over all helicities can easily be performed.

For this thesis, the helicity amplitudes have been calculated by using the Dirac spinor formalism of Ref. [69]. This method allows one to express the complete Dirac algebra and the polarization vectors of external gauge bosons in terms of two basic spinor products,

$$s(p_1,p_2) \equiv \bar{u}_+(p1)\, u_-(p_2) = -s(p2,p1), \tag{4.20}$$

$$t(p_1,p_2) \equiv \bar{u}_-(p1)\, u_+(p_2) = \big(s(p2,p1)\big)^*, \tag{4.21}$$

where $u_\pm$ denote massless Dirac spinors with positive/negative helicity and $s(p_1,p_2)$ can be determined according to

$$p_i^\mu = (p_i^0, p_i^{\mathrm{x}}, p_i^{\mathrm{y}}, p_i^{\mathrm{z}}), \tag{4.22}$$

$$s(p_1,p_2) = (p_1^{\mathrm{y}} + ip_1^{\mathrm{z}})\sqrt{\frac{p_2^0 - p_2^{\mathrm{x}}}{p_1^0 - p_1^{\mathrm{x}}}} - (p_2^{\mathrm{y}} + ip_2^{\mathrm{z}})\sqrt{\frac{p_1^0 - p_1^{\mathrm{x}}}{p_2^0 - p_2^{\mathrm{x}}}}. \tag{4.23}$$

If the denominators in (4.23) become singular, x and y can be interchanged.

In this work, the diagrams and amplitudes are generated with the package *FeynArts* [35]. Appropriate *Mathematica* routines have been written which, after simplification of the Dirac and Lorentz algebra, transform the *FeynArts* output into helicity amplitudes in terms of the spinor products s and t. These expression are then exported into a C++ program which performs the numerical evaluation and the phase space integration.

The integration over the phase space of a n-particle final state can be written as

$$I = \int \mathrm{d}\sigma = \int \mathrm{d}^{3n-4}y\ \rho\big(k_i(\vec{y})\big)\, f\big(k_i(\vec{y})\big), \tag{4.24}$$

$$f(k_i) = \frac{(2\pi)^{3n-4}}{2s}\, \big|\mathcal{M}(p_{e^+}, p_{e^-}, k_i)\big|^2, \tag{4.25}$$

where a suitable set of variables $\vec{y} = (y_i)$ has been chosen as a parametrization of the final state momenta $k_1, \ldots, k_n$. Usually invariants and angles are taken for the y_i, see e. g. Ref. [70]. An easily implementable parametrization is obtained by decomposition of the n-particle final state into a $2 \to 2$ scattering process with subsequent $1 \to 2$ decays. The variables y_i then consist of the invariant virtualities of the intermediate particle propagators and the polar and azimuthal angles of the 2-particle sub-phase-spaces. In order to increase the numerical stability, it is useful to render resonant propagators flat by an appropriate mapping of the integration variables to new variables $\vec{x} = (x_i)$, $\vec{y} = \vec{\Psi}(\vec{x})$, yielding

$$I = \int \mathrm{d}^{3n-4}x\ \frac{f\big(k_i(\vec{\Psi}(\vec{x}))\big)}{g\big(k_i(\vec{\Psi}(\vec{x}))\big)}. \tag{4.26}$$

The corresponding density function (integration Jacobian) g is given by

$$\frac{1}{g\big(k_i(\vec{\Psi}(\vec{x}))\big)} = \rho\big(k_i(\vec{\Psi}(\vec{x}))\big) \left|\frac{\partial\vec{\Psi}(\vec{x})}{\partial\vec{x}}\right|. \tag{4.27}$$

Now the mapping function $\vec{\Psi}(\vec{x})$ is chosen so that the resulting density function g mimics the behaviour of f, and thus large peak values in the integrand of (4.26) are cancelled. More precisely, a resonant Breit-Wigner propagator $1/((y_i - M_\mathrm{X}^2)^2 + M_\mathrm{X}^2\Gamma_\mathrm{X}^2)$ in the integrand f can be rendered flat by the variable mapping

$$y_i = M_\mathrm{X}^2 + M_\mathrm{X}\Gamma_\mathrm{X}\tan x_i, \tag{4.28}$$

$$\arctan\left(\frac{y_{i,\min} - M_\mathrm{X}^2}{M_\mathrm{X}\Gamma_\mathrm{X}}\right) < x_i < \arctan\left(\frac{y_{i,\max} - M_\mathrm{X}^2}{M_\mathrm{X}\Gamma_\mathrm{X}}\right). \tag{4.29}$$

In general, also massless propagators in the t- or u-channel may become resonant in the collinear limit and therefore would require a suitable variable mapping. However, for the processes studied in this thesis, such contributions do not occur or are excluded by simple cuts.

Since the full matrix element exhibits a complicated resonance structure, it is impossible to describe the peaks in the integrand $f(\vec{y})$ by a single density $g(\vec{y})$. Each peaking topology would require a suitable set of integration variables $\vec{y}_k$ and a specific mapping of integration variables $\vec{y}_k = \vec{\Psi}_k(\vec{x})$, so that resonant propagators are rendered flat by the resulting density g_k. Therefore the integration over the phase space of the final state particles is performed by a multi-channel Monte Carlo method [71]. In this approach all densities g_k are joined into a combined density g_tot which renders the integrand sufficiently smooth over the whole phase-space region. The phase-space integral of (4.26) then reads

$$I = \sum_{k=1}^{K} \int \mathrm{d}^{3n-4}x \, \frac{f\big(k_i(\vec{\Psi}_k(\vec{x}))\big)}{g_\mathrm{tot}\big(k_i(\vec{\Psi}_k(\vec{x}))\big)}, \tag{4.30}$$

with

$$g_\mathrm{tot}(k_i) = \sum_{l=1}^{K} g_l(k_i), \qquad \frac{1}{g_l\big(k_i(\vec{\Psi}_l(\vec{x}))\big)} = \rho_l\big(k_i(\vec{\Psi}_l(\vec{x}))\big) \left|\frac{\partial\vec{\Psi}_l(\vec{x})}{\partial\vec{x}}\right|. \tag{4.31}$$

The different mappings $\vec{\Psi}_k(\vec{x})$ are called channels, with K being the number of all channels.

For a further reduction of the Monte Carlo error, the method of weight optimization according to Ref. [72] is employed. Here, each channel k is furnished with a weight α_k, $k \in \{1, \ldots, K\}$. For the generation of a Monte Carlo event, one of the channels is picked randomly according to the weights α_k, which determine the probability of picking the channel k. The integral is then given by

$$I = \sum_{k=1}^{K} \alpha_k \int \mathrm{d}^{3n-4}x \, \frac{f\big(k_i(\vec{\Psi}_k(\vec{x}))\big)}{g_\mathrm{tot}\big(k_i(\vec{\Psi}_k(\vec{x}))\big)}, \tag{4.32}$$

with

$$g_{\text{tot}}(k_i) = \sum_{l=1}^{K} \alpha_l \, g_l(k_i), \tag{4.33}$$

and $\sum_{l=1}^{K} \alpha_l = 1$.

After the generation of N Monte Carlo points $\vec{x}^j$ one obtains the following estimate I_N of the phase-space integral,

$$I_N = \frac{1}{N} \sum_{j=1}^{N} w(\vec{x}^j), \tag{4.34}$$

where $w = f/g_{\text{tot}}$ is the weight of a Monte Carlo point $\vec{x}_j$. The expected Monte Carlo error is given by

$$\delta I_N = \sqrt{\frac{W_N - I_N^2}{N}}, \qquad W_N = \frac{1}{N} \sum_{j=1}^{N} w^2(\vec{x}^j). \tag{4.35}$$

The idea of the weight optimization method is now to minimize the expected Monte Carlo error by choosing on optimal set of weights α_k. This can be achieved by an adaptive procedure [72], starting with evenly distributed weights α_k. After a certain number N of Monte Carlo points a new set of weights is calculated according to

$$\alpha_k^{\text{new}} \propto \alpha_k \sqrt{\frac{1}{N} \sum_{j=1}^{N} \frac{g_k\big(k_i(\vec{\Psi}_k(\vec{x}^j))\big) \, w^2(\vec{x}^j)}{g_{\text{tot}}\big(k_i(\vec{\Psi}_k(\vec{x}^j))\big)}}, \tag{4.36}$$

with the normalization $\sum_{k=1}^{K} \alpha_k^{\text{new}} = 1$.

For some purposes in the following the narrow-width approximation is used. This consists in taking a zero width in resonant propagators, i.e. the corresponding intermediate particle is considered on-shell. The corresponding Breit-Wigner propagator then reduces to a Delta function,

$$\frac{M\Gamma}{(k^2 - M^2)^2 + M^2\Gamma^2} \xrightarrow{\Gamma \to 0} \pi \, \delta(k^2 - M^2). \tag{4.37}$$

When studying the production cross-section of some particle α near the kinematical threshold, it is in most cases safe to apply the narrow-width approximation for all other particles which appear in the full $2 \to 4$ process. The relative effect of the finite width of the particle α is of order $\mathcal{O}\Big(\frac{\Gamma_\alpha}{\sqrt{s}/2 - M_\alpha}\Big)$, which is sizeable near the threshold $\sqrt{s} \approx 2M_\alpha$. If the mass M_β of any background particle β does not accidentally coincide with M_α, the effect due to its width Γ_β is of minor importance, $\mathcal{O}\Big(\frac{\Gamma_\beta}{\sqrt{s}/2 - M_\beta}\Big)$. In addition, it is further reduced by cuts that are applied to decrease the β background.

The effect of Γ_β in interference contributions between production diagrams for α and β or in cascade decays is of order $\mathcal{O}\Big(\frac{\Gamma_\alpha \Gamma_\beta}{(M_\beta - M_\alpha)^2}\Big)$ if M_α and M_β are sufficiently far separated and therefore clearly suppressed in this case. As a consequence, if $|M_\alpha - M_\beta| \gg \Gamma_{\alpha,\beta}$, one may safely neglect the finite width of the particle β when focusing on the threshold of particle α.

condition	variable	accepted range
reject lepton in forward/backward region	lepton polar angle θ_{l}	$\lvert\cos\theta_{\mathrm{l}}\rvert < 0.95$
require minimal lepton energy	lepton energy E_{l}	$E_{\mathrm{l}} > 5$ GeV
reject missing momentum p_{miss} in forward/backward region	missing momentum polar angle $\theta_{\vec{p}_{\mathrm{miss}}}$	$\lvert\cos\theta_{\vec{p}_{\mathrm{miss}}}\rvert < 0.90$
angular separation of two leptons	angle $\phi_{\mathrm{l}^+\mathrm{l}^-}$ between leptons	$\lvert 1 - \cos\phi_{\mathrm{l}^+\mathrm{l}^-}\rvert > 0.002$
angular separation of two quark or tau jets	angle ϕ_{jj} between jets	$\lvert 1 - \cos\phi_{\mathrm{jj}}\rvert > 0.015$

Table 4.1: *General cuts to account for the detector geometry and resolution and to reduce photonic background. The first two cuts also apply for jets.*

4.4 Signatures and backgrounds

This section discusses how the aspired slepton signal can be extracted from potential backgrounds. Throughout, some general cuts given in Tab. 4.1 are applied to account for the basic detector geometry. However, some of the cuts are far more conservative than required by the hardware layout. The reason is that they also effectively reduce background from soft and collinear photon emission, which is typically one of the major backgrounds.

4.4.1 Production of right-chiral sleptons

For most scenarios (in particular those considered in App. A), the partners of the right-handed leptons predominantly decay into the corresponding leptons and the lightest neutralino, which in many cases is the LSP,

$$\tilde{l}^{\pm}_{\mathrm{R}} \to l^{\pm}\,\tilde{\chi}^0_1. \tag{4.38}$$

In mSUGRA and GMSB scenarios this assertion follows from the fact that in these models the $\tilde{\chi}^0_1$ has a dominant bino component and the R-sleptons only couple via the U(1) gauge coupling (and their supersymmetric equivalent Yukawa coupling). If kinematically allowed, in AMSB scenarios R-sleptons can have a dominant decay branching fraction into the second-lightest neutralino $\tilde{\chi}^0_2$, since this carries a dominant bino component. Here this case will not be considered further.

With the above-mentioned decay, the pair production of R-sleptons at an e^+e^- collider results in the simple final state of two leptons plus missing energy, $l^+l^- + \not{E}$. The most important Standard Model background arises from contributions with the final state $l^+l^-\nu\bar{\nu}$. This includes dominant contributions from WW and ZZ pair production as well as two-photon contributions. The Standard Model backgrounds are large and need to be reduced by appropriate cuts [73].

condition	variable	accepted range
cut on Z decaying into lepton pair	di-lepton invariant mass $m_{l^+l^-}$	$\lvert m_{l^+l^-} - M_Z\rvert > 10$ GeV
cut on invisibly decaying Z	invariant recoil mass m_{recoil}	$\lvert m_{\text{recoil}} - M_Z\rvert > 15$ GeV
reject back-to-back leptons from W pairs	angle $\phi_{l^+l^-}$ between leptons	$\lvert\cos\phi_{l^+l^-}\rvert < 0.7$

Table 4.2: *Cuts for the reduction of large resonant ZZ and WW contributions to the signature $l^+l^- + \not{E}$.*

resonant production	followed by	
$e^+e^- \to \tilde{\chi}^0_k\,\tilde{\chi}^0_1$	$\tilde{\chi}^0_k \to l^+\,l^-\,\tilde{\chi}^0_1$	
$e^+e^- \to \tilde{\chi}^0_k\,\tilde{\chi}^0_1$	$\tilde{\chi}^0_k \to \tau^+\,\tau^-\,\tilde{\chi}^0_1$	$\tau^\pm \to l^\pm\,\bar{\nu}_l\,\nu_\tau$
$e^+e^- \to \tilde{\chi}^0_2\,\tilde{\chi}^0_2$	$\tilde{\chi}^0_2 \to l^+\,l^-\,\tilde{\chi}^0_1$	$\tilde{\chi}^0_2 \to \nu\,\bar{\nu}\,\tilde{\chi}^0_1$
$e^+e^- \to \tilde{\chi}^+_1\,\tilde{\chi}^-_1$	$\tilde{\chi}^\pm_1 \to l^\pm\,\nu_l\,\tilde{\chi}^0_1$	
$e^+e^- \to Z\,Z$	$Z \to l^+\,l^-$	$Z \to \tilde{\chi}^0_1\,\tilde{\chi}^0_1$
$e^+e^- \to Z\,h_0/H_0$	$Z \to l^+\,l^-$	$h_0/H_0 \to \tilde{\chi}^0_1\,\tilde{\chi}^0_1$

Table 4.3: *Significant doubly resonant supersymmetric background processes to $e^+e^- \to l^+\,l^- + \not{E}$.*

The reduction of photonic background was already discussed at the beginning of this section. The background from resonant Z production can be easily reduced by applying an cut on the invariant lepton pair mass $m_{l^+l^-} = \sqrt{(k_+ + k_-)^2}$ and on the invariant mass $m_{\text{recoil}} = \sqrt{s - \sqrt{s}(E_+ + E_-) + (k_+ + k_-)^2}$ of the invisible recoil momentum, see Tab. 4.2. Here $k_\pm$ and $E_\pm$ are the momenta and energies of the leptons $l^\pm$, respectively. Contributions from WW pair production have a characteristic angular distribution of the final state leptons. Because of the spin correlations and the boost factor, the leptons tend to be aligned back to back and along the beam direction. Therefore this background can be effectively reduced by rejecting signatures with back-to-back leptons (Tab. 4.2).

In addition, a large number of supersymmetric backgrounds are involved (see e.g. [74]). The most important doubly resonant contributions are listed in Tab. 4.3. Their treatment strongly depends on the scenario.

The background from $\tilde{\chi}^0_2\tilde{\chi}^0_1$ production can be reduced by requiring the missing energy $\not{E}$ below the cut

$$\not{E} \lesssim \not{E}_{\text{cut}} = \sqrt{s}\left[1 - \frac{(m^2_{\tilde{\chi}^0_2} - m^2_{\tilde{\chi}^0_1})\big(s - m^2_{\tilde{\chi}^0_1} + m^2_{\tilde{\chi}^0_2} + \lambda^{1/2}(s, m^2_{\tilde{\chi}^0_1}, m^2_{\tilde{\chi}^0_2})\big)}{4\,m^2_{\tilde{\chi}^0_2}\,s}\right], \tag{4.39}$$

with $\lambda(a,b,c)$ defined in (4.17). Here one may exploit the tendency for the neutralino background to have a larger fraction of missing energy than the signal since one of the

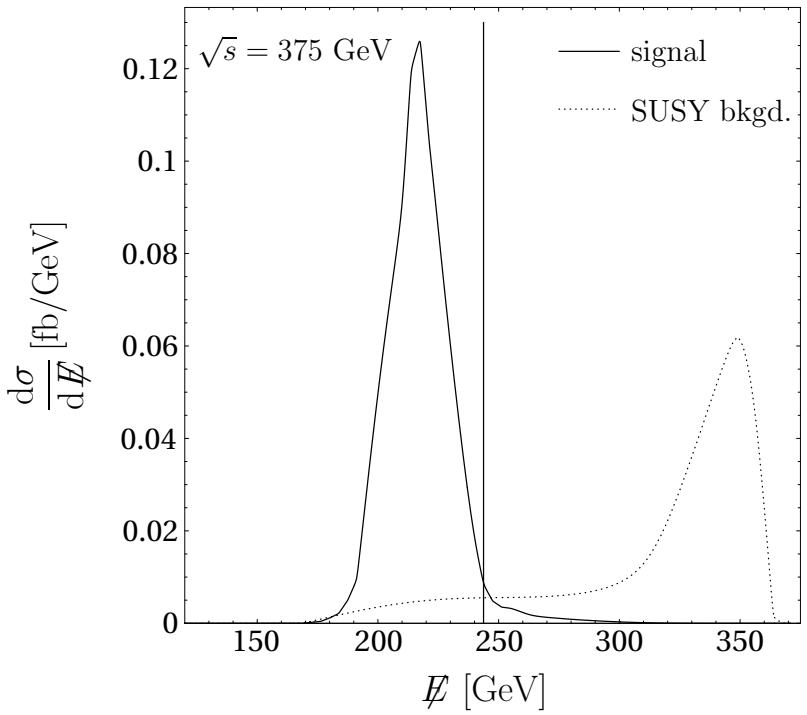

Figure 4.4: *Distribution in the missing energy $\not{E}$ of the signal contributions, from diagrams Fig. 4.1, and the supersymmetric backgrounds to $e^+e^- \to e^+e^- + \not{E}$. A possible cut according to* (4.39) *is shown as vertical line. Numerical values for RR2 scenario.*

two produced neutralinos remains completely invisible. The effect of this cut can be seen from Fig. 4.4. The same argument applies even more strongly to $\tilde{\chi}_2^0\tilde{\chi}_2^0$ and $\chi_1^+\chi_1^-$ production since the processes result in additional invisible neutrinos in the final state. For large $\tan\beta$, the bulk of the neutralinos and charginos decays into staus. These taus could then decay into the lepton l and thereby imitate the signal of l^+l^-. However, again this decay chain leads to additional neutrinos in the final state and is easily accounted for by the missing-energy cut.

In addition to the pair production of resonant particles as in Tab. 4.3, for the analysis in the next section background contributions with one or no resonant particles are also taken into account by considering the full matrix element for $e^+e^- \to e^+e^-\,\tilde{\chi}_1^0\,\tilde{\chi}_1^{02}$. While the total amount of these background contributions is definitely smaller than the signal cross-section, they can still have a non-negligible effect on high precision measurements. In particular after application of cuts these sub-dominant contributions are only sightly reduced and may be of the same order as the remaining, originally doubly-resonant and dominant, background.

The signal-to-background ratio can further be enhanced by applying appropriate polarizations. In the following it is assumed that the electron beam can be polarized with a degree of 80%, while for the positron beam 50% polarization is taken. For the pair production of sleptons in e^+e^- annihilation, the optimal combination is a right-polarized electron beam and a left-polarized positron beam, $P_{e^-} = +80\%$, $P_{e^+} = -50\%$.

[2]The full matrix element is needed also for gauge-invariance reasons, cf. sec. 4.1

The production of scalar electrons is also possible in the e^-e^- mode. The final state signature consists of two like-sign electrons plus missing energy, $e^-e^- + \not{E}$. One virtue of this options is the very low background contamination. The Standard Model backgrounds $e^-e^- \to e^-e^-\,\nu\bar{\nu}$ involve dominant contributions from the resonant production of single W- and Z-bosons. The Z background can easily be reduced [75] by observing that for a Z decaying into two neutrinos, the missing energy is always below

$$\not{E} < \frac{s + M_{\mathrm{Z}}^2}{2\sqrt{s}} \approx \frac{\sqrt{s}}{2} \qquad \text{for } s \gg M_{\mathrm{Z}}^2. \tag{4.40}$$

Since the selectrons decay into massive neutralinos they typically lead to larger fractions of missing energy. Accordingly, with the condition $\not{E} > \sqrt{s}/2$, the Z background can be almost completely eliminated. Background from single W production can be effectively reduced by using right-polarized electron beams, $P_{e^-} = +80\%$ [75]. In addition, this would lead to a significant enhancement of the signal cross-section.

Supersymmetric backgrounds in the e^-e^- mode are low and do not require any special treatment, since they do not involve any resonant pair production sub-processes.

4.4.2 Production of left-chiral sleptons

In all typical breaking scenarios, left-chiral sleptons of the first two generations are heavier than their right-chiral companions. Accordingly, L-sleptons are produced over a huge background from R-sleptons. Thus, in order to disentangle the two states, one should consider other decay modes of the L-sleptons than $\tilde{l}_{\mathrm{L}}^{\pm} \to l^{\pm}\,\tilde{\chi}_1^0$. A unique property of left-chiral sleptons is the decay into a chargino and a neutrino, cf. (3.19). This is however unfavourable for slepton production in e^+e^- annihilation, since the neutrino escapes undetected and no identification of the flavour of the produced sleptons is possible[3]. Therefore, here the decay into a heavier neutralino is considered,

$$\begin{aligned} \tilde{l}_{\mathrm{L}}^{\pm} &\to l^{\pm}\,\tilde{\chi}_2^0 \\ &\qquad \hookrightarrow \tau^+\,\tau^-\,\tilde{\chi}_1^0, \end{aligned} \tag{4.41}$$

with a subsequent decay of the neutralino $\tilde{\chi}_2^0$ into a pair of taus $\tau^+\tau^-$ and the lightest neutralino. For scenarios with $\tan\beta \gtrsim 10$ the tau final state is favourable since it is strongly enhanced with respect to the first two generation leptons. The mixed selectron pair production, $e^+e^- \to \tilde{e}_{\mathrm{R}}^{\pm}\tilde{e}_{\mathrm{L}}^{\mp}$, for instance, is then characterized by the final state signature $e^+e^-\,\tau^+\tau^- + \not{E}$, where a reasonable tau detection performance is presumed. The decay of a R-slepton into a heavier neutralino, $\tilde{l}_{\mathrm{R}}^{\pm} \to l^{\pm}\,\tilde{\chi}_2^0$ is strongly suppressed if the lightest neutralino $\tilde{\chi}_1^0$ is bino-like. Furthermore, this channel is also disfavoured due to kinematical reasons because of the mass difference between $\tilde{l}_{\mathrm{L}}$ and $\tilde{l}_{\mathrm{R}}$. The appearance of additional tau jets can therefore be interpreted as a clear signal of L-sleptons.

In the e^+e^- mode, the production of mixed selectron pairs, $\tilde{e}_{\mathrm{R}}^{\pm}\tilde{e}_{\mathrm{L}}^{\mp}$, is best suited for the examination of the left-chiral selectron. In contrast to the production of L-selectron pairs, the cross-section rises faster at threshold due to the S-wave excitation. In addition,

[3] Thanks to H. U. Martyn for stressing this point.

as explained before, using same-sign polarization for the e^- and e^+ beams reduces supersymmetric backgrounds. The cross-section for left-chiral smuon production is too small to perform any measurements at the threshold.

The main Standard Model backgrounds arise from triple gauge boson production $\mathrm{W^+W^-Z}$ and $\mathrm{W^+W^-}\gamma^*$ with a leptonic decay of the W-bosons and the Z-boson or photon. The total cross-section of these processes is well below 1 fb [76] and can be further reduced by applying cuts on the invariant di-lepton masses. Therefore, Standard Model background will be neglected here.

Supersymmetric backgrounds to $\tilde{e}_\mathrm{R}^\pm \tilde{e}_\mathrm{L}^\mp$ are included by computing the complete matrix element for $e^+e^- \to e^+e^-\,\tilde{\chi}_1^0\,\tilde{\chi}_2^0$. In the scenarios of App. A, the width of $\tilde{\chi}_2^0$ is small so that it can safely be treated as an on-shell final-state particle. Accordingly, the decay of the $\tilde{\chi}_2^0$ factorizes; nevertheless, spin correlations have to be taken into account.

The full process $e^+e^- \to e^+e^-\,\tilde{\chi}_1^0\,\tilde{\chi}_2^0$ includes a possibly large background from $\tilde{\chi}_2^0\tilde{\chi}_2^0$ production. Another potential background source could stem from the production of scalar taus, $e^+e^- \to \tilde{\tau}^+\tilde{\tau}^- \to \tau^+\tau^-\,\tilde{\chi}_1^0\,neu_2 \to \tau^+\tau^-\,e^+e^-\,\tilde{\chi}_1^0\,\tilde{\chi}_1^0$. Both contributions are suppressed due to the small branching fraction of the neutralino $\tilde{\chi}_2^0$ into electrons (see App. A). Furthermore the signal-to-background ratio can be improved by a suitable application of beam polarization. For the pair production of mixed selectron pairs, $\tilde{e}_\mathrm{R}^\pm \tilde{e}_\mathrm{L}^\mp$, the polarization for both electron and positron beams with the same helicity, $P_{e^-} = -80\%, P_{e^+} = -50\%$ or $P_{e^-} = +80\%, P_{e^+} = +50\%$, leads to an enhancement of the signal cross-section while the background from stau pair production is suppressed.

In e^-e^- scattering left-chiral selectrons can best be studied when they are produced in pairs, $\tilde{e}_\mathrm{L}^-\,\tilde{e}_\mathrm{L}^-$. Compared the production of mixed pairs, this production of diagonal L-selectron pairs has a larger cross-section and rises more rapidly in an S-wave excitation near threshold. The production via

$$e^-\,e^- \to (\tilde{e}_\mathrm{L}^-\,\tilde{e}_\mathrm{L}^-) \to e^-\,e^-\,\tilde{\chi}_2^0\,\tilde{\chi}_2^0 \to e^-\,e^-\,\tau\tau\tau\tau\,\tilde{\chi}_1^0\,\tilde{\chi}_1^0 \tag{4.42}$$

is practically background-free. Nevertheless, for consistency reasons, the full matrix element $e^-e^- \to \tilde{e}_\mathrm{L}^-\tilde{e}_\mathrm{L}^-\,\tilde{\chi}_2^0\,\tilde{\chi}_2^0$ is computed as before. By using left-polarized electron beams, $P_{e^-} = -80\%$, the signal can be further enhanced.

4.4.3 Specialized cuts near threshold

Near threshold the scalar leptons are produced almost at rest (with a typical energy spread of the order of the width). If one now considers a two-body decay of the sleptons, for example $\tilde{l}_\mathrm{R}^\pm \to l^\pm\,\tilde{\chi}_1^0$, the energy of the decay products is sharply defined. For instance, the final state lepton energy in the above-mentioned decay is given by

$$E_l \approx \frac{m_{\tilde{l}}^2 - m_{\tilde{\chi}_1^0}^2}{2m_{\tilde{l}}}. \tag{4.43}$$

When the masses of the slepton and the neutralino are roughly known, for example from end-points kinematics, this can be used to construct a specialized selection criterion. By cutting on the lepton energy, the total background can be reduced very effectively since

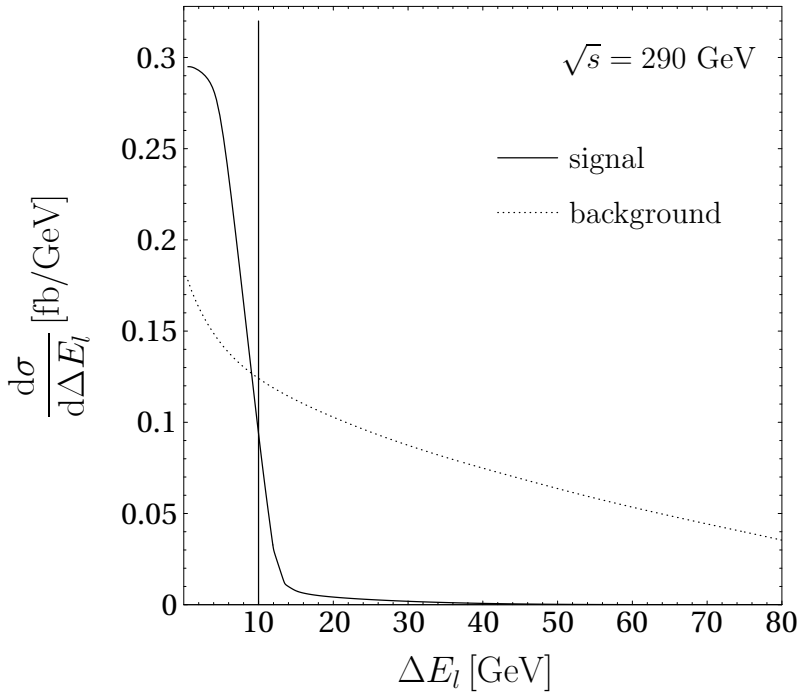

Figure 4.5: *Distribution in the lepton energy difference* $\Delta E_l = |E_+ - E_-|$ *of the signal contributions and the backgrounds to* $e^+e^- \to e^+\, e^- + \not{E}$ *near the threshold for R-selectron production,* $\sqrt{s} = 290$ *GeV (the nominal threshold is at* $2m_{\tilde{e}_R} = 286$ *GeV). A possible cut according to* (4.44) *is indicated by the vertical lines. Numerical values for SPS1 scenario.*

it is extremely unlikely that any background contribution could mimic the characteristic, sharply constrained energy distribution.

Even without any information about the neutralino mass, (4.43) can help to extract the signal for $\tilde{l}_\mathrm{R}^+\tilde{l}_\mathrm{R}^-$ production near threshold. In this case one would like to study the production of two charge-conjugated particles, which naturally have the same mass. As a consequence, final state leptons originating from two-body decays of these particles have roughly the same energy near threshold. Therefore the cut condition

$$|E_+ - E_-| < E_{l,\mathrm{cut}} \tag{4.44}$$

reduces most of the background while only slightly affecting the signal near threshold, see Fig. 4.5. Reasonable values for the cut energy are $E_{l,\mathrm{cut}} \approx 10$ GeV.

4.5 Analysis of smuon and selectron pair production near threshold

Since it is the purpose of this study to examine the effect of the finite widths in the pair production of scalar leptons, the decay of the sleptons cannot be separated from the production process. Thus, in order to preserve gauge-invariance, the computation always encompasses the full $2 \to 4$ matrix elements with the two-particle decay products of the sleptons in the final state. The potential subsequent decay of the second-lightest

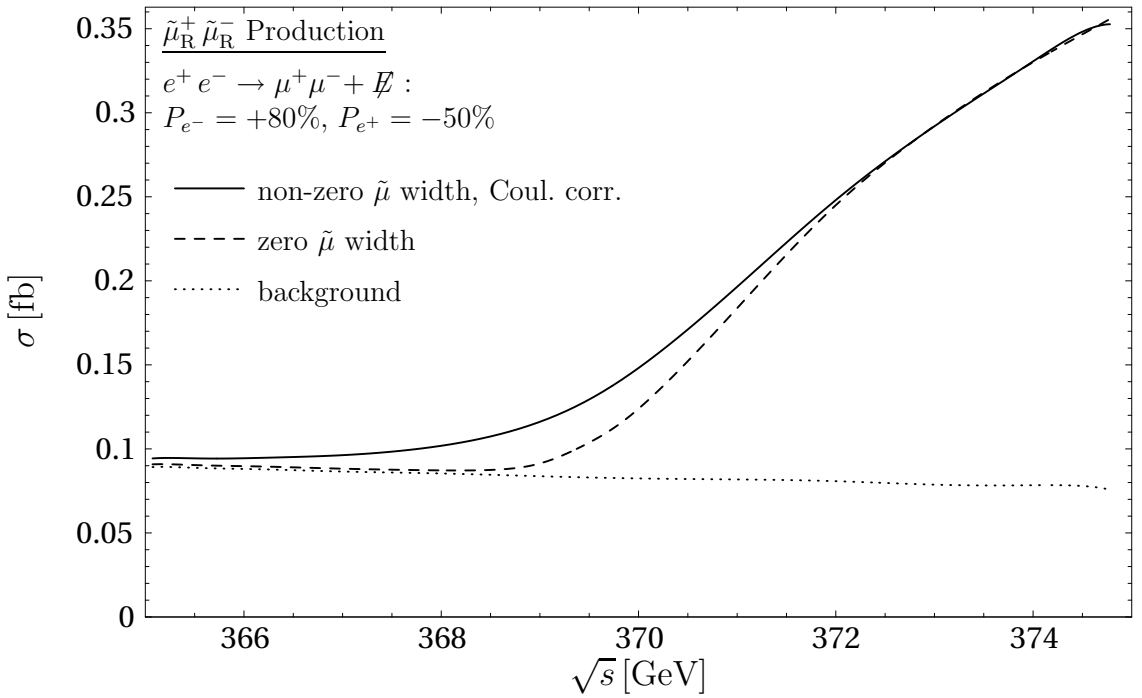

Figure 4.6: *The excitation curve for $\tilde{\mu}_R^+\tilde{\mu}_R^-$ production over Standard Model and supersymmetric backgrounds. The signal contribution with non-zero widths and Coulomb rescattering is compared with the case of zero width and no higher order corrections. Beam polarization $P_{e^-} = +80\%$ and $P_{e^+} = -50\%$ is used. Values for RR2 scenario.*

neutralino $\tilde{\chi}_2^0$ is then treated in the narrow-width approximation, i.e. the neutralino $\tilde{\chi}_2^0$ is taken on-shell.

Results for smuon production in e^+e^- annihilation and selectron production in e^-e^- scattering including supersymmetric backgrounds have been published in Ref. [74, 77]. Here the background from Standard Model processes is added and in addition the production of selectrons in e^+e^- annihilation is discussed and compared with the e^-e^- mode.

In Fig. 4.6 the threshold excitation curve for right-chiral smuon $\tilde{\mu}_R$ production is shown, including initial-state radiation and beamstrahlung. The Standard Model and supersymmetric backgrounds with the same visible final state $\mu^+\mu^- + \not{E}$ are reduced using the cut on the muon energy difference, eq. (4.44). As evident from the figure, the remaining background is smooth and almost flat so that it can be subtracted experimentally in a model-independent way.

In order to illustrate the effect of the finite smuon widths and the Coulomb rescattering corrections, also the threshold excitation curve for zero width and without radiative corrections is shown.

The production of right-chiral selectrons $\tilde{e}_R$ in e^+e^- and e^-e^- scattering is shown in Fig. 4.7. As before the curves include ISR and beamstrahlung effects and the influence of the non-zero widths and the Coulomb correction is demonstrated. In e^+e^- annihilation large background contributions arise both from Standard Model and supersymmetric

processes and are reduced with the electron energy cut (4.44). In the e^-e^- mode the backgrounds are relatively small and can be controlled with the cut (4.40).

From the figure the distinct features of the two different collider modes become apparent. Due to the S-wave excitation, the cross-section in the e^-e^- mode rises sharply at the kinematical threshold and exceeds the e^+e^- cross-section by almost two orders of magnitude in the threshold region. As a consequence, in the e^-e^- mode the effects of the finite selectron width and the Coulomb correction become more pronounced. This could open up the possibility to measure both the mass and the width of the selectron from a threshold scan.

For the measurement of the left-chiral selectron $\tilde{e}_\mathrm{L}$ mass, the most favourable processes are the production of mixed selectron pairs, $\tilde{e}_\mathrm{R}^\pm\tilde{e}_\mathrm{L}^\mp$ in the e^+e^- mode and the production of L-selectron pairs, $\tilde{e}_\mathrm{L}^-\tilde{e}_\mathrm{L}^-$ in the e^-e^- mode, respectively. In both processes the selectron pairs are produced in S-waves, thus suggesting promising prospects for precision measurements. The threshold cross-sections are depicted in Fig. 4.8.

The production of mixed pairs $\tilde{e}_\mathrm{R}^\pm\tilde{e}_\mathrm{L}^\mp$ is characterized by the final state signature $e^+e^-\,\tau^+\tau^-\,+\not{E}$, where the decay channel (4.41) of the L-selectron has been considered. The backgrounds from Standard Model and supersymmetric contributions are small and well under control.

The signal for L-selectron production in e^-e^- scattering with the decay chain (4.42) has a very distinctive pattern of two electrons, four tau jets and missing energy. Therefore, despite the relatively low signal cross-section, measurements in this channel seem promising because of the absence of relevant backgrounds.

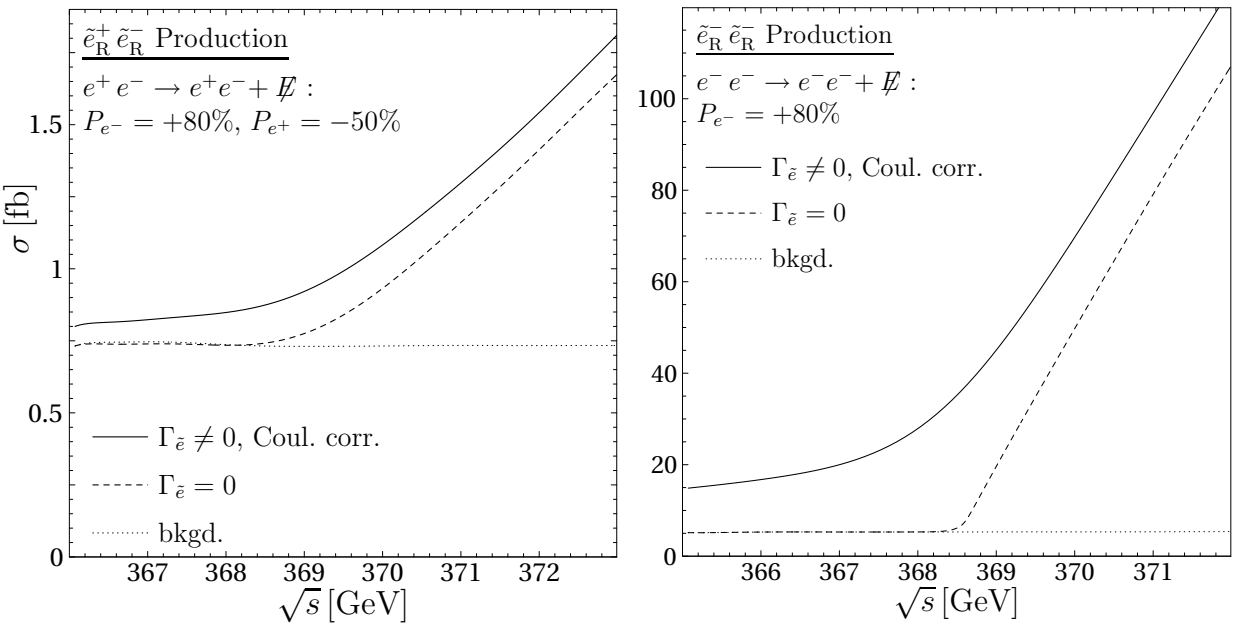

Figure 4.7: *The excitation curves for $\tilde{e}_R$ pair production over Standard Model and supersymmetric backgrounds for e^+e^- annihilation (left) and e^-e^- scattering (right). The signal contribution with non-zero widths and Coulomb rescattering is compared with the case of zero width and no higher order corrections. The signal is enhanced with beam polarization as indicated. Values for RR2 scenario.*

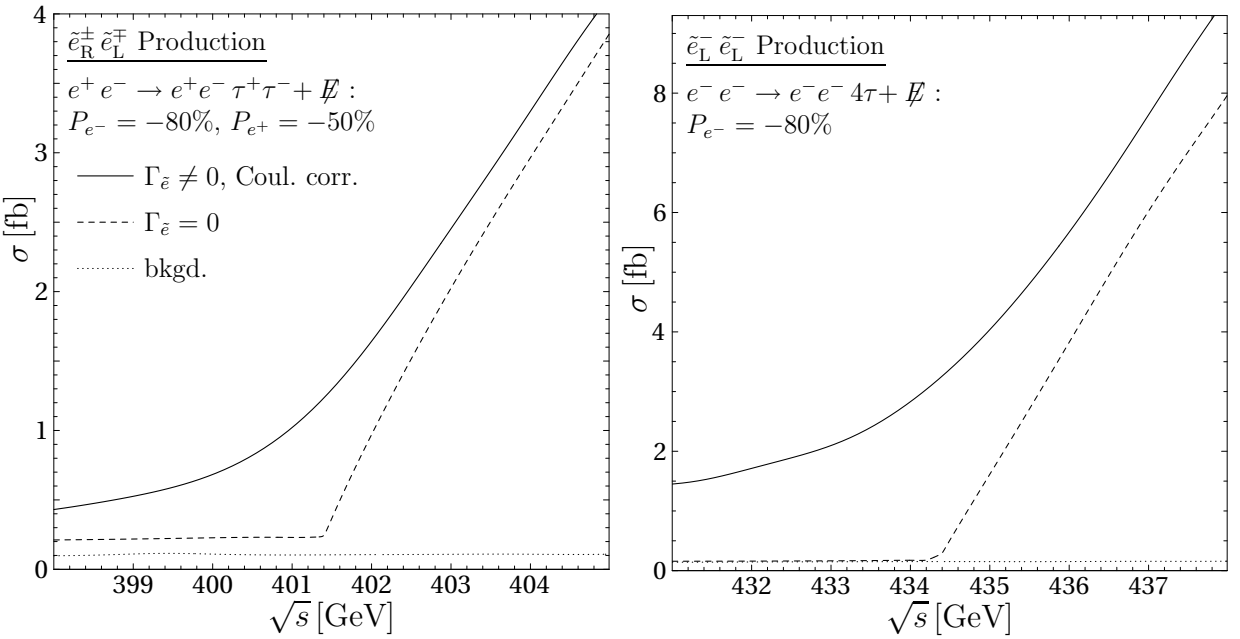

Figure 4.8: *The excitation curves mixed selectron pair production, $\tilde{e}_R^\pm \tilde{e}_L^\mp$, in e^+e^- annihilation (left) and L-selectron pair production, $\tilde{e}_L^- \tilde{e}_L^-$, in e^-e^- scattering (right). The signal contribution with non-zero widths and Coulomb rescattering is compared with the case of zero width and no higher order corrections. The signal is enhanced with beam polarization as indicated. Values for RR2 scenario.*

Chapter 5

Radiative corrections to on-shell slepton pair production

One of the most fundamental predictions of supersymmetry is the equivalence between gauge couplings of fermions and sfermions, and supersymmetric Yukawa couplings of fermions, sfermions and gauginos. Therefore, it will be one of the most interesting tasks to test this relation with high precision. At a linear collider, the couplings of scalar leptons can be extracted with an accuracy at the per-cent level or even below (see section 6.2) from the measurement of slepton pair-production cross-sections in the continuum.

Clearly, in order to match this precision, it is necessary to include radiative corrections in the theoretical predictions. In the continuum, i.e. sufficiently far above the production threshold, the effect of the finite slepton widths is less important than near threshold. Therefore, as a first step, radiative corrections are studied for the production of on-shell sleptons. As one important building block, the complete electroweak one-loop corrections to the decay of sfermions into charginos and neutralinos have been published recently [78].

Here, electroweak $\mathcal{O}(\alpha)$ corrections to the pair production of scalar leptons are studied. In particular, complete one-loop results are presented for the production of the first two generation right-chiral sleptons, i.e. the processes $e^+e^- \to \tilde{\mu}_{\mathrm{R}}^+\tilde{\mu}_{\mathrm{R}}^-$, $e^+e^- \to \tilde{e}_{\mathrm{R}}^+\tilde{e}_{\mathrm{R}}^-$ and $e^-e^- \to \tilde{e}_{\mathrm{R}}^-\tilde{e}_{\mathrm{R}}^-$. The virtual contributions are supplemented by the corresponding real photon bremsstrahlung corrections, so that a physically sound result is obtained.

In principle, these calculations could easily be extended to the production of left-chiral sleptons. However, for brevity, the complete analysis has not been performed for this case.

Since there is no standard convention for the renormalization of the superpartners of the MSSM (i.e. particles that are not present in the Standard Model), the renormalization procedure will be described in detail in the next section. The following sections will then address the other relevant issues for the calculation and discuss the results.

5.1 Renormalization of the MSSM

5.1.1 Regularization

Within non-supersymmetric gauge theories, dimensional regularization (DREG) [79] is the most widely used method of regularization. In DREG all objects which are represen-

tations of the Lorentz group (i.e. Dirac algebra, vector fields, momenta, metric tensor) are extended from 4 to $D = 4 - \epsilon$ dimensions. All loop and soft bremsstrahlung integrals are thus rendered finite. Since this procedure preserves gauge invariance, it is for most purposes[1] a very convenient prescription.

For supersymmetric theories, however, it is less suited, since there is a mismatch between bosonic and fermionic degrees of freedom causing a violation of supersymmetry. In particular, in DREG a vector boson carries $D - 2$ instead of 2 transverse degrees of freedom, while the fermionic degrees of freedom remain unaffected.

In general it is not necessary to employ a regularization prescription which preserves all symmetries of the theory. However, the procedure would then be as follows: After performing the regularization with an arbitrary method and cancelling the UV divergences with appropriate counterterms, additional finite counterterms have to be added in order to restore the Slavnov-Taylor identity of the theory. The general application of this concept to supersymmetric theories is described in detail in [80, 81].

While generally this approach is very cumbersome from a technical point of view, for practical calculations of physical one-loop amplitudes there exists a convenient procedure. Since DREG does not violate gauge invariance, no symmetry-restoring counterterms are needed for the renormalization of gauge couplings, also in supersymmetric theories. The on-shell masses are unambiguously fixed by the propagator pole position. Therefore the only possibly dangerous type of couplings in physical amplitudes are scalar-fermion-fermion and fermion-sfermion-gaugino Yukawa couplings as well as quartic scalar couplings. The finite supersymmetry-restoring counterterms that have to be added to these couplings when using DREG have been worked out at the one-loop level in [82].

A promising alternative is the method of dimensional reduction (DRED) [83, 84]. In contrast to DREG, within DRED the dimensions of the momentum integrals are compactified to $D < 4$ dimensions while the number of field components remains unchanged. As an effect, the regularized Lagrangian can be divided into a D-dimensional and an ϵ-dimensional part. The contributions from the latter are often referred to as "evanescent couplings" [85]. In non-supersymmetric theories this bears the problem that the evanescent couplings require a different renormalization as the couplings in the D-dimensional part [86]. Fortunately this is not the case for supersymmetric theories, where the evanescent couplings are linked to the normal couplings in order to preserve supersymmetry.

As a consequence, within DRED, no extra counterterms are needed besides those which cancel the UV divergences. This assertion is valid at least up to 1-loop order which is reflected by the fact that the supersymmetric Ward identity is satisfied within DRED at this order [84][2]. Therefore in this work, DRED is employed for the regularization of the loop integrals.

It should be noted, however, that in higher orders DRED may also cause symmetry violations in supersymmetric theories [87]. This is due to intrinsic ambiguities in the treatment of the antisymmetric Levi-Civita tensor [88].

[1] An exception are problems in connection with the axial anomaly.

[2] Strictly speaking, in Ref. [84] this has only been investigated for the Yang-Mills part and not for the complete MSSM. Nevertheless, up to the present day, no situation is known where DRED violates symmetries of the MSSM at 1-loop.

5.1.2 Renormalization of the gauge sector

In comparison to the Standard Model, the introduction of (unbroken) supersymmetry does not induce any new independent couplings. Consequently, the gauge sector of the MSSM can be renormalized in the same way as the Standard Model gauge sector. Here the conventions of Ref. [89] are adopted.

For the massive gauge bosons, counterterms are introduced according to

$$M_{\mathrm{W}}^2 \to M_{\mathrm{W}}^2 + \delta M_{\mathrm{W}}^2, \qquad M_{\mathrm{Z}}^2 \to M_{\mathrm{Z}}^2 + \delta M_{\mathrm{Z}}^2 \tag{5.1}$$

They are fixed by the condition that the gauge boson masses coincide with the poles of the propagators, i.e. the zeros of the transverse part of renormalized one-particle-irreducible two-point functions[3] $\hat{\Gamma}^{ab}_{\mathrm{T}}(k^2) = -i\big((k^2 - M_a^2)\delta_{ab} + \hat{\Sigma}^{ab}_{\mathrm{T}}(k^2)\big)$,

$$\Re e\, \hat{\Gamma}^{aa}_{\mathrm{T}}(M_a^2) = 0, \qquad a = \mathrm{W,Z}. \tag{5.2}$$

At one-loop order this leads to the following equations for the mass counterterms,

$$\delta M_{\mathrm{W}}^2 = \Re e\ \Sigma^{\mathrm{WW}}_{\mathrm{T}}(M_{\mathrm{W}}^2), \qquad \delta M_{\mathrm{Z}}^2 = \Re e\ \Sigma^{\mathrm{ZZ}}_{\mathrm{T}}(M_{\mathrm{Z}}^2). \tag{5.3}$$

Here $\Sigma(k^2)$ and $\hat{\Sigma}(k^2)$ denote the unrenormalized and renormalized self-energies, respectively. As apparent from (2.13), the gauge couplings g and g' can be expressed in terms of the electromagnetic coupling and the weak mixing angle. Consequently, their renormalization can be determined by the renormalization of the electromagnetic charge and the gauge boson masses as follows,

$$e \to (1 + \delta Z_e)e \qquad \delta Z_e = \frac{1}{2}\left.\frac{\partial \Sigma^{\gamma\gamma}_{\mathrm{T}}(k^2)}{\partial k^2}\right|_{k^2=0} - \frac{s_{\mathrm{W}}}{c_{\mathrm{W}}}\frac{\Sigma^{\gamma Z}_{\mathrm{T}}(0)}{M_{\mathrm{Z}}^2}, \tag{5.4}$$

$$s_{\mathrm{W}} \to s_{\mathrm{W}} + \delta s_W, \qquad \frac{\delta s_W}{s_{\mathrm{W}}} = \frac{c_{\mathrm{W}}^2}{2s_{\mathrm{W}}^2}\left[\frac{\delta M_{\mathrm{Z}}^2}{M_{\mathrm{Z}}^2} - \frac{\delta M_{\mathrm{W}}^2}{M_{\mathrm{W}}^2}\right]. \tag{5.5}$$

Furthermore, for the calculation of radiative corrections to $e^{\pm}e^{-}$ scattering processes, the field renormalizations of the incoming electrons and positron are needed,

$$e_{\mathrm{L}} \to (1 + \tfrac{1}{2}\delta Z^{e\mathrm{L}})\, e_{\mathrm{L}}, \qquad e_{\mathrm{R}} \to (1 + \tfrac{1}{2}\delta Z^{e\mathrm{R}})\, e_{\mathrm{R}}. \tag{5.6}$$

They are given by the condition that the residues of the renormalized propagators are normalized to unity,

$$\frac{\partial}{\partial \not{p}}\, \Re e\big\{\hat{\Gamma}^e(p)\big\}\ u_i(p), \Big|_{p^2=m_{\mathrm{e}}^2} = i\, u_i(p), \qquad \frac{\partial}{\partial \not{p}}\, \bar{u}_i(p)\ \Re e\big\{\hat{\Gamma}^e(p)\big\}\Big|_{p^2=m_{\mathrm{e}}^2} = i\, \bar{u}_i(p), \tag{5.7}$$

with the electron two-point function given by $\hat{\Gamma}^e(p) = i\big((\not{p} - m_{\mathrm{e}}) + \hat{\Sigma}^e(p)\big)$. Using the decomposition

$$\Sigma^e(p) \;=\; \not{p}\,\omega_{\mathrm{L}}\Sigma^{e\mathrm{L}}(p^2) \;+\; \not{p}\,\omega_{\mathrm{R}}\Sigma^{e\mathrm{R}}(p^2) + \Sigma^{e\mathrm{S}}(p^2) \tag{5.8}$$

[3] In the following the hat indicates renormalized quantities.

the field renormalization constants are given by

$$\delta Z^{e\mathrm{L}} = -\Re e\left\{\Sigma^{e\mathrm{L}}(m_\mathrm{e}^2) + m_\mathrm{e}^2\,\frac{\partial}{\partial p^2}\Big[\Sigma^{e\mathrm{L}}(p^2) + \Sigma^{e\mathrm{R}}(p^2) + 2/m_\mathrm{e}\,\Sigma^{e\mathrm{S}}(p^2)\Big]_{p^2=m_\mathrm{e}^2}\right\}, \tag{5.9}$$

$$\delta Z^{e\mathrm{R}} = -\Re e\left\{\Sigma^{e\mathrm{R}}(m_\mathrm{e}^2) + m_\mathrm{e}^2\,\frac{\partial}{\partial p^2}\Big[\Sigma^{e\mathrm{L}}(p^2) + \Sigma^{e\mathrm{R}}(p^2) + 2/m_\mathrm{e}\,\Sigma^{e\mathrm{S}}(p^2)\Big]_{p^2=m_\mathrm{e}^2}\right\}. \tag{5.10}$$

Apart from the QED corrections, the electron mass may be safely neglected, which considerably simplifies (5.9) and (5.10).

5.1.3 Renormalization of the sfermion sector

In this work only scalar leptons of the first two generations are considered as external particles, for which mixing can be neglected, as explained in section 2.2.3. As a consequence, the partners of the left- and right-handed leptons (L-/R-sleptons) can be renormalized independently. However, for completeness, in this section also the general case including mixing between L- and R-sfermions is discussed [90–92].

The tree-level Lagrangian for the bilinear sfermion terms reads

$$\mathcal{L}_{\tilde{\mathrm{f}}} = \left(\tilde{f}_\mathrm{L}^*,\ \ \tilde{f}_\mathrm{R}^*\right) k^2 \begin{pmatrix}\tilde{f}_\mathrm{L}\\ \tilde{f}_\mathrm{R}\end{pmatrix} - \left(\tilde{f}_\mathrm{L}^*,\ \ \tilde{f}_\mathrm{R}^*\right) M_{\tilde{\mathrm{f}}}^2 \begin{pmatrix}\tilde{f}_\mathrm{L}\\ \tilde{f}_\mathrm{R}\end{pmatrix}, \tag{5.11}$$

with k denoting the momentum of the sfermions and $M_{\tilde{\mathrm{f}}}$ given in (2.27). The mass matrix and the fields are renormalized according to

$$M_{\tilde{\mathrm{f}}}^2 \to M_{\tilde{\mathrm{f}}}^2 + \delta M_{\tilde{\mathrm{f}}}^2, \tag{5.12}$$

$$\begin{pmatrix}\tilde{f}_\mathrm{L}\\ \tilde{f}_\mathrm{R}\end{pmatrix} \to \left(1 + \tfrac{1}{2}\delta Z^{\tilde{\mathrm{f}}}\right)\begin{pmatrix}\tilde{f}_\mathrm{L}\\ \tilde{f}_\mathrm{R}\end{pmatrix}, \tag{5.13}$$

where the mass counterterm $\delta M_{\tilde{\mathrm{f}}}$ is defined in terms of the fundamental parameters of the mass matrix,

$$\delta M_{\tilde{\mathrm{f}}}^2 = \begin{pmatrix}\delta m_\mathrm{f}^2 + \delta m_{\tilde{\mathrm{f}}_\mathrm{L}}^2 + \delta\big(M_\mathrm{Z}^2\cos 2\beta\ (I_\mathrm{f}^3 - Q_\mathrm{f} s_\mathrm{W}^2)\big) & \delta\big[m_\mathrm{f}\big(A_\mathrm{f} - \mu(\cot\beta)^{2I_\mathrm{f}^3}\big)\big]\\ \delta\big[m_\mathrm{f}\big(A_\mathrm{f} - \mu(\cot\beta)^{2I_\mathrm{f}^3}\big)\big] & \delta m_\mathrm{f}^2 + \delta m_{\tilde{\mathrm{f}}_\mathrm{R}}^2 + \delta\big(M_\mathrm{Z}^2\cos 2\beta\ Q_\mathrm{f} s_\mathrm{W}^2\big)\end{pmatrix}, \tag{5.14}$$

and field renormalization constants are diagonal,

$$\delta Z^{\tilde{\mathrm{f}}} = \begin{pmatrix}\delta Z_\mathrm{L}^{\tilde{\mathrm{f}}} & 0\\ 0 & \delta Z_\mathrm{R}^{\tilde{\mathrm{f}}}\end{pmatrix}. \tag{5.15}$$

This choice is sufficient for the cancellation of UV-divergences [80] and compatible with the most general ansatz when in addition a renormalized mixing matrix is properly defined. To start with, the interaction eigenstates $\tilde{f}_\mathrm{L}, \tilde{f}_\mathrm{R}$ are related to the mass eigenstates $\tilde{f}_1, \tilde{f}_2$ by an arbitrary complex mixing matrix $R_{\tilde{\mathrm{f}}}$,

$$\begin{pmatrix}\tilde{f}_1\\ \tilde{f}_2\end{pmatrix} = R_{\tilde{\mathrm{f}}}\begin{pmatrix}\tilde{f}_\mathrm{L}\\ \tilde{f}_\mathrm{R}\end{pmatrix}. \tag{5.16}$$

Following [92], it can be written as

$$R_{\tilde{\mathrm{f}}} = \left(1 + \tfrac{1}{2}\delta Z^{U_{\tilde{\mathrm{f}}}}\right) U_{\tilde{\mathrm{f}}}, \tag{5.17}$$

where the tree-level mixing matrix $U_{\tilde{\mathrm{f}}}$ can be taken unitary. Note that the correction term $\delta Z^{U_{\tilde{\mathrm{f}}}}$ is finite since all divergences are already absorbed by the counterterms in (5.12), (5.13).

Since the constants $\delta Z^{\tilde{\mathrm{f}}}, \delta Z^{U_{\tilde{\mathrm{f}}}}$ only appear in a specific combination in the transformations of the fields, they can be combined into one renormalization constant $\delta\tilde{Z}^{\tilde{\mathrm{f}}}$:

$$\begin{aligned}\begin{pmatrix}\tilde{f}_{\mathrm{L}}\\ \tilde{f}_{\mathrm{R}}\end{pmatrix} \to \left(1 + \tfrac{1}{2}\delta Z^{\tilde{\mathrm{f}}}\right) R_{\tilde{\mathrm{f}}}^{-1} \begin{pmatrix}\tilde{f}_1\\ \tilde{f}_2\end{pmatrix} &= U_{\tilde{\mathrm{f}}}^{\dagger}\left[1 + \tfrac{1}{2}U_{\tilde{\mathrm{f}}}\left(\delta Z^{\tilde{\mathrm{f}}} U_{\tilde{\mathrm{f}}}^{\dagger} - U_{\tilde{\mathrm{f}}}^{\dagger}\delta Z^{U_{\tilde{\mathrm{f}}}}\right)\right]\begin{pmatrix}\tilde{f}_1\\ \tilde{f}_2\end{pmatrix}\\ &\equiv U_{\tilde{\mathrm{f}}}^{\dagger}\left[1 + \tfrac{1}{2}\delta\tilde{Z}^{\tilde{\mathrm{f}}}\right]\begin{pmatrix}\tilde{f}_1\\ \tilde{f}_2\end{pmatrix}\end{aligned} \tag{5.18}$$

with

$$\delta\tilde{Z}^{\tilde{\mathrm{f}}} = U_{\tilde{\mathrm{f}}}\delta Z^{\tilde{\mathrm{f}}} U_{\tilde{\mathrm{f}}}^{\dagger} - \delta Z^{U_{\tilde{\mathrm{f}}}}. \tag{5.19}$$

With these definitions the renormalized Lagrangian reads

$$\begin{aligned}&\mathcal{L}_{\tilde{\mathrm{f}}} \to \mathcal{L}_{\tilde{\mathrm{f}}} + \delta\mathcal{L}_{\tilde{\mathrm{f}}},\\ &\mathcal{L}_{\tilde{\mathrm{f}}} = \left(\tilde{f}_1^*,\, \tilde{f}_2^*\right)\left[k^2 - U_{\tilde{\mathrm{f}}} M_{\tilde{\mathrm{f}}}^2 U_{\tilde{\mathrm{f}}}^{\dagger}\right]\begin{pmatrix}\tilde{f}_1\\ \tilde{f}_2\end{pmatrix},\\ &\delta\mathcal{L}_{\tilde{\mathrm{f}}} = \left(\tilde{f}_1^*,\, \tilde{f}_2^*\right)\left[\frac{k^2}{2}\left(\delta\tilde{Z}^{\tilde{\mathrm{f}}\dagger} + \delta\tilde{Z}^{\tilde{\mathrm{f}}}\right) - \frac{1}{2}\left(\delta\tilde{Z}^{\tilde{\mathrm{f}}\dagger} U_{\tilde{\mathrm{f}}} M_{\tilde{\mathrm{f}}}^2 U_{\tilde{\mathrm{f}}}^{\dagger} + U_{\tilde{\mathrm{f}}} M_{\tilde{\mathrm{f}}}^2 U_{\tilde{\mathrm{f}}}^{\dagger}\delta\tilde{Z}^{\tilde{\mathrm{f}}}\right) - U_{\tilde{\mathrm{f}}}\,\delta M_{\tilde{\mathrm{f}}}^2\, U_{\tilde{\mathrm{f}}}^{\dagger}\right]\begin{pmatrix}\tilde{f}_1\\ \tilde{f}_2\end{pmatrix}.\end{aligned} \tag{5.20}$$

By exploiting the tree-level relation for the mass matrix diagonalization

$$U_{\tilde{\mathrm{f}}} M_{\tilde{\mathrm{f}}}^2 U_{\tilde{\mathrm{f}}}^{\dagger} = M_{\tilde{\mathrm{f}}}^{\mathrm{D}} \equiv \begin{pmatrix} m_{\tilde{\mathrm{f}}1}^2 & 0\\ 0 & m_{\tilde{\mathrm{f}}2}^2\end{pmatrix} \tag{5.21}$$

the renormalized self-energy for the sfermions $\tilde{f}_i$ and $\tilde{f}_j$ takes on the form

$$\hat{\Sigma}_{ij}^{\tilde{\mathrm{f}}}(k^2) = \Sigma_{ij}^{\tilde{\mathrm{f}}}(k^2) + \frac{k^2}{2}\left(\delta\tilde{Z}_{ji}^{\tilde{\mathrm{f}}\,*} + \delta\tilde{Z}_{ij}^{\tilde{\mathrm{f}}}\right) - \frac{1}{2}\left(m_{\tilde{\mathrm{f}}j}^2\,\delta\tilde{Z}_{ji}^{\tilde{\mathrm{f}}\,*} + m_{\tilde{\mathrm{f}}i}^2\,\delta\tilde{Z}_{ij}^{\tilde{\mathrm{f}}}\right) - (U_{\tilde{\mathrm{f}}}\,\delta M_{\tilde{\mathrm{f}}}^2\, U_{\tilde{\mathrm{f}}}^{\dagger})_{ij}. \tag{5.22}$$

Now, on-shell renormalization conditions are imposed for the sfermions. They define the mass eigenvalues as the poles of the propagators. In addition, it can be demanded that the matrix of the renormalized two-point vertex functions $\hat{\Gamma}_{ij}^{\tilde{\mathrm{f}}}(k^2) = i\left((k^2 - m_{\tilde{\mathrm{f}}i}^2)\delta_{ij} + \hat{\Sigma}_{ij}^{\tilde{\mathrm{f}}}(k^2)\right)$ is diagonal for on-shell external momenta. This leads to the following conditions,

$$\Re e\,\hat{\Gamma}_{ij}^{\tilde{\mathrm{f}}}(m_{\tilde{\mathrm{f}}i}^2) = 0, \qquad \Re e\,\hat{\Gamma}_{ij}^{\tilde{\mathrm{f}}}(m_{\tilde{\mathrm{f}}j}^2) = 0, \qquad (i,j = 1,2). \tag{5.23}$$

Furthermore, the normalization of the physical fields is fixed by the condition that the residues of the renormalized propagators are unity,

$$\frac{\partial}{\partial k^2}\Re e\,\hat{\Gamma}_{ii}^{\tilde{\mathrm{f}}}(k^2)\bigg|_{k^2 = m_{\tilde{\mathrm{f}}i}^2} = i, \qquad (i = 1,2). \tag{5.24}$$

From the requirement that the Lagrangian is hermitian and invariant under the CPT transformation, one obtains the relation

$$\hat{\Gamma}^{\tilde{\mathrm{f}}}_{ij}(k^2) = -\,\hat{\Gamma}^{\tilde{\mathrm{f}}\ *}_{ji}(k^2), \tag{5.25}$$

so that the two conditions in (5.23) are equivalent. It may be illustrative to note that the tree-level mass matrix diagonalization (5.21) and the unitarity of the tree-level mixing matrix $U_{\tilde{\mathrm{f}}}$ can also be derived from the above renormalization conditions.

At one-loop level the renormalization conditions yield

$$(U_{\tilde{\mathrm{f}}}\,\delta M^2_{\tilde{\mathrm{f}}}\,U^\dagger_{\tilde{\mathrm{f}}})_{ii} = \Re e\,\Sigma^{\tilde{\mathrm{f}}}_{ii}(m^2_{\tilde{\mathrm{f}}_i}), \tag{5.26}$$

$$\delta\tilde{Z}^{\tilde{\mathrm{f}}}_{ii} = -\Re e\,\frac{\partial\Sigma^{\tilde{\mathrm{f}}}_{ii}(k^2)}{\partial k^2}\bigg|_{k^2=m^2_{\tilde{\mathrm{f}}_i}}, \tag{5.27}$$

$$\delta\tilde{Z}^{\tilde{\mathrm{f}}}_{ij} = \frac{2}{m^2_{\tilde{\mathrm{f}}_i} - m^2_{\tilde{\mathrm{f}}_j}}\left[\Re e\,\Sigma^{\tilde{\mathrm{f}}}_{ij}(m^2_{\tilde{\mathrm{f}}_j}) - (U_{\tilde{\mathrm{f}}}\,\delta M^2_{\tilde{\mathrm{f}}}\,U^\dagger_{\tilde{\mathrm{f}}})_{ij}\right] \quad \text{for } i \neq j. \tag{5.28}$$

Here it has been assumed that the sfermion mass matrix is free of CP-violating phases, so that the counterterms $(U_{\tilde{\mathrm{f}}}\,\delta M^2_{\tilde{\mathrm{f}}}\,U^\dagger_{\tilde{\mathrm{f}}})$ and $\delta\tilde{Z}^{\tilde{\mathrm{f}}}$ are real. In the case of CP-violation, the renormalization conditions (5.23), (5.24) only fix the real part of the field renormalization constants $\delta\tilde{Z}^{\tilde{\mathrm{f}}}_{ij}$.

Using (5.26), two parameter counterterms of the sfermion mass matrix (5.14), for example $\delta m^2_{\tilde{\mathrm{f}}_\mathrm{L}}$ and $\delta m^2_{\tilde{\mathrm{f}}_\mathrm{R}}$, can be determined in terms of the two mass eigenvalues $m_{\tilde{\mathrm{f}}1}, m_{\tilde{\mathrm{f}}2}$. The remaining counterterms in (5.14), e.g. the counterterms to the trilinear couplings A_f, cannot be fixed with the conditions (5.23), (5.24). They have to be defined via additional observable processes, such as decays of heavy Higgs bosons into sfermions or gauge coupling asymmetries of sfermions. Considering the renormalization of a whole squark generation, there are four independent mass eigenvalues, which can be used to determine the counterterms to $m^2_{\tilde{\mathrm{q}}_\mathrm{L}}, m^2_{\tilde{\mathrm{u}}_\mathrm{R}}, m^2_{\tilde{\mathrm{d}}_\mathrm{R}}$ and one of the trilinear couplings. For the case of the sleptons, the situation is somewhat similar, but upon neglect of R-sneutrinos in the MSSM, there are only three mass eigenvalues within one mass generation, which can be used to fix the counterterms for $m^2_{\tilde{\mathrm{l}}_\mathrm{L}}, m^2_{\tilde{\mathrm{e}}_\mathrm{R}}$ and the trilinear coupling A_e.

In this connection it is understood that the renormalization of the remaining parameters in the mass counterterm (5.14) is performed in other sectors. The Z-boson mass M_Z and the weak mixing angle s_W are specified within the gauge boson sector. The renormalization of $\tan\beta$ and μ is conveniently achieved in the Higgs and higgsino sector, respectively, and will be described in the following sections.

Now the special case of vanishing mixing within one slepton generation shall be discussed. In this case the off-diagonal entries of the field renormalization constants $\delta\tilde{Z}^{\tilde{\mathrm{f}}}_{ij}$ in (5.28) trivially become zero. The combination in (5.19) then simplifies to $\delta\tilde{Z}^{\tilde{\mathrm{f}}} = \delta Z^{\tilde{\mathrm{f}}}$. From (5.26), (5.27), one obtains for $i = \mathrm{L,R}$:

$$(\delta M^2_{\tilde{\mathrm{f}}})_{ii} = \Re e\,\Sigma^{\tilde{\mathrm{f}}}_{ii}(m^2_{\tilde{\mathrm{f}}_i}), \tag{5.29}$$

$$\delta Z^{\tilde{\mathrm{f}}}_{ii} = -\Re e\,\frac{\partial\Sigma^{\tilde{\mathrm{f}}}_{ii}(k^2)}{\partial k^2}\bigg|_{k^2=m^2_{\tilde{\mathrm{f}}_i}}. \tag{5.30}$$

With the condition (5.29), it is possible to determine the counterterms to the parameters $m^2_{\tilde{l}_L}, m^2_{\tilde{e}_R}$ in terms of the mass eigenvalues $m_{\tilde{l}1}, m_{\tilde{l}2}$. Since both the mass of the L-slepton and the sneutrino within one generation depend on the supersymmetry breaking parameter $m^2_{\tilde{l}_L}$, one can only use one of the two masses, say the L-slepton mass, as independent input. The mass of the sneutrino can then be calculated as a function of the L-slepton mass, including the corresponding one-loop corrections. However, this is not an issue for this thesis, since sneutrinos only appear inside the loops for slepton pair production processes.

5.1.4 Renormalization of the charginos and neutralinos

The mass spectrum of the two chargino and four neutralino eigenstates depends on only two supersymmetry breaking parameters M_1, M_2 and on the superpotential parameter μ. Here it is assumed that $\tan\beta$ is already defined in the Higgs sector, as will be described in the next section. As a consequence, when taking three of the six mass eigenvalues as given input parameters, the other three masses are determined as a function of the first three masses. This relation between the masses receives corrections from higher orders [93–95]. Because of this close connection between charginos and neutralinos, in this section the renormalization for both is discussed, although only the renormalization of the neutralinos is required for the loop corrections to selectron production.

The different renormalization prescriptions for charginos and neutralinos in [93–95] are in accordance with each other in predictions for relations between physical quantities at the one-loop level. For Refs. [93] and [95] this can easily be checked by direct computation. While in principle the renormalization scheme proposed in Ref. [94] is equivalent to [93,95], it leads to substantial differences in practical calculations. Following the formalism of Ref. [96], the mass matrix counterterms in [94] are required to be diagonal in the mass eigenstate basis. This additional condition results in finite shifts between the radiatively corrected values for the fundamental parameters M_1, M_2 and μ in [94] and [93, 95], thus making a direct comparison difficult. For technical reasons, here the formalism of [95] is adopted.

Starting from the chargino Lagrangian

$$\mathcal{L}_{\text{ch}} = i\big[\psi^{-\top}\sigma^\mu\partial_\mu\,\overline{\psi^-} + \overline{\psi^+}^{\top}\bar\sigma^\mu\partial_\mu\,\psi^+\big] - \big[\psi^{-\top}X\,\psi^+ + \overline{\psi^+}^{\top}X^\dagger\,\overline{\psi^-}\big], \tag{5.31}$$

where

$$\psi^+ \equiv \begin{pmatrix}\psi_1^+\\ \psi_2^+\end{pmatrix} = \begin{pmatrix}\widetilde{W}^+\\ \widetilde{H}_{\text{u}}^+\end{pmatrix}, \qquad \psi^- \equiv \begin{pmatrix}\psi_1^-\\ \psi_2^-\end{pmatrix} = \begin{pmatrix}\widetilde{W}^-\\ \widetilde{H}_{\text{d}}^-\end{pmatrix} \tag{5.32}$$

are the chargino interaction eigenstates and X is given in (2.30), the following renormalization constants are introduced,

$$X \to X + \delta X, \tag{5.33}$$

$$\psi^+ \to \big(1 + \tfrac{1}{2}\delta Z^{\text{L}}\big)\,\psi^+,$$

$$\psi^- \to \big(1 + \tfrac{1}{2}\delta Z^{\text{R}}\big)\,\psi^-. \tag{5.34}$$

As before, the mass matrix counterterm δX is constructed from the counterterms of the parameters in X,

$$\delta X = \begin{pmatrix} \delta M_2 & \sqrt{2}\,\delta\,(M_\mathrm{W}\sin\beta) \\ \sqrt{2}\,\delta\,(M_\mathrm{W}\cos\beta) & \delta\mu \end{pmatrix}, \tag{5.35}$$

and the field renormalization constants $\delta Z^\mathrm{L}, \delta Z^\mathrm{R}$ are diagonal. In addition, finite correction terms to the mixing matrices are introduced,

$$\begin{aligned} \chi^+ &= R_\mathrm{L}\,\psi^+, & R_\mathrm{L} &= \left(1+\tfrac{1}{2}\delta Z^V\right) V, \\ \chi^- &= R_\mathrm{R}\,\psi^-, & R_\mathrm{R} &= \left(1+\tfrac{1}{2}\delta Z^U\right) U, \end{aligned} \tag{5.36}$$

with $\chi^\pm$ denoting the mass eigenstates and U, V the unitary tree-level matrices from (2.31). $\delta Z^U, \delta Z^V$ are arbitrary 2×2 matrices. The transformation of the fields can then be written as

$$\begin{aligned} \psi^+ &\to \left(1+\tfrac{1}{2}\delta Z^\mathrm{L}\right) V^\dagger \left(1-\tfrac{1}{2}\delta Z^V\right)\chi^+ \equiv V^\dagger\left(1+\tfrac{1}{2}\delta\tilde{Z}^\mathrm{L}\right)\chi^+, \\ \psi^- &\to \left(1+\tfrac{1}{2}\delta Z^\mathrm{R}\right) U^\dagger \left(1-\tfrac{1}{2}\delta Z^U\right)\chi^- \equiv U^\dagger\left(1+\tfrac{1}{2}\delta\tilde{Z}^\mathrm{R}\right)\chi^-, \end{aligned} \tag{5.37}$$

where

$$\delta\tilde{Z}^\mathrm{L} = V\delta Z^\mathrm{L} V^\dagger - \delta Z^V, \qquad \delta\tilde{Z}^\mathrm{R} = U\delta Z^\mathrm{R} U^\dagger - \delta Z^U \tag{5.38}$$

have been introduced as shorthand notation. These transformations yield for the Lagrangian, after a Fourier transformation,

$$\begin{aligned} \mathcal{L}_\mathrm{ch} &\to \mathcal{L}_\mathrm{ch} + \delta\mathcal{L}_\mathrm{ch}, \\ \mathcal{L}_\mathrm{ch} &= \left(\overline{\tilde{\chi}_1^+},\ \overline{\tilde{\chi}_2^+}\right)\left[\not{p} - U^* X V^\dagger\,\omega_\mathrm{L} - V X^\dagger U^\top \omega_\mathrm{R}\right]\begin{pmatrix}\tilde{\chi}_1^+\\ \tilde{\chi}_2^+\end{pmatrix}, \end{aligned} \tag{5.39}$$

$$\begin{aligned} \delta\mathcal{L}_\mathrm{ch} = \left(\overline{\tilde{\chi}_1^+},\ \overline{\tilde{\chi}_2^+}\right)\Bigg[&\frac{\not{p}}{2}\left(\delta\tilde{Z}^{\mathrm{L}\dagger} + \delta\tilde{Z}^\mathrm{L}\right)\omega_\mathrm{L} + \frac{\not{p}}{2}\left(\delta\tilde{Z}^{\mathrm{R}*} + \delta\tilde{Z}^{\mathrm{R}\top}\right)\omega_\mathrm{R} \\ &- \left(\tfrac{1}{2}\delta\tilde{Z}^{\mathrm{R}\top} U^* X V^\dagger + \tfrac{1}{2} U^* X V^\dagger \delta\tilde{Z}^\mathrm{L} + U^*\delta X V^\dagger\right)\omega_\mathrm{L} \\ &- \left(\tfrac{1}{2}\delta\tilde{Z}^{\mathrm{L}\dagger} V X^\dagger U^\top + \tfrac{1}{2} V X^\dagger U^\top \delta\tilde{Z}^{\mathrm{R}*} + V\delta X^\dagger U^\top\right)\omega_\mathrm{R}\Bigg]\begin{pmatrix}\tilde{\chi}_1^+\\ \tilde{\chi}_2^+\end{pmatrix}, \end{aligned} \tag{5.40}$$

where the 4-component Dirac spinors specified in (2.32) and the projectors $\omega_{\mathrm{L,R}} = \frac{1}{2}(1\mp\gamma_5)$ have been used. With the help of the tree-level relation (2.31), the renormalized self-energies with respect to the fields $\overline{\tilde{\chi}_i^+}$ and $\tilde{\chi}_j^+$ can be cast into the form

$$\hat{\Sigma}_{ij}^\pm(p) = \not{p}\,\omega_\mathrm{L}\hat{\Sigma}_{ij}^{\pm\mathrm{L}}(p^2) + \not{p}\,\omega_\mathrm{R}\hat{\Sigma}_{ij}^{\pm\mathrm{R}}(p^2) + \omega_\mathrm{L}\hat{\Sigma}_{ij}^{\pm\mathrm{SL}}(p^2) + \omega_\mathrm{R}\hat{\Sigma}_{ij}^{\pm\mathrm{SR}}(p^2), \tag{5.41}$$

$$\hat{\Sigma}_{ij}^{\pm\mathrm{L}}(p^2) = \Sigma_{ij}^{\pm\mathrm{L}}(p^2) + \tfrac{1}{2}\left(\delta\tilde{Z}_{ij}^\mathrm{L} + \delta\tilde{Z}_{ji}^{\mathrm{L}*}\right), \tag{5.42}$$

$$\hat{\Sigma}_{ij}^{\pm\mathrm{R}}(p^2) = \Sigma_{ij}^{\pm\mathrm{R}}(p^2) + \tfrac{1}{2}\left(\delta\tilde{Z}_{ij}^{\mathrm{R}*} + \delta\tilde{Z}_{ji}^\mathrm{R}\right), \tag{5.43}$$

$$\hat{\Sigma}_{ij}^{\pm\mathrm{SL}}(p^2) = \Sigma_{ij}^{\pm\mathrm{SL}}(p^2) - \tfrac{1}{2}\left(m_{\tilde{\chi}_i^\pm}\delta\tilde{Z}_{ij}^\mathrm{L} + m_{\tilde{\chi}_j^\pm}\delta\tilde{Z}_{ji}^\mathrm{R}\right) - (U^*\delta X V^\dagger)_{ij}, \tag{5.44}$$

$$\hat{\Sigma}_{ij}^{\pm\mathrm{SR}}(p^2) = \Sigma_{ij}^{\pm\mathrm{SR}}(p^2) - \tfrac{1}{2}\left(m_{\tilde{\chi}_i^\pm}\delta\tilde{Z}_{ij}^{\mathrm{R}*} + m_{\tilde{\chi}_j^\pm}\delta\tilde{Z}_{ji}^{\mathrm{L}*}\right) - (V\delta X^\dagger U^\top)_{ij}. \tag{5.45}$$

The bilinear part of the neutralino Lagrangian reads

$$\mathcal{L}_{\rm n} = \frac{i}{2}\big[{\psi^0}^\top \sigma^\mu \partial_\mu \overline{\psi^0} + \overline{\psi^0}^\top \bar{\sigma}^\mu \partial_\mu \psi^0\big] - \frac{1}{2}\big[{\psi^0}^\top Y\, \psi^0 + \overline{\psi^0}^\top Y^\dagger\, \overline{\psi^0}\big], \tag{5.46}$$

with ψ^0 and Y given in (2.33) and (2.34), respectively. In analogy to the chargino case, the mass matrix Y and the fields are renormalized according to

$$Y \to Y + \delta Y, \tag{5.47}$$
$$\psi^0 \to \big(1 + \tfrac{1}{2}\delta Z^0\big)\, \psi^0, \tag{5.48}$$

Furthermore, a finite one-loop correction to the mixing is introduced,

$$\chi^0 = R_0\, \psi^0, \qquad R_0 = \big(1 + \tfrac{1}{2}\delta Z^N\big)\, N, \tag{5.49}$$

where χ^0 denotes the mass eigenstates and N is the unitary tree-level matrix from (2.35), whereas δZ^N is an arbitrary 4×4 matrix. The renormalization and redefinition of the fields then results in

$$\psi^0 \to N^\dagger \left(1 + \tfrac{1}{2}\delta \tilde{Z}^0\right) \chi^0, \qquad \text{with} \qquad \delta \tilde{Z}^0 = N \delta Z^0 N^\dagger - \delta Z^N. \tag{5.50}$$

Using the renormalization transformation and the 4-component Majorana spinors from (2.36), the Lagrangian reads

$$\begin{aligned}
&\mathcal{L}_{\rm n} \to \mathcal{L}_{\rm n} + \delta\mathcal{L}_{\rm n}, \\
&\mathcal{L}_{\rm n} = \frac{1}{2}\left(\overline{\tilde{\chi}^0_1},\ \overline{\tilde{\chi}^0_2}\right)\left[\not{p} - N^* Y N^\dagger\, \omega_{\rm L} - N Y^\dagger N^\top \omega_{\rm R}\right]\begin{pmatrix}\tilde{\chi}^0_1 \\ \tilde{\chi}^0_2\end{pmatrix}, \qquad (5.51) \\
&\delta\mathcal{L}_{\rm n} = \frac{1}{2}\left(\overline{\tilde{\chi}^0_1},\ \overline{\tilde{\chi}^0_2}\right)\Big[\frac{\not{p}}{2}\big(\delta\tilde{Z}^{0\dagger} + \delta\tilde{Z}^0\big)\,\omega_{\rm L} + \frac{\not{p}}{2}\big(\delta\tilde{Z}^{0*} + \delta\tilde{Z}^{0\top}\big)\,\omega_{\rm R} \\
&\qquad - \big(\tfrac{1}{2}\delta\tilde{Z}^{0\top} N^* Y N^\dagger + \tfrac{1}{2} N^* Y N^\dagger \delta\tilde{Z}^0 + N^* \delta Y N^\dagger\big)\,\omega_{\rm L} \qquad (5.52) \\
&\qquad - \big(\tfrac{1}{2}\delta\tilde{Z}^{0\dagger} N Y^\dagger N^\top + \tfrac{1}{2} N Y^\dagger N^\top \delta\tilde{Z}^{0*} + N \delta Y^\dagger N^\top\big)\,\omega_{\rm R}\Big]\begin{pmatrix}\tilde{\chi}^0_1 \\ \tilde{\chi}^0_2\end{pmatrix}.
\end{aligned}$$

From this one obtains the following expressions for the Lorentz decomposition of the renormalized self-energies, where the tree-level relation (2.35) has been used:

$$\hat{\Sigma}^0_{ij}(p) = \not{p}\omega_{\rm L}\hat{\Sigma}^{0{\rm L}}_{ij}(p^2) + \not{p}\omega_{\rm R}\hat{\Sigma}^{0{\rm R}}_{ij}(p^2) + \omega_{\rm L}\hat{\Sigma}^{0{\rm SL}}_{ij}(p^2) + \omega_{\rm R}\hat{\Sigma}^{0{\rm SR}}_{ij}(p^2), \tag{5.53}$$
$$\hat{\Sigma}^{0{\rm L}}_{ij}(p^2) = \Sigma^{0{\rm L}}_{ij}(p^2) + \tfrac{1}{2}\big(\delta\tilde{Z}^0_{ij} + \delta\tilde{Z}^{0\,*}_{ji}\big), \tag{5.54}$$
$$\hat{\Sigma}^{0{\rm R}}_{ij}(p^2) = \Sigma^{0{\rm R}}_{ij}(p^2) + \tfrac{1}{2}\big(\delta\tilde{Z}^{0\,*}_{ij} + \delta\tilde{Z}^0_{ji}\big), \tag{5.55}$$
$$\hat{\Sigma}^{0{\rm SL}}_{ij}(p^2) = \Sigma^{0{\rm SL}}_{ij}(p^2) - \tfrac{1}{2}\big(m_{\tilde{\chi}^0_i}\delta\tilde{Z}^0_{ij} + m_{\tilde{\chi}^0_j}\delta\tilde{Z}^0_{ji}\big) - (N^*\delta Y N^\dagger)_{ij}, \tag{5.56}$$
$$\hat{\Sigma}^{0{\rm SR}}_{ij}(p^2) = \Sigma^{0{\rm SR}}_{ij}(p^2) - \tfrac{1}{2}\big(m_{\tilde{\chi}^0_i}\delta\tilde{Z}^{0\,*}_{ij} + m_{\tilde{\chi}^0_j}\delta\tilde{Z}^{0\,*}_{ji}\big) - (N\delta Y^\dagger N^\top)_{ij}. \tag{5.57}$$

The above expressions for the chargino and neutralino self-energies can be simplified by considering the CPT invariance and hermiticity of the Lagrangian and the Majorana

nature of the neutralinos, yielding the relations

$$\hat{\Sigma}^{\pm\mathrm{L}}_{ij}(p^2) = \hat{\Sigma}^{\pm\mathrm{L}^*}_{ji}(p^2), \qquad \hat{\Sigma}^{\pm\mathrm{R}}_{ij}(p^2) = \hat{\Sigma}^{\pm\mathrm{R}^*}_{ji}(p^2), \qquad \hat{\Sigma}^{\pm\mathrm{SL}}_{ij}(p^2) = \hat{\Sigma}^{\pm\mathrm{SR}^*}_{ji}(p^2), \tag{5.58}$$

$$\hat{\Sigma}^{0\mathrm{L}}_{ij}(p^2) = \hat{\Sigma}^{0\mathrm{L}^*}_{ji}(p^2), \qquad \hat{\Sigma}^{0\mathrm{R}}_{ij}(p^2) = \hat{\Sigma}^{0\mathrm{R}^*}_{ji}(p^2), \qquad \hat{\Sigma}^{0\mathrm{SL}}_{ij}(p^2) = \hat{\Sigma}^{0\mathrm{SR}^*}_{ji}(p^2), \tag{5.59}$$

$$\hat{\Sigma}^{0\mathrm{L}}_{ij}(p^2) = \hat{\Sigma}^{0\mathrm{R}}_{ji}(p^2), \qquad \hat{\Sigma}^{0\mathrm{SL}}_{ij}(p^2) = \hat{\Sigma}^{0\mathrm{SL}}_{ji}(p^2), \qquad \hat{\Sigma}^{0\mathrm{SR}}_{ij}(p^2) = \hat{\Sigma}^{0\mathrm{SR}}_{ji}(p^2). \tag{5.60}$$

In order to fix the renormalization constants for the charginos and neutralinos, the following on-shell renormalization conditions are imposed, which are similar to the sfermion case. The mass eigenvalues are defined as the poles of the propagators, while in addition it is required that the matrix of the renormalized two-point vertex functions $\hat{\Gamma}^t_{ij}(p) = i\big((\not{p} - m_{\tilde{\chi}^t_i})\delta_{ij} + \hat{\Sigma}^t_{ij}(p)\big)$ becomes diagonal for on-shell external momenta. The residues of the on-shell propagators are normalized to unity. The corresponding conditions read ($t = 0, \pm$ for neutralinos and charginos, respectively)

$$\Re e\big\{\hat{\Gamma}^t_{ij}(p)\big\}\; u_j(p)\Big|_{p^2=m^2_{\tilde{\chi}^t_j}} = 0, \qquad \bar{u}_i(p)\; \Re e\big\{\hat{\Gamma}^t_{ij}(p)\big\}\Big|_{p^2=m^2_{\tilde{\chi}^t_i}} = 0, \tag{5.61}$$

$$\frac{\partial}{\partial \not{p}}\, \Re e\big\{\hat{\Gamma}^t_{ii}(p)\big\}\; u_i(p)\Big|_{p^2=m^2_{\tilde{\chi}^t_i}} = i\, u_i(p), \qquad \frac{\partial}{\partial \not{p}}\, \bar{u}_i(p)\; \Re e\big\{\hat{\Gamma}^t_{ii}(p)\big\}\Big|_{p^2=m^2_{\tilde{\chi}^t_i}} = i\, \bar{u}_i(p). \tag{5.62}$$

From these renormalization conditions one can derive explicit expressions for the counterterms to the MSSM parameters M_1, M_2 and μ [95]. They can be fixed by the on-shell renormalization of three chargino or neutralino masses, for which here the two charginos and the lightest neutralino have been chosen. The following formulae are valid for the special case of CP conservation, i.e. when all parameters can be taken real:

$$\begin{aligned}\delta M_2 = \frac{1}{\mu^2 - M_2^2}\Big[&(m_{\tilde{\chi}^\pm_2}\mu - m_{\tilde{\chi}^\pm_1} M_2)\; \delta m_{\tilde{\chi}^\pm_1} + (m_{\tilde{\chi}^\pm_1}\mu - m_{\tilde{\chi}^\pm_2} M_2)\; \delta m_{\tilde{\chi}^\pm_2} \\ &+ M_2\; \delta M^2_{\mathrm{W}} + \mu\; \delta\big(M^2_{\mathrm{W}} \sin 2\beta\big)\Big],\end{aligned} \tag{5.63}$$

$$\begin{aligned}\delta \mu = \frac{1}{M_2^2 - \mu^2}\Big[&(m_{\tilde{\chi}^\pm_2} M_2 - m_{\tilde{\chi}^\pm_1}\mu)\; \delta m_{\tilde{\chi}^\pm_1} + (m_{\tilde{\chi}^\pm_1} M_2 - m_{\tilde{\chi}^\pm_2}\mu)\; \delta m_{\tilde{\chi}^\pm_2} \\ &+ \mu\; \delta M^2_{\mathrm{W}} + M_2\; \delta\big(M^2_{\mathrm{W}} \sin 2\beta\big)\Big],\end{aligned} \tag{5.64}$$

$$\text{with} \quad \delta m_{\tilde{\chi}^\pm_k} = \frac{1}{2}\,\Re e\big\{m_{\tilde{\chi}^\pm_k}\Sigma^{\pm\mathrm{L}}_{kk}(m^2_{\tilde{\chi}^\pm_k}) + m_{\tilde{\chi}^\pm_k}\Sigma^{\pm\mathrm{R}}_{kk}(m^2_{\tilde{\chi}^\pm_k}) + 2\,\Sigma^{\pm\mathrm{SL}}_{kk}(m^2_{\tilde{\chi}^\pm_k})\big\},$$

$$\begin{aligned}\delta M_1 = \frac{1}{N_{11}^2}\Big[&\Re e\big\{m_{\tilde{\chi}^0_1}\Sigma^{0\mathrm{L}}_{11}(m^2_{\tilde{\chi}^0_1}) + \Sigma^{0\mathrm{SL}}_{11}(m^2_{\tilde{\chi}^0_1})\big\} - N_{12}^2\,\delta M_2 + 2N_{13}N_{14}\,\delta\mu \\ &+ 2N_{11}\big[N_{13}\;\delta\big(M_{\mathrm{Z}} s_{\mathrm{W}} \cos\beta\big) - N_{14}\;\delta\big(M_{\mathrm{Z}} s_{\mathrm{W}} \sin\beta\big)\big] \\ &+ 2N_{12}\big[N_{13}\;\delta\big(M_{\mathrm{Z}} c_{\mathrm{W}} \cos\beta\big) - N_{14}\;\delta\big(M_{\mathrm{Z}} c_{\mathrm{W}} \sin\beta\big)\big]\Big].\end{aligned} \tag{5.65}$$

Accordingly, this choice for the renormalization of the parameters M_1, M_2 and μ corresponds to the extension of the tree-level relation between these parameters and the on-shell masses of the two charginos and one neutralino to the one-loop level. The other three neutralino mass eigenvalues then receive non-zero corrections at the one-loop level.

Eqs. (5.63) – (5.65) still depend on the counterterms for the gauge boson masses and the weak mixing angle, which can be obtained from the gauge sector, and the counterterm for $\tan\beta$, which is a parameter of the Higgs sector. The renormalization of $\tan\beta$ will be discussed in the next section.

For completeness also the expressions for the field renormalization matrices of the neutralinos are given, while they are not needed in loop calculations without external neutralinos:

$$\delta\tilde{Z}^0_{ii} = -\Re e\Big\{\Sigma^{0\mathrm{L}}_{ii}(m^2_{\tilde{\chi}^0_i}) + 2m^2_{\tilde{\chi}^0_i}\Sigma^{0\mathrm{L}\prime}_{ii}(m^2_{\tilde{\chi}^0_i}) + 2m_{\tilde{\chi}^0_i}\Sigma^{0\mathrm{SL}\prime}_{ii}(m^2_{\tilde{\chi}^0_i})\Big\}, \tag{5.66}$$

$$\delta\tilde{Z}^0_{ij} = \frac{2}{m_{\tilde{\chi}^0_i} - m_{\tilde{\chi}^0_j}}\left[m_{\tilde{\chi}^0_j}\,\Re e\,\Sigma^{0\mathrm{L}}_{ij}(m^2_{\tilde{\chi}^0_1}) + \Re e\,\Sigma^{0\mathrm{SL}}_{ij}(m^2_{\tilde{\chi}^0_1}) - (N\delta Y N^\top)_{ij}\right], \tag{5.67}$$

where the prime in Σ' denotes the derivate of the corresponding self-energy.

5.1.5 Renormalization of the Higgs sector

In contrast to the renormalization of masses and gauge couplings, there is no standard on-shell prescription for the renormalization of $\tan\beta$. This is related to the fact that $\tan\beta$ is not directly connected with any observable. In the following, three requirements are put up that are desirable for a renormalization scheme:

- Since $\tan\beta$ originates from the Higgs sector, see (2.19), its renormalization should not involve quantities from other sectors.
- The renormalization condition should lead to a gauge-independent numerical value for $\tan\beta$.
- A good convergence behaviour of the perturbation series is required, i.e. quantum correction to $\tan\beta$ should not grow too large.

In Ref. [97] a variety of different renormalization schemes has been studied with respect to these requirements. The findings are briefly sketched here. With the following decomposition of the Higgs doublets,

$$H_\mathrm{u} = \begin{pmatrix} \phi^+_\mathrm{u} \\ v_\mathrm{u} + \frac{1}{\sqrt{2}}(\phi_\mathrm{u} + i\rho_\mathrm{u}) \end{pmatrix}, \qquad H_\mathrm{d} = \begin{pmatrix} v_\mathrm{d} + \frac{1}{\sqrt{2}}(\phi_\mathrm{d} + i\rho_\mathrm{d}) \\ -\phi^-_\mathrm{d} \end{pmatrix}, \tag{5.68}$$

the linear and quadratic terms of the Higgs potential of the MSSM can quite generally be written as

$$\begin{aligned} V_\mathrm{bilin} = t_\mathrm{u}\phi_\mathrm{u} + t_\mathrm{d}\phi_\mathrm{d} + m_1^2\left(\tfrac{1}{2}\phi_\mathrm{d}^2 + \tfrac{1}{2}\rho_\mathrm{d}^2 + |\phi_\mathrm{d}^-|^2\right) + m_2^2\left(\tfrac{1}{2}\phi_\mathrm{u}^2 + \tfrac{1}{2}\rho_\mathrm{u}^2 + |\phi_\mathrm{u}^+|^2\right) \\ + m_3^2\left(\phi_\mathrm{u}\phi_\mathrm{d} + \rho_\mathrm{u}\rho_\mathrm{d} + \phi_\mathrm{u}^+\phi_\mathrm{d}^- + \phi_\mathrm{u}^{+*}\phi_\mathrm{d}^{-*}\right). \end{aligned} \tag{5.69}$$

with $m_1^2 = \mu^2 + m^2_{\mathrm{H_d}}$, $m_2^2 = \mu^2 + m^2_{\mathrm{H_u}}$ and $m_3^2 = -b$. The tadpole parameters $t_{\mathrm{u,d}}$ vanish at tree-level. The soft-breaking parameters $m_{1,2,3}$ can be re-expressed in terms of $v_\mathrm{u}, v_\mathrm{d}, M_{\mathrm{A^0}}$,

leading to the relations

$$\frac{t_\mathrm{u}}{v_\mathrm{u}} + \frac{t_\mathrm{d}}{v_\mathrm{d}} = \sqrt{2}(m_1^2 + m_2^2) + \sqrt{2}\, m_3^2 \left(t_\beta + \frac{1}{t_\beta}\right), \tag{5.70}$$

$$M_{\mathrm{A}^0}^2 = -m_3^2 \left(t_\beta + \frac{1}{t_\beta}\right) + c_\beta^2 \frac{t_\mathrm{u}}{\sqrt{2} v_\mathrm{u}} + s_\beta^2 \frac{t_\mathrm{d}}{\sqrt{2} v_\mathrm{d}}, \tag{5.71}$$

where the abbreviations $t_\beta = \tan\beta$, $s_\beta = \sin\beta$ and $c_\beta = \cos\beta$ have been introduced. These formulae will be of use later.

The renormalization of the parameters in (5.68) and (5.69) is given by

$$m_{1,2,3}^2 \to m_{1,2,3}^2 + \delta m_{1,2,3}^2, \qquad v_\mathrm{u,d} \to v_\mathrm{u,d}\left(1 + \tfrac{1}{2}\delta Z_\mathrm{u,d}\right) - \delta v_\mathrm{u,d}, \tag{5.72}$$

$$t_\mathrm{u,d} \to t_\mathrm{u,d} + \delta t_\mathrm{u,d}. \tag{5.73}$$

Here $\delta Z_\mathrm{u,d}$ denote the field renormalization constants of the Higgs doublets $H_\mathrm{u,d}$. Their specific form is of no importance here. Now the counterterm for $\tan\beta = v_\mathrm{u}/v_\mathrm{d}$ follows as

$$\delta t_\beta = \frac{v_\mathrm{u}}{v_\mathrm{d}} \left[\tfrac{1}{2}\delta Z_\mathrm{u} - \tfrac{1}{2}\delta Z_\mathrm{d} - \frac{\delta v_\mathrm{u}}{v_\mathrm{u}} + \frac{\delta v_\mathrm{d}}{v_\mathrm{d}}\right]. \tag{5.74}$$

The tadpoles are renormalized so that they also vanish in higher orders, $t_\mathrm{u,d} + \delta t_\mathrm{u,d} = 0$.

In the literature, the renormalization scheme introduced by Dabelstein [98] and by Chankowski et al. [99] has frequently been used. It is defined by the conditions

$$\frac{\delta v_\mathrm{u}}{v_\mathrm{u}} \stackrel{!}{=} \frac{\delta v_\mathrm{d}}{v_\mathrm{d}}, \qquad \Re e\, \Gamma_{\mathrm{A}^0\mathrm{Z}}(M_{\mathrm{A}^0}^2) \stackrel{!}{=} 0. \tag{5.75}$$

At one-loop level this leads to

$$\text{DCPR:} \quad \frac{\delta t_\beta}{t_\beta} = -\frac{1}{M_\mathrm{Z} \sin 2\beta}\, \Im m\, \Sigma_{A^0 Z}(M_{\mathrm{A}^0}^2) \tag{5.76}$$

with the A^0–Z mixing self-energy $\Sigma_{A^0 Z}$. While at the first glance the unmixing of the A^0 and Z looks like an on-shell condition, this is in fact not the case since the longitudinal part of the Z boson is associated with the unphysical Goldstone boson G^0. An alternative method [100], using the condition that the charged Higgs boson $H^\pm$ does not mix with the W boson, is similar to the DCPR scheme.

Another renormalization prescription for t_β that has been used in practice [101] is the $\overline{\mathrm{DR}}$ scheme. It is defined by only taking the divergent part, i.e. the term of order $\Delta = \frac{2}{4-D} - \gamma_\mathrm{E} + \log 4\pi$ in dimensional reduction, of the counterterm δt_β.

It turns out that both the DCPR scheme and the $\overline{\mathrm{DR}}$ scheme are gauge-dependent in the sense that the value for $\tan\beta$ in predictions for physical observables depends on the gauge parameters. The gauge-dependence can generally be shown [97] using the tool of extended Slavnov-Taylor identities [102]. By accident, the $\overline{\mathrm{DR}}$ renormalization of $\tan\beta$ is independent of a covariant R_ξ gauge at the one-loop level. However, gauge-dependent terms are obtained from two-loop order on in the R_ξ gauge [103] and even at the one-loop level in a more general gauge [97].

	$\tan\beta = 3$			$\tan\beta = 50$		
	$M_{\mathrm{h}^0}^{\max}$	large μ	no mixing	$M_{\mathrm{h}^0}^{\max}$	large μ	no mixing
$\overline{\mathrm{DR}}$	−0.06	−0.06	−0.06	−0.17	−0.17	−0.17
GI1	0.81	−0.46	−0.04	285.29	127.11	4.92
GI2	4.50	−0.21	1.24	370.73	140.11	34.53

Table 5.1: *Dependence $\partial t_\beta/\partial \log\bar{\mu}$ on the renormalization scale $\bar{\mu}$ for the $\overline{\mathrm{DR}}$, GI1 and GI2 schemes, for three typical scenarios from [105] and $M_{\mathrm{A}^0} = 500$ GeV.*

One can construct gauge-independent renormalization schemes for $\tan\beta$ by observing that the symmetric soft-breaking parameters $m_{1,2,3}$ are gauge-independent to all orders [104]. In practice, this can be realized by using a $\overline{\mathrm{DR}}$ renormalization for the counterterms $\delta m_{1,2,3}$. From eqs. (5.70), (5.71) the following two alternative relations for the finite part of δt_β can then be deduced,

$$\text{GI1:}\quad \delta t_\beta^{\mathrm{fin}} \stackrel{!}{=} \frac{1}{m_3^2(1-\cot^2\beta)}\left[-(\delta M_{A^0}^2)^{\mathrm{fin}} + c_\beta^2\frac{\delta t_{\mathrm{u}}^{\mathrm{fin}}}{\sqrt{2}v_{\mathrm{u}}} + s_\beta^2\frac{\delta t_{\mathrm{d}}^{\mathrm{fin}}}{\sqrt{2}v_{\mathrm{d}}}\right] \tag{5.77}$$

or

$$\text{GI2:}\quad \delta t_\beta^{\mathrm{fin}} \stackrel{!}{=} \frac{1}{\sqrt{2}m_3^2(1-\cot^2\beta)}\left[\frac{\delta t_{\mathrm{u}}^{\mathrm{fin}}}{v_{\mathrm{u}}} + \frac{\delta t_{\mathrm{d}}^{\mathrm{fin}}}{v_{\mathrm{d}}}\right]. \tag{5.78}$$

The superscript "fin" denotes the purely finite part of the counterterms. The divergent part of δt_β of order Δ can be obtained from the DCPR scheme, for example.

A third gauge-independent scheme can be obtained by extending the Higgs mass relation

$$\text{GI3:}\quad \cos^2 2\beta \stackrel{!}{=} \frac{M_{\mathrm{h}^0}^2 M_{\mathrm{H}^0}^2}{M_{\mathrm{A}^0}^2(M_{\mathrm{H}^0}^2 + M_{\mathrm{h}^0}^2 - M_{\mathrm{A}^0}^2)}, \tag{5.79}$$

which follows from (2.24), to one-loop order.

While all the three schemes GI1, GI2, and GI3 are manifestly gauge-invariant, they turn out to lead to serious numerical problems. Two indications for the magnitude of the higher-order corrections are the scale-dependence (for the $\overline{\mathrm{DR}}$, GI1 and GI2 schemes) and the size of the finite part of the δt_β counterterm.

It can be seen from Tab. 5.1 and 5.2 that the $\overline{\mathrm{DR}}$ and the DCPR scheme are well-behaved in the sense that the magnitude of the higher order corrections is suppressed with respect to the tree-level parameter. However, for the three gauge-invariant schemes GI1–3 very large scale dependences and finite shifts to $\tan\beta$ can be obtained, signalling the breakdown of the validity of perturbation theory. As a consequence, the schemes GI1–3 cannot be employed for practical calculations. In fact, it can be proven that it is impossible to construct any renormalization scheme for $\tan\beta$ from quantities of the Higgs sector that is both gauge-invariant and numerically stable in higher orders [97].

In order to circumvent these problems one could try to define the renormalization of $\tan\beta$ by relating it to a specific physical process. This method has been adopted in [106],

	$\tan\beta = 3$			$\tan\beta = 50$		
	$M_{\mathrm{h}^0}^{\max}$	large μ	no mixing	$M_{\mathrm{h}^0}^{\max}$	large μ	no mixing
$\overline{\mathrm{DR}}$	0	0	0	0	0	0
DCPR	−0.10	−0.06	−0.08	3.56	14.47	0.46
GI1	0.56	−0.08	−0.04	490.45	−67.14	−4.85
GI2	2.64	−0.46	0.33	624.70	−76.46	0.92
GI3	−2.44	−1.83	−1.33	−426.54	−1995.93	−413.50

Table 5.2: *Finite contribution of the counterterm $\delta t_\beta^{\mathrm{fin}}$ in various renormalization schemes, for three typical scenarios from [105] and $M_{\mathrm{A}^0} = 500$ GeV.*

where it was suggested to use the decay $H^+ \to \tau^+\nu_\tau$. The one-loop corrected decay width to this process reads

$$\Gamma[H^+ \to \tau^+\nu_\tau] = \frac{\alpha\, m_\tau^2\, M_{H^\pm}^2\, t_\beta^2}{8 M_{\mathrm{W}}^2 s_{\mathrm{W}}^2} \Bigg[1 + 2\,\delta Z_e + 2\frac{\delta m_\tau}{m_\tau} + 2\frac{\delta t_\beta}{t_\beta} - \frac{\delta M_{\mathrm{W}}^2}{M_{\mathrm{W}}^2} - 2\frac{\delta s_W}{s_{\mathrm{W}}} + \delta Z^{\nu\mathrm{L}} + \delta Z^{\tau\mathrm{R}} + \delta Z^{H^\pm} - \frac{1}{t_\beta}\,\delta Z^{G^\pm H^\pm} + F_\tau \Bigg], \tag{5.80}$$

where F_τ is the form factor describing the vertex corrections to the amplitude $H^+ \to \tau^+\nu_\tau$. The field renormalization constants of the neutrino, $\delta Z^{\nu\mathrm{L}}$, and the tau, $\delta Z^{\tau\mathrm{R}}$, are defined in (5.9), (5.10), while the charged Higgs and the Higgs-Goldstone mixing field renormalizations are given by [100]

$$\delta Z^{H^\pm} = -\Re e\, \frac{\partial}{\partial k^2} \Sigma^{H^\pm}(k^2)\Big|_{k^2 = M_{H^\pm}^2}, \qquad \delta Z^{G^\pm H^\pm} = -\frac{2}{M_{\mathrm{W}}}\, \Re e\, \Sigma^{W^\pm H^\pm}(M_{H^\pm}^2). \tag{5.81}$$

By requiring that the radiatively corrected decay width retains the same form as the tree-level formula, eq. (5.80) can be understood as a definition of the counterterm δt_β. As a consequence of the relation to a physical observable, this definition of $\tan\beta$ is manifestly gauge-invariant.

However, this scheme also has several drawbacks. At first, for the computation of the counterterm to $\tan\beta$, it is necessary to compute loop corrections to the three-particle vertex in F_τ, which can be difficult beyond one-loop order[4]. Furthermore, by defining $\tan\beta$ in a specific process, it becomes a non-universal, flavour-dependent quantity, in contrast to the conception that $\tan\beta$ is a parameter of the Higgs sector.

Finally, the decay vertex $H^+ \to \tau^+\nu_\tau$ also receives QED corrections, which necessarily include contributions with real photon emission so as to cancel the IR divergences. It is not possible to separate the QED contributions from the rest of the electroweak corrections since they are not individually UV-finite. At first glance this fact may seem surprising and in contradiction to the situation for gauge boson decays, where it is known that

[4]For the purposes of this thesis, only one-loop corrections are needed. Nevertheless, a renormalization scheme should be general enough to be extendible to potential future two-loop calculations.

the QED corrections form a gauge-invariant and UV-finite subset. The reason is that in the case of gauge bosons the finiteness of the QED corrections is guaranteed by gauge invariance whereas no such symmetry argument applies to the decays of Higgs bosons. As a consequence, there is no a-priori argument that would require the QED corrections to $H^+ \to \tau^+\nu_\tau$ to be separately finite, and indeed it turns out from an explicit calculation that this is not the case. For practical calculations, however, it is unacceptable to include real bremsstrahlung corrections into the definition of a counterterm.

The problem posed by the QED corrections can be avoided by choosing the process $A^0 \to \tau^+\tau^-$ instead of the decay $H^+ \to \tau^+\nu_\tau$. The QED corrections to this process form a UV-finite subset of the full one-loop corrections. This can be explained by imagining the QED corrections as being generated by an effective theory consisting of the local QED gauge group and the $A^0\tau\tau$ vertex and are therefore naturally finite. Nevertheless, any process-dependent scheme is afflicted with the disadvantages of being flavour-dependent and requiring the computation of vertex loop corrections.

To conclude, it seems impossible to find any renormalization prescription for $\tan\beta$ which satisfies all three requirements that were put up at the beginning of this section. For this thesis, the $\overline{\text{DR}}$ scheme has been used for δt_β, since it is technically most convenient. However, it should be borne in mind that this definition is in general gauge-dependent. Nevertheless, since $\tan\beta$ is not a physical quantity but can only be interpreted as an auxiliary parameter, practical reasons are the decisive factor for the choice of its renormalization.

5.2 Outline of the calculation

5.2.1 Virtual and soft-photonic $\mathcal{O}(\alpha)$ corrections

The generation of the diagrams and amplitudes for the virtual loop contributions and real photonic corrections was performed with the package *FeynArts* [35]. A general covariant R_ξ gauge has been used in order to facilitate an additional check of the result.

For the treatment of the Lorentz and Dirac algebra and the tensor loop integrals, the program *FeynCalc 2.2* [107] was employed. For the purpose of this thesis it was supplemented with an appropriate treatment of dimensional reduction (DRED). The results obtained with DRED have been checked against the package *FormCalc* [108, 109] which uses a different regularization prescription called constrained differential renormalization [110], that has been shown to be equivalent to DRED at the one-loop level [108].

The results for the virtual loop contributions have been reduced to a set of fundamental scalar functions by the well-known Passarino-Veltman method [111], so that an explicit check of the gauge-parameter independence of the result can be performed.

After addition of the on-shell counterterms (see previous section), the result for the virtual contributions is UV-finite. However, they contain another type of singularity which arises from virtual photon exchange between charged external particles in the limit of vanishing photon momentum. These IR-divergences are cancelled by the corresponding real contributions where a photon is emitted from one of the external particles. For very small photon energies the photon radiation process cannot be distinguished experimentally

from the non-radiative slepton pair production process. Therefore only the sum of the virtual and real corrections form a physically sound quantity.

Usually the real corrections are divided into a soft and a hard regime. In order to obtain a IR-finite result, it is sufficient to include the real contributions in the soft-photon limit where the photon energy E_γ is small compared to all other relevant scales of the process, $E_\gamma < \Delta E \ll \sqrt{s}, M_\mathrm{Z}, \ldots$. Here ΔE is a suitable soft-photon cut-off energy. The corresponding real bremsstrahlung integrals in the soft-photon limit are known analytically [112]. For the calculations in this thesis, it was explicitly verified that the total result including virtual and soft-photonic real corrections is UV- and IR-finite.

The hard contributions with $E_\gamma > \Delta E$ are free of singularities and are treated without any approximation, as described in the following section.

Although in the described approach it is possible to extract the gauge-dependent and UV-/IR-divergent expressions algebraically, it may sometimes be difficult to see that they actually vanish. In these cases numerical values for different MSSM scenarios have been inserted and it was checked that the gauge-dependent and divergent terms yield zero within the numerical accuracy.

Finally the renormalized result has been exported into a C++ program for the numerical evaluation of the matrix element and the scalar one-loop functions and the final state phase-space integration. Analytical formulae for the fundamental one-loop integrals are available in the literature [112] and were implemented in the package *LoopTools* [113].

5.2.2 Bremsstrahlung of hard photons

For a complete next-to-leading calculation, the virtual and soft-photonic $\mathcal{O}(\alpha)$ corrections have to be supplemented by the contributions which take into account the emission of hard photons with energies E_γ above the cut-off ΔE. The total inclusive result including soft and hard photon radiation should then be independent of the value of ΔE.

It is convenient to perform the integration over the phase space of the process $e^+e^- \to \tilde{l}^+\tilde{l}^-\gamma$ using Monte-Carlo techniques. This allows one to incorporate appropriate experimental cuts if necessary. It should be noted that the squared matrix elements can grow large when the photon energy E_γ approaches the soft-photon cut-off ΔE (which is generally small compared to other scales in the process) and in the collinear regime. The latter originates from the emission of a photon in the direction of an incoming electron or positron, yielding large QED corrections $\propto (\alpha/\pi)\log(s/m_\mathrm{e}^2)$ (see also section 4.2.1).

In both the soft-photon and the collinear regime, the Monte-Carlo error can be significantly reduced by applying an appropriate mapping of the integration variables so that the integrand is rendered sufficiently flat. From the matrix element $\mathcal{M}_\gamma$ the total hard-photon cross-section is obtained as

$$\sigma_\mathrm{hard} = \frac{1}{2s}\,\frac{1}{2(2\pi)^2}\int \mathrm{d}\Gamma_{+-}\int_{-1}^{1}\mathrm{d}\cos\theta_\gamma\int_{\Delta E}^{\frac{1}{2}\sqrt{s}(1-4m_{\tilde{l}}^2/s)}\mathrm{d}E_\gamma\,E_\gamma\,\frac{1}{4}\sum_\mathrm{pol}\left|\mathcal{M}_\gamma\right|^2, \qquad (5.82)$$

where $\mathrm{d}\Gamma_{+-}$ denotes the sub-phase-space of the two charged sleptons and θ_γ is the polar angle of the photon with respect to the incoming positron, see Fig. 5.1. $\sum_\mathrm{pol}$ stands for the summation over the initial- and final-state polarizations. In the soft-photon regime,

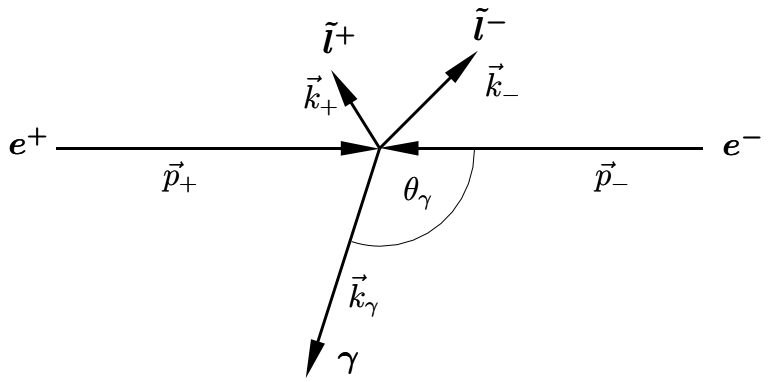

Figure 5.1: *Kinematics for photon radiation contributions.*

the matrix element exhibits the behaviour $\mathcal{M}_{\gamma,\mathrm{soft}} \sim 1/E_\gamma$. Thus the integrand can be flattened by transforming E_γ to the new integration variable r according to

$$r = \ln \frac{E_\gamma}{\sqrt{s}}. \tag{5.83}$$

Note that the Jacobian $|\partial r/\partial E_\gamma|$ exactly mimics the behaviour of the integrand in the soft-photon limit.

In the collinear region, the matrix element is dominated by the propagator of the electron or positron from which the photon is radiated, see (4.5). For photon emission in the direction of the electron momentum p_+, the leading term of the squared matrix element is given by $|\mathcal{M}_{\gamma,\mathrm{coll}}| \sim 1/(p_+k_\gamma)$. A smooth integrand in this region is obtained by using the following transformation from $\cos\theta_\gamma$ to the new variable t,

$$t = \ln \frac{p_+k_\gamma}{\sqrt{s}}, \qquad p_+k_\gamma = \frac{\sqrt{s}E_\gamma}{2}\left[1 - \sqrt{1 - \frac{4m_\mathrm{e}^2}{s}}\cos\theta_\gamma\right]. \tag{5.84}$$

Another technique for the numerical treatment of the collinear regime involves a subtraction procedure (for a discussion in the context of W pair production, see e.g. Ref. [53]). In this method, the large collinear terms are subtracted from the full matrix element. For these terms the integration over the photon phase-space is performed analytically, while the subtracted matrix element can be integrated with standard Monte-Carlo techniques without difficulties. In the limit of collinear hard-photon radiation in the direction of the incoming positron momentum p_+, for instance, $|\mathcal{M}_\gamma|^2$ can be approximated by

$$|\mathcal{M}_{\gamma,\mathrm{coll}}(p_+,p_-,k_+,k_-,k_\gamma)|^2 = e^2\, f^+_{\mathrm{coll}}(p_+,k_\gamma)\; |\mathcal{M}_{\mathrm{Born}}(x_+p_+,p_-,k_+,k_-)|^2\,, \tag{5.85}$$

with $x_+ = 1 - 2E_\gamma/\sqrt{s}$. In the unpolarized case, i.e. after summation over the photon and positron helicities, the collinear factor f^+_{coll} reads

$$\sum_{\mathrm{pol}} f^+_{\mathrm{coll}}(p_+,k_\gamma) = \frac{1+x_+^2}{x_+(1-x_+)}\,\frac{1}{(p_+k_\gamma)} - \frac{m_\mathrm{e}^2}{(p_+k_\gamma)^2} + \mathcal{O}(m_\mathrm{e}^0). \tag{5.86}$$

(Note that $(p_+k_\gamma) = \mathcal{O}(m_\mathrm{e}^2)$ in the collinear limit). After integration over the photon angle, the result for the collinear factor contains the typical large QED logarithms,

$$\int_{-1}^{1} \mathrm{d}\cos\theta_\gamma \sum_{\mathrm{pol}} f_{\mathrm{coll}}^{+}(p_+, k_\gamma) = \frac{4}{sx_+}\left[\frac{1+x_+^2}{(1-x_+)^2}\left(\ln\frac{s}{m_\mathrm{e}^2} - 1\right) + 1\right]. \tag{5.87}$$

For this thesis both the variable mapping method and the subtraction method have been applied to the Monte-Carlo integration of the hard-photon phase-space and it was checked that they agree numerically. In comparison, the subtraction method proves to be more efficient and results in a faster convergence of the Monte-Carlo error.

5.3 Results for smuon pair production

This section gives a brief summary of the numerical results for the $\mathcal{O}(\alpha)$ calculation to $e^+e^- \to \tilde{\mu}_\mathrm{R}^+\tilde{\mu}_\mathrm{R}^-$. More information can be found in Ref. [114].

Since this process only involves gauge couplings and no Yukawa couplings at tree-level, it can be computed both with dimensional regularization and dimensional reduction without the requirement of introducing symmetry-restoring counterterms (for discussion, see section 5.1.1). The computation has been performed for the two regularization schemes and it was checked that the results agree algebraically.

In the following numerical results are given for the input values of the SPS1 scenario, see App. A. In Fig. 5.2 the effect of the one-loop corrections is shown. For demonstration of the loop effects, the relative correction

$$\Delta_\alpha = \frac{\sigma_\alpha - \sigma_{\mathrm{Born}}}{\sigma_{\mathrm{Born}}} \tag{5.88}$$

is depicted, where σ_α is the full next-to-leading order cross-section. Here the Born cross-section σ_{Born} already includes the universal shift $\Delta\alpha$ to the fine-structure constant α, which is induced by light-fermion loops in the photon self-energy. In other words, the on-shell α is replaced by the QED-running effective fine-structure constant $\alpha(s)$ at the scale $\sqrt{s}$.

Furthermore, the virtual and real QED corrections contain universal large logarithmic contributions from emission of soft and collinear photons. These generic terms can be taken into account by a convolution of the Born cross-section with a radiator structure function, see (4.7) and (4.9). Therefore, here these universal terms are subtracted from the $\mathcal{O}(\alpha)$ result, so that Δ_α only depends on the non-universal, i.e. process-dependent QED corrections.

After exclusion of these dominant effects, the remaining QED and weak loop contributions both amount to about 5%, which underlines the importance of the full one-loop calculation for envisaged future precision measurements.

5.4 Results for selectron pair production

In comparison to smuon pair production, the one-loop calculation to selectron pair production entails additional complexities. For instance, one has to deal with an extra technical

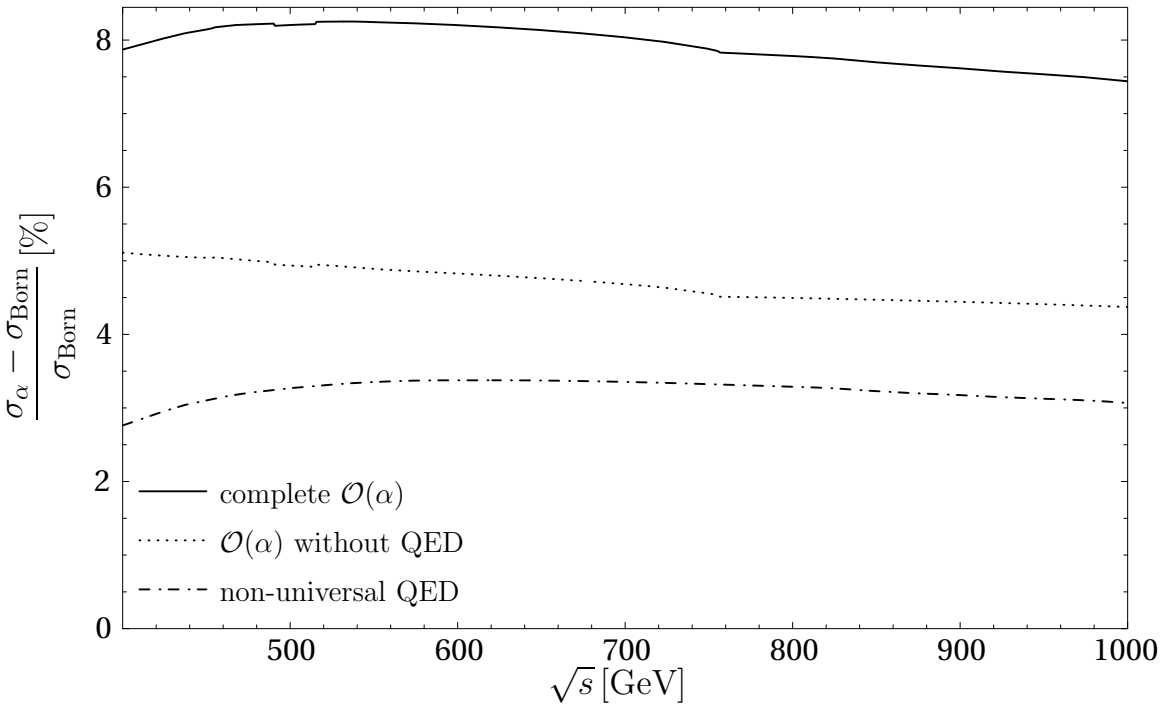

Figure 5.2: *Electroweak corrections to the cross-section for $e^+e^- \to \tilde{\mu}_{\rm R}^+\tilde{\mu}_{\rm R}^-$, relative to the Born cross-section. Separately shown are the QED corrections, including soft and hard real bremsstrahlung contributions but no universal ISR terms, the genuine weak (non-QED) corrections and the full effect of the $\mathcal{O}(\alpha)$ contributions. Input parameters taken from SPS1 scenario.*

challenge, since the number of diagrams is almost doubled compared to smuon production due to the additional t- and u-channel neutralino exchange, but also with conceptual issues like the renormalization of the neutralino sector.

The calculation of the virtual loop diagrams has been performed using dimensional reduction to regulate the divergences.

As before, the numerical results are presented in terms of the relative correction $\Delta_\alpha = (\sigma_\alpha - \sigma_{\rm Born})/\sigma_{\rm Born}$. If not stated otherwise, the SPS1 scenario (see App. A) is chosen for the MSSM input parameters.

Fig. 5.3 and Fig. 5.4 show the effect of the $\mathcal{O}(\alpha)$ corrections on the total cross-section for $e^+e^- \to \tilde{e}_{\rm R}^+\tilde{e}_{\rm R}^-$ and $e^-e^- \to \tilde{e}_{\rm R}^-\tilde{e}_{\rm R}^-$, respectively. The total effect of the next-to-leading order contributions amounts to about 5–10%. For illustration also the contributions from various subsets of diagrams are shown. For instance, the set of diagrams with closed lepton and slepton loops forms a gauge invariant subset since these loop contributions are proportional to the lepton number. A similar argument holds for diagrams with closed loops involving quarks and squarks. Both the lepton/slepton loops and the quark/squark loops yield an effect of a few per-cent on the total cross-section each.

The diagrams involving massive gauge bosons, Higgs bosons, gauginos and higgsinos in the loops cannot be separated in a gauge-invariant manner from the QED contributions. The reason for this is that the set of diagrams with virtual photons in the loops alone is not UV-finite. In particular, in the loop corrections to the electron-selectron-neutralino

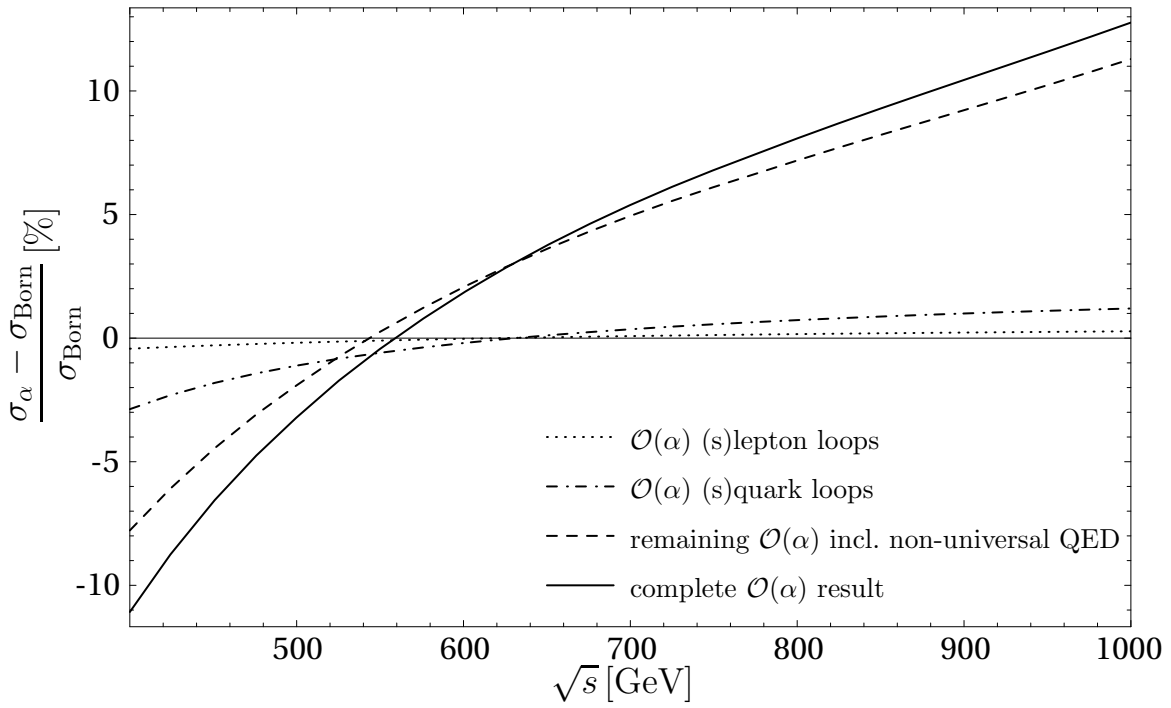

Figure 5.3: *Electroweak corrections to the cross-section for* $e^+e^- \to \tilde{e}_{\rm R}^+\tilde{e}_{\rm R}^-$*, relative to the Born cross-section. Besides the full* $\mathcal{O}(\alpha)$ *result, contributions from different subsets of diagrams are shown. Input parameters taken from SPS1 scenario.*

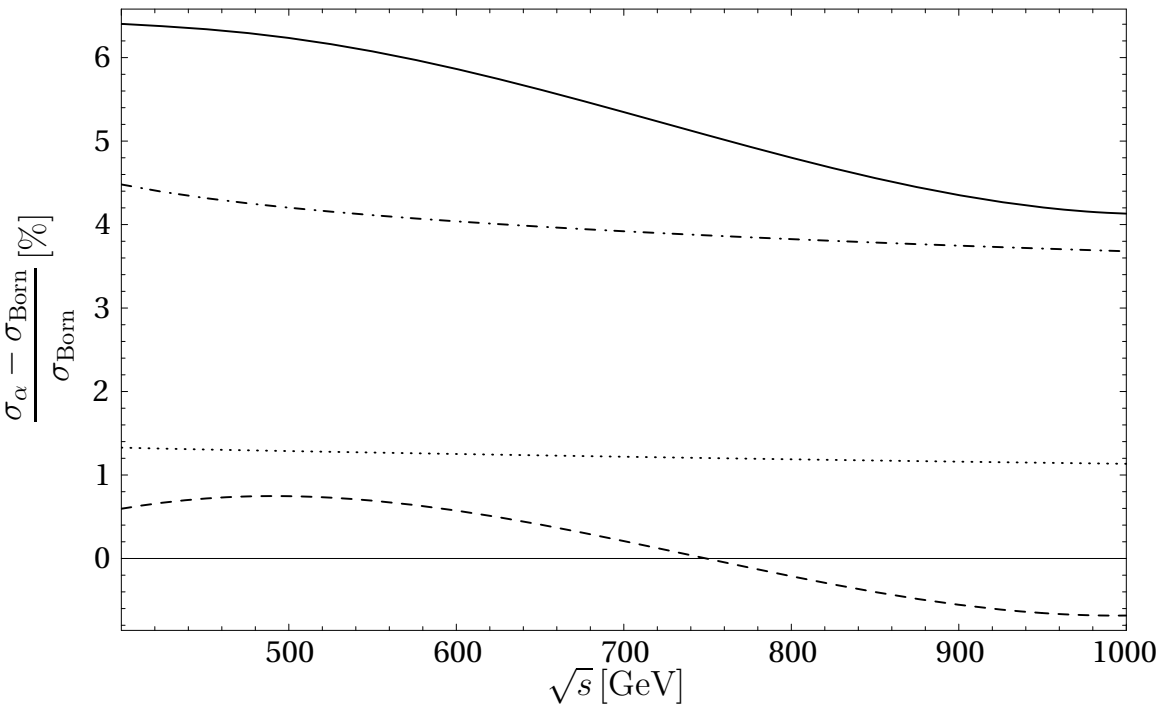

Figure 5.4: *Electroweak corrections to the cross-section for* $e^-e^- \to \tilde{e}_{\rm R}^-\tilde{e}_{\rm R}^-$*, similar to Fig. 5.3.*

vertex in the t-channel contributions, the diagram with a virtual photon exchange has be to supplemented by the corresponding diagram with a photino exchange in order to obtain a finite quantity. However, since the photino is not a mass eigenstate, this contribution is necessarily linked to the weak loop corrections. Therefore, in the figures the remaining $\mathcal{O}(\alpha)$ corrections without closed lepton/slepton and quark/squark loops but including QED corrections are shown in one curve.

In the following the dependence of the one-loop result on genuine supersymmetric corrections shall be studied in more detail. Since in the processes under consideration, supersymmetric particles are also present in the final state, it is not possible to distinguish formally between Standard Model and supersymmetric loop corrections. However, besides the obvious dependence of the cross-section on selectron parameters, important effects can also arise from other sectors of the MSSM which only enter via the loop corrections. In principle, the one-loop result is a function of almost all parameters of the MSSM. Depending on how well these parameters can be extracted from other processes, their limited knowledge may significantly influence the measurement of the selectron parameters from selectron pair production.

The influence on parameters of the Higgs sector, M_{A^0} and $\tan\beta$, is rather mild, since the couplings of the Higgs bosons to the electron and selectron are negligible. The nominal effect of Higgs bosons in the self-energies of the s-channel Z-boson and the t-channel neutralinos may be expected to be somewhat larger. However the leading self-energy contributions that depend on the Higgs sector are proportional to the logarithm of the mass ratio of two Higgs bosons, such as $\log M_{\mathrm{H}^0}/M_{\mathrm{A}^0}$. As a consequence, these terms are naturally suppressed.

A significant influence on the one-loop corrections arises from the gaugino sector, which depends on the parameters M_1, M_2 and μ. As an example, in Fig. 5.5 and Fig. 5.6 the dependence of the one-loop corrections on the parameters M_2 and μ is shown. For the values given in the figures, the variation of these parameters has an effect of about half a per-cent on the cross-section, which is clearly above the experimental accuracy of about two per-mille (see section 6.2). It can be seen that the dependence is strongest for low values of μ. This is due to the influence of higgsino loops in the Z and W boson self-energies which affect the renormalization of the weak mixing angle. The deviations along the line $M_2 = \mu$ originate from the level crossing between the $\tilde{\chi}^0_2$ and $\tilde{\chi}^0_{3,4}$ states, which occurs for this parameter configuration. Near level crossings the relative radiative corrections can grow unusually large since here the relation between the mass eigenstates and the gaugino parameters becomes singular.

It is also important to consider the dependence on the sfermion masses (besides the selectron masses which of course enter at tree-level already). This will be discussed in the next section.

5.5 Superoblique corrections

In general, the effect of quantum corrections decreases with increasing mass scale of the virtual particles inside the quantum loops. This behaviour is the statement of the decoupling theorem [115]. However, this theorem does not apply in the case of broken

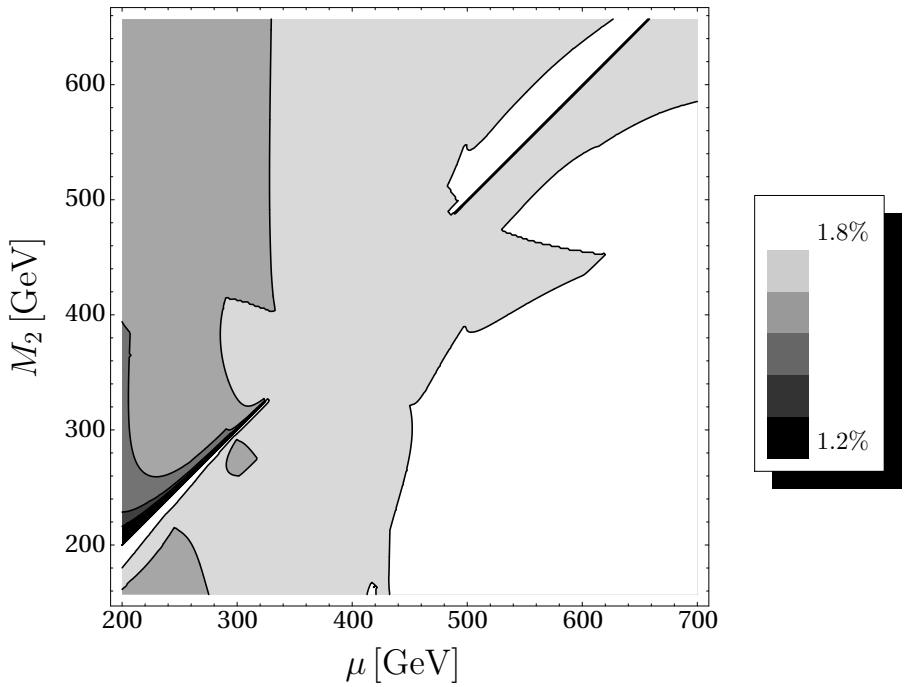

Figure 5.5: *Dependence of the relative one-loop corrections Δ_α to $\tilde{e}_{\mathrm{R}}^{+}\tilde{e}_{\mathrm{R}}^{-}$ production on the gaugino parameters M_2 and μ at $\sqrt{s} = 600$ GeV. Values of other parameters from SPS1 scenario.*

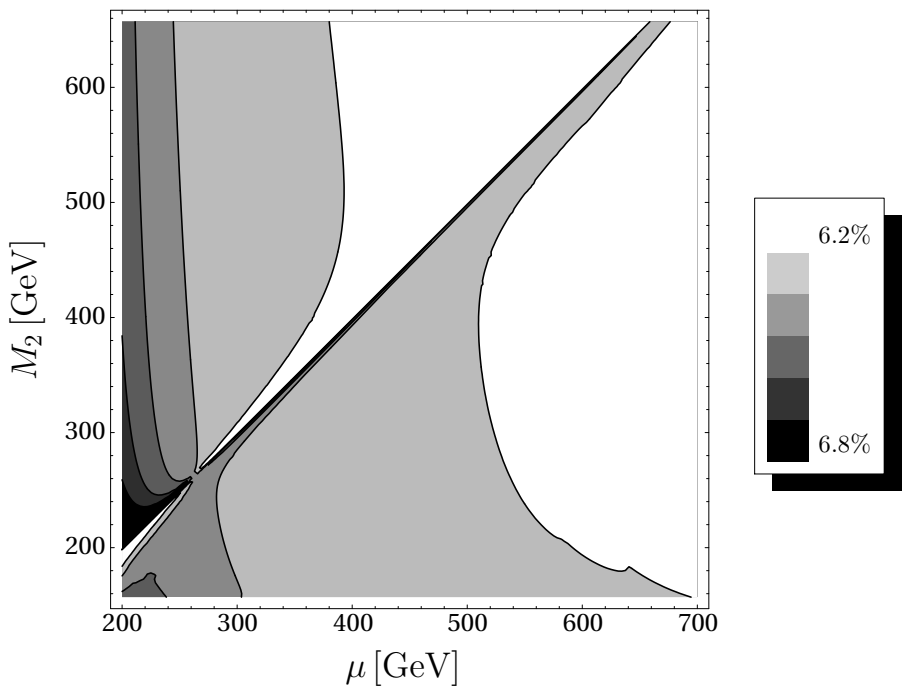

Figure 5.6: *Dependence of the relative one-loop corrections Δ_α to $\tilde{e}_{\mathrm{R}}^{-}\tilde{e}_{\mathrm{R}}^{-}$ production on the gaugino parameters M_2 and μ at $\sqrt{s} = 400$ GeV. Values of other parameters from SPS1 scenario.*

symmetries. As a consequence, in such theories it is possible to obtain radiative effects that grow with increasing violation of the broken symmetry, in contrast to the usual decoupling behaviour. Therefore these non-decoupling corrections may be expected to yield possibly large effects in predictions of physical observables.

In the case of the MSSM, supersymmetry is required to be broken so that non-decoupling corrections may arise from the supersymmetry-breaking masses, for example gaugino and sfermion masses. In the case that *all* superpartner masses are very heavy they are known to decouple from the Standard Model sector. Nevertheless, non-decoupling corrections are possible in scenarios with large hierarchies between different superpartner masses.

A particular class of non-decoupling supersymmetric effects has been studied in Ref. [116, 117]. It was found that large sfermion masses result in corrections proportional to $\ln M_{\tilde{\mathrm{f}}}$ in the renormalization of the gauge boson and gaugino propagators, where $M_{\tilde{\mathrm{f}}}$ is the characteristic heavy sfermion mass. In analogy to the so-called oblique corrections [118] of the Standard Model, which arise from the mass splittings inside the fermion SU(2) doublets, the authors of Ref. [117] called them "superoblique corrections."

For the present purposes, let us consider scenarios where the masses of the gluino and all squarks are relatively heavy while the masses of the sleptons reside near the weak scale, $M_{\tilde{\mathrm{q}}} \gg m_{\tilde{l}}$. In this case the slepton production cross-section could receive significant corrections due to the logarithmic non-decoupling effects $\propto \ln M_{\tilde{\mathrm{q}}}$ which arise from squark loops. Accordingly, in Ref. [119] it was argued that this may serve as probe of supersymmetric particles at the multi-TeV scale which will escape direct detection.

In [116, 117], the effect of the logarithmic terms $\propto \ln M_{\tilde{\mathrm{q}}}$ were studied in the language of $\overline{\mathrm{DR}}$ running couplings. In particular, the gauge couplings $g_{\overline{\mathrm{DR}}}$ and the corresponding supersymmetric gaugino-fermion-sfermion Yukawa couplings $\hat{g}_{\overline{\mathrm{DR}}}$ evolve differently below the scale of the heavy superpartners, $M_{\tilde{\mathrm{q}}}$, thereby leading to a modification of the fundamental relation $g_{\overline{\mathrm{DR}}} = \hat{g}_{\overline{\mathrm{DR}}}$ at the weak scale. On the other hand, for the calculations presented in the previous sections, the on-shell renormalization scheme has been employed where all couplings are manifestly scale-invariant. Therefore, within the on-shell scheme, the relation $g_{\mathrm{os}} = \hat{g}_{\mathrm{os}}$ remains valid to all orders of perturbation theory. However, in this case, the non-decoupling logarithmic corrections are present in loop corrections to the gauge bosons in gauge coupling vertices and the gauginos in gaugino-fermion-sfermion vertices.

The pair production of smuons, $e^+e^- \to \tilde{\mu}^+\tilde{\mu}^-$ is free of any superoblique corrections since it only involves gauge couplings and no gauginos at tree-level. In fact, all non-decoupling logarithms exactly cancel between the renormalization of the gauge couplings and the renormalization of the s-channel gauge bosons. This is a consequence of gauge invariance which is not violated by the supersymmetry-breaking terms. The decoupling behaviour is illustrated by Fig. 5.7, where the dependence of the one-loop radiative corrections to $\tilde{\mu}^+_{\mathrm{R}}\tilde{\mu}^-_{\mathrm{R}}$ production on the squark masses is shown. Here the soft-breaking scalar quark masses $M_{\tilde{\mathrm{Q}}} = m_{\tilde{\mathrm{q}}_{\mathrm{L}}} = m_{\tilde{\mathrm{u}}_{\mathrm{R}}} = m_{\tilde{\mathrm{d}}_{\mathrm{R}}}$ are taken to be equal for all generations and for left/right chiralities. It can be seen that for increasing squark masses, $M_{\tilde{\mathrm{Q}}}$, the size of the radiative corrections quickly reaches an asymptotic behaviour, which is an indication for the decoupling of the squarks.

In the case of selectron production, superoblique effects enter via the t-channel neu-

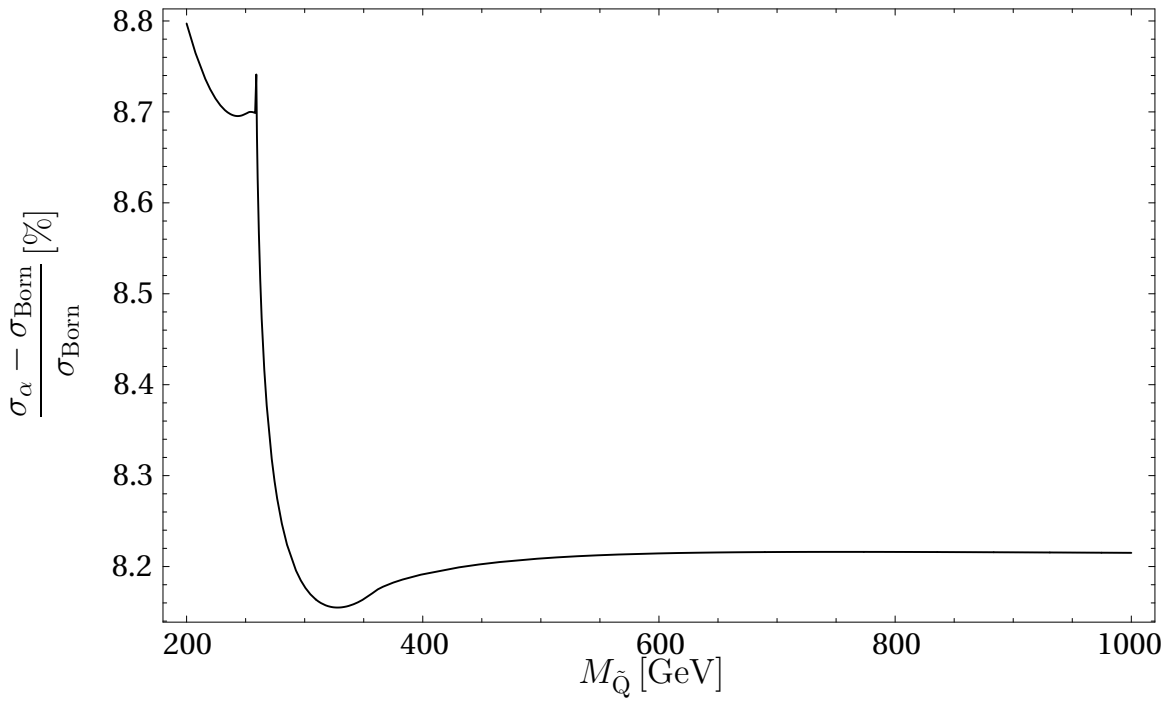

Figure 5.7: *Dependence of the relative one-loop corrections Δ_α to $\tilde{\mu}_{\rm R}^+\tilde{\mu}_{\rm R}^-$ production on the universal squark soft-breaking parameter $M_{\tilde{\rm Q}}$ for $\sqrt{s} = 500$ GeV. Values of other parameters from SPS1 scenario.*

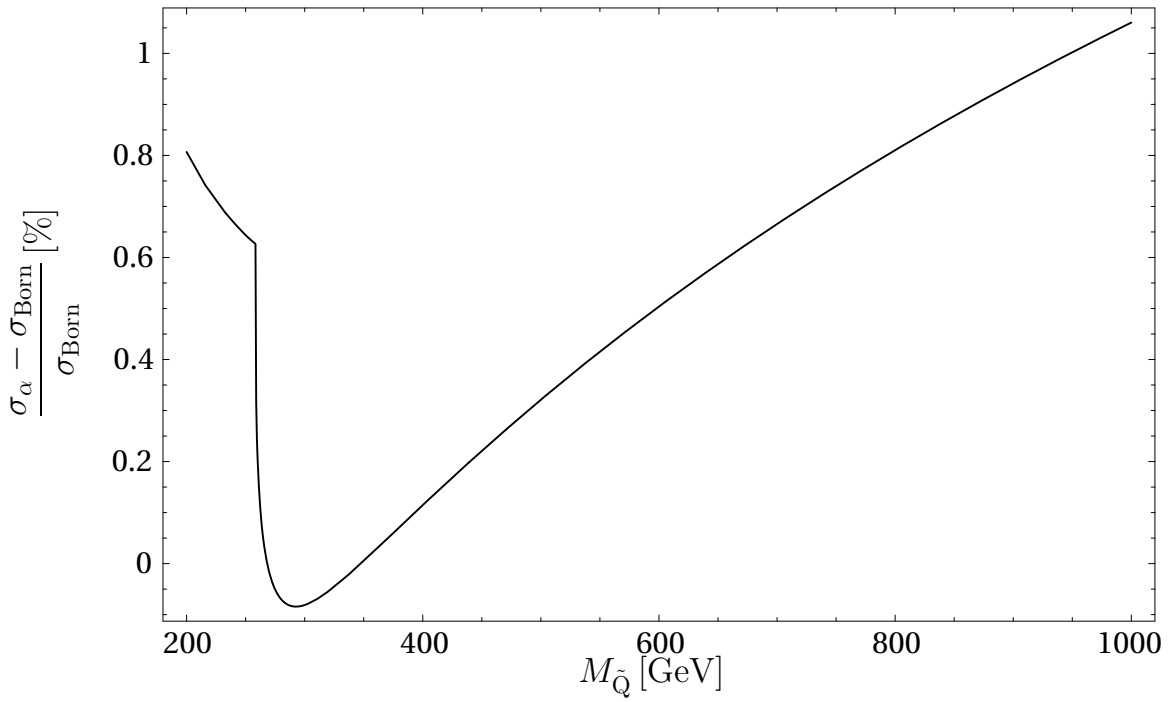

Figure 5.8: *Dependence of the relative one-loop corrections Δ_α to $\tilde{e}_{\rm R}^-\tilde{e}_{\rm R}^-$ production on the universal squark soft-breaking parameter $M_{\tilde{\rm Q}}$ for $\sqrt{s} = 400$ GeV. Values of other parameters from SPS1 scenario.*

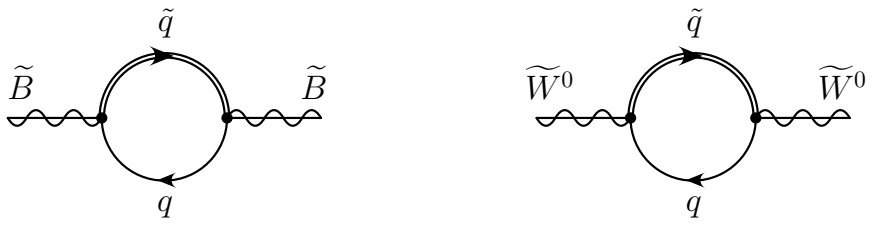

(a) (b)

Figure 5.9: *Quark-squark loop corrections to the U(1) (a) and SU(2) (b) neutral gaugino self-energies.*

tralino exchange contributions. The neutralino propagators receive corrections from quark-squark loops which are sensitive to a tentative high-scale squark mass. It is possible to extract the leading-logarithmic terms $\propto \ln M_{\tilde{\mathrm{Q}}}$ from the complete MSSM loop corrections by performing an expansion in the heavy squark mass $M_{\tilde{\mathrm{Q}}}$ and only keeping the logarithmic coefficients.

When considering a pure bino state, see Fig. 5.9 (a), one obtains the following non-decoupling contributions to the self-energy from heavy squarks,

$$\Sigma^0_{\tilde{\mathrm{B}},\log}(p) = -\not{p}\,\frac{g'^2}{16\pi^2}\,\frac{11}{2}\,\ln M^2_{\tilde{\mathrm{Q}}}. \tag{5.89}$$

One can interpret this result as a shift of the effective Yukawa couplings. This means that the superoblique corrections to the neutralino propagator are regarded as contributions to the bino-electron-selectron Yukawa couplings $\hat{g}'$ which are connected by this propagator. As a consequence, the effective Yukawa coupling $\hat{g}'_{\mathrm{eff}}$ is shifted by the leading-logarithmic correction term,

$$\frac{\hat{g}'^2_{\mathrm{eff,log}}}{\hat{g}'^2} = 1 + \frac{g'^2}{16\pi^2}\,\frac{11}{2}\,\ln M^2_{\tilde{\mathrm{Q}}}. \tag{5.90}$$

In the one-loop correction, the distinction between the gauge coupling g' and the Yukawa coupling $\hat{g}'$ is consistently dropped. The corresponding leading-logarithmic term in the gauge coupling renormalization reads

$$\frac{g'^2_{\mathrm{eff,log}}}{g'^2} = 1 - \delta Z^{\mathrm{B}} = 1 + \frac{g'^2}{16\pi^2}\,\frac{11}{6}\,\ln M^2_{\tilde{\mathrm{Q}}}, \tag{5.91}$$

where δZ^{B} is the field renormalization constant of the B-boson field. Since the scale invariant couplings g' and $\hat{g}'$ are equal by definition, (5.90) and (5.91) result in a splitting between the effective gauge and Yukawa coupling,

$$\frac{\hat{g}'^2_{\mathrm{eff,log}}}{g'^2_{\mathrm{eff,log}}} = 1 + \frac{g'^2}{16\pi^2}\,\frac{11}{3}\,\ln M^2_{\tilde{\mathrm{Q}}}, \tag{5.92}$$

in agreement with [117][5].

[5]Note that in [117] the hypercharge U(1) group is multiplied by the GUT factor 5/3. Accordingly, the correction term in (5.92) has to be multiplied by 3/5 in order to reproduce their numbers.

Similarly, the superoblique corrections to the SU(2) gauge and Yukawa couplings can be extracted. From the neutral wino self-energy correction, see Fig. 5.9 (b), one obtains for the effective SU(2) Yukawa coupling

$$\frac{\hat{g}^2_{\text{eff,log}}}{\hat{g}^2} = 1 + \frac{g^2}{16\pi^2}\,\frac{9}{2}\,\ln M^2_{\tilde{\text{Q}}}, \tag{5.93}$$

whereas the gauge coupling renormalization yields

$$\frac{g^2_{\text{eff,log}}}{g^2} = 1 - \delta Z^{\text{W}^3} = 1 + \frac{g^2}{16\pi^2}\,\frac{3}{2}\,\ln M^2_{\tilde{\text{Q}}}. \tag{5.94}$$

Here δZ^{W^3} denotes the field renormalization constant of the neutral SU(2) gauge boson. Thus, the ratio of the two effective couplings is given by

$$\frac{\hat{g}^2_{\text{eff,log}}}{g^2_{\text{eff,log}}} = 1 + \frac{g^2}{16\pi^2}\,3\,\ln M^2_{\tilde{\text{Q}}}, \tag{5.95}$$

which is consistent with [117].

The situation gets more involved when considering the complete neutralino mixing. In particular, when expressing the neutralino masses in terms of the soft-breaking parameters, not all neutralinos masses can be taken as free parameters but they are linked by non-trivial relations. At higher orders, these relations receive radiative corrections which contain also non-decoupling logarithmic corrections from quark-squark loops. This fact has not been considered in Ref. [119] and would severely complicate any effort to extract information about possibly heavy squarks at the multi-TeV scale from the superoblique coupling corrections to selectron production. In particular, since the superoblique corrections do not only enter in the relation between gauge and Yukawa couplings, but also in the neutralino masses, they depend on the process under consideration and cannot be regarded as universal.

In contrast to smuon production, the presence of non-decoupling supersymmetric corrections in $\tilde{e}^-_{\text{R}}\tilde{e}^-_{\text{R}}$ production can be seen from Fig. 5.8. For increasing values of the squark soft-breaking parameter, $M_{\tilde{\text{Q}}}$, the size of the radiative corrections grows unboundedly. For very large values of $M_{\tilde{\text{Q}}} \sim \mathcal{O}(100\text{ TeV})$ the effect of the superoblique correction on the cross-section for R-selectron pair production can amount up to a few percent. While this contribution is clearly non-negligible, it yet is of the same order as the remaining one-loop corrections.

Chapter 6

Determination of supersymmetric masses and couplings

In order to establish supersymmetry experimentally at future colliders, two categories of properties of the newly detected particles have to be determined. First, all quantum numbers with the exception of spin are required to be equal between partners of a supermultiplet. Thus it is important to test the equivalence of Standard Model and MSSM couplings with high accuracy. Secondly, their masses have to be measured with high precision, which would allow one to construct the spectrum of the soft-breaking parameters. This is a crucial prerequisite to discriminate between different tentative breaking mechanisms with the help of renormalization group extrapolation to higher scales, see section 2.3.

6.1 Measurement of masses in threshold scans

In supersymmetric theories with R-parity conservation, the masses of supersymmetric particles cannot be directly reconstructed from their decay products since the lightest supersymmetric particle is stable and escapes detection. Nevertheless, it is possible to determine the superpartner masses by measuring the endpoints of the kinematical distributions of the visible decay products [10, 15, 52, 120].

On the other hand, at a linear collider with high luminosity the masses of scalar leptons can be determined in threshold scans with unparallelled precision. Several studies have been performed as to explore the potential of this method [15–18]. For the case of selectrons it was investigated which advantages one can gain from the e^-e^- collider mode [17] and how beam polarization can help to single out the desired signal contributions [18].

Since all these studies are based upon specific idealizations, a more realistic and theoretically sound analysis of threshold measurements is desirable. Here, the previous studies are improved in the context of the calculations of chapter 4. In order to match the experimental accuracy, it is required to incorporate several non-leading effects. Finite widths, which considerably affect the cross-section near threshold, are included in a gauge-invariant manner. As a consequence, the full $2 \to 4$ matrix elements including the decay of the sleptons as well as potential MSSM backgrounds and interference contribu-

tions are computed. The Standard Model backgrounds with the same final state signature are added. Beamstrahlung and leading photon emission corrections in the initial state and the Coulomb correction in the final state are taken into account.

Threshold scan measurements are performed by measuring the cross-section of a given process at different centre-of-mass energies near threshold and fitting the theoretical prediction to the experimental values. This procedure can then be used to constrain the parameters which enter into the theoretical prediction. Because of the distinct slope of the excitation curve near the kinematical threshold, measurements in this region are particularly sensitive on the mass of the produced particle. For the present analysis both the "measurement" and the theoretical predictions are simulated with the Monte-Carlo techniques explained in section 4.3.

The optimization of the scan strategy is a non-trivial question [17,121] and will not be further addressed here. For simplicity, for each threshold measurement five equidistant scan points in a centre-of-mass energy range of 10 GeV are considered and the expended luminosity is equally distributed among these points. The precision on the mass measurements that are obtained by this method can therefore not be interpreted as the final answer but may be improved by dedicated scan strategies.

For the fit of the theoretical prediction and the extraction of statistical bounds on the masses, the binned likelihood method is employed, see e.g. [122]. The likelihood function $\mathcal{L}$ for a histogram of N scan points is given by

$$\ln \mathcal{L} = \sum_{i=1}^{N} \left(n_i - y_i + n_i \ln \frac{y_i}{n_i} \right), \tag{6.1}$$

where n_i is the measured number of events at the scan point i and y_i is the number of events predicted by the model. The model prediction $\{y_i\}$ is a function of the unknown slepton mass $m_{\tilde{l}}$ which is to be determined from the fitting procedure. In the ansatz of (6.1) it is assumed that the individual cross-section measurements at each scan point comply with Poisson statistics.

The best-fit value for $m_{\tilde{l}}$ is obtained by maximizing $\ln \mathcal{L}$, while the squared standard deviation is defined as

$$\chi^2 = 2(\ln \mathcal{L}_{\max} - \ln \mathcal{L}). \tag{6.2}$$

Technically the fitting procedure is performed as follows. A reference "measurement" is generated by calculating the observable cross-section for a given fixed slepton mass. Now, the tentative mass parameter $m_{\tilde{l}}$ is varied in a certain region and for each value of $m_{\tilde{l}}$ a prediction for the cross-section is computed. The number of events obtained from these computations is then used to evaluate $\ln \mathcal{L}$ for each parameter point. Finally, the parameter value $m_{\tilde{l},\mathrm{opt}}$ which corresponds to the maximum value of $\ln \mathcal{L}$ is considered as the best-fit value. The 1σ bounds are obained by searching parameter points which satisfy $\ln \mathcal{L}_{\max} - \ln \mathcal{L} = 1/2$.

In the second column of Tab. 6.1 the resulting one-standard deviation errors in the determination of smuon and selectron masses are given for the example of the SPS1 scenario. For the e^+e^- mode a total luminosity of 50 fb^{-1} for each threshold scan is assumed, corresponding to 10 fb^{-1} per scan point. In the e^-e^- the anti-pinch effect leads to a somewhat reduced machine luminosity. Therefore it is presumed that a total amount

process	one-parameter fit	four-parameter fit
$e^+e^- \to (\tilde{e}_R^+\tilde{e}_R^-) \to e^+e^- + \not{E}$	$m_{\tilde{e}_R} = 143.0^{+0.21}_{-0.19}$ GeV	$m_{\tilde{e}_R} = 143.0^{+0.21}_{-0.19}$ GeV $\Gamma_{\tilde{e}_R} = 150^{+300}_{-250}$ MeV
$e^-e^- \to (\tilde{e}_R^-\tilde{e}_R^-) \to e^-e^- + \not{E}$	$m_{\tilde{e}_R} = 142.95^{+0.032}_{-0.032}$ GeV	$m_{\tilde{e}_R} = 142.95^{+0.048}_{-0.053}$ GeV $\Gamma_{\tilde{e}_R} = 200^{+50}_{-40}$ MeV
$e^+e^- \to (\tilde{e}_R^\pm\tilde{e}_L^\mp) \to e^+e^-\,\tau^+\tau^- + \not{E}$	$m_{\tilde{e}_L} = 202.2^{+0.32}_{-0.29}$ GeV	$m_{\tilde{e}_L} = 202.2^{+0.37}_{-0.33}$ GeV $\Gamma_{\tilde{e}_L} = 240^{+20}_{-20}$ MeV
$e^-e^- \to (\tilde{e}_L^-\tilde{e}_L^-) \to e^-e^-\,\tau\tau\tau\tau + \not{E}$	$m_{\tilde{e}_L} = 202.1^{+0.54}_{-0.36}$ GeV	$m_{\tilde{e}_L} = 202.1^{+0.62}_{-0.44}$ GeV $\Gamma_{\tilde{e}_L} = 240^{+500}_{-240}$ MeV
$e^+e^- \to (\tilde{\mu}_R^+\tilde{\mu}_R^-) \to \mu^+\mu^- + \not{E}$	$m_{\tilde{\mu}_R} = 143.0^{+0.39}_{-0.34}$ GeV	$m_{\tilde{\mu}_R} = 143.0^{+0.42}_{-0.38}$ GeV $\Gamma_{\tilde{\mu}_R} = 350^{+400}_{-400}$ MeV

Table 6.1: *Expected precision for the determination of slepton masses from threshold scans in e^+e^- and e^-e^- scattering. The values in the second column are based on the assumption that all other model parameters are known, while the third column is independent on the structure of the neutralino sector. Values for SPS1 scenario.*

of 5 fb^{-1} is avaible for each scan measurement, corresponding to 1 fb^{-1} per scan point. The signal-to-background ratio is enhanced by using suitable cuts and beam polarization as explained in section 4.4.

As far as the measurement of the right-chiral selectron mass $m_{\tilde{e}_R}$ is concerned the e^-e^- mode is clearly superior to the e^+e^- mode, with almost one order of magnitude difference in the precision. This can be explained by the lower cross-section in the threshold region and the substantial background contamination for e^+e^- annihilation. For illustration, in Fig. 6.1 the threshold cross-sections for right-chiral selectron production in the two cases are shown with the 1σ error bars of the cross-section measurements at each individual scan point. Nevertheless, it should be noted that the impressive accuracy of $\delta m_{\tilde{e}_R} = 33$ MeV, that can be obtained in e^-e^- scattering, would definitly require to be checked by some further studies on sytematics.

For the determination of the left-chiral selectron mass $m_{\tilde{e}_L}$ the differences of the two collider modes are less pronounced. In the e^+e^- mode, one can capitalize on the possibility to measure the L-selectron mass at the threshold for the production of mixed pairs, $\tilde{e}_R^\pm\tilde{e}_L^\mp$, which—similar to $\tilde{e}_L^-\tilde{e}_L^-$ production—profits from S-wave excitation. On the other hand, the measurement of the $\tilde{e}_L^-\tilde{e}_L^-$ threshold suffers from limited statistics due to the reduced luminosity and the low cross-section in the chosen decay channel. Therefore, measurements in both e^+e^- and e^-e^- scattering result in roughly comparable errors for $m_{\tilde{e}_L}$.

For illustration, it is also interesting to discuss the measurement of $m_{\tilde{e}_L}$ at the threshold for mixed pairs in the e^-e^- mode, $e^-e^- \to (\tilde{e}_R^-\tilde{e}_L^-) \to e^-e^-\,\tau^+\tau^- + \not{E}$. This case may be of particular importance if the threshold for $\tilde{e}_L^-\tilde{e}_L^-$ production is beyond the kinematical reach of the collider. However, the small cross-section and the smooth P-wave threshold

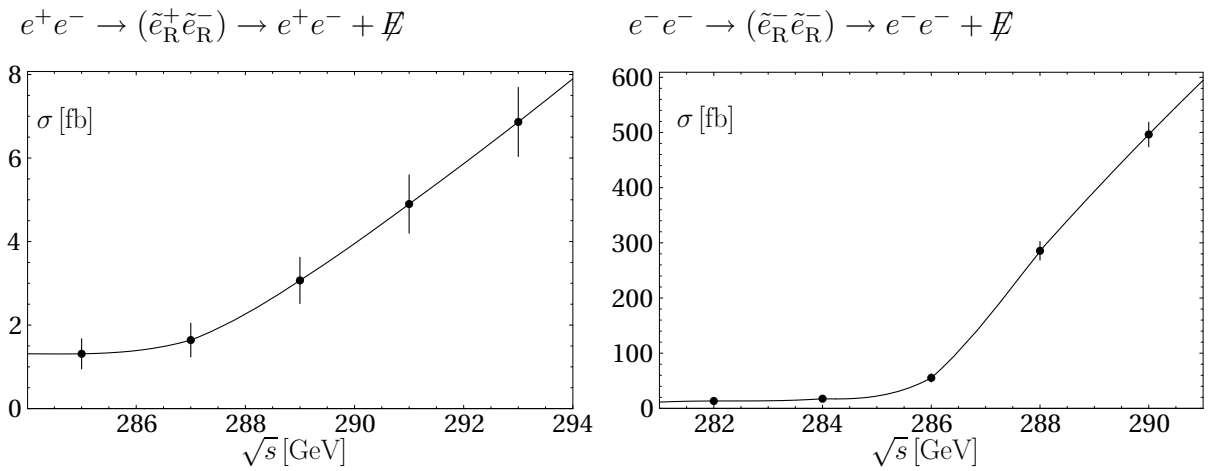

Figure 6.1: *Threshold behaviour of R-selectron pair production for e^+e^- and e^-e^- scattering. The error bars indicate the statistical error of the cross-section measurements at each scan point for $L = 10$ fb^{-1} in e^+e^- and $L = 1$ fb^{-1} in e^-e^-, respectively. Values for SPS1 scenario.*

excitation of this channel result in a rather large statistical error of $\delta m_{\tilde{e}_L} = 1.5$ GeV.

For the same reasons the measurement of the right-chiral smuon mass from a threshold scan is afflicted with a rather large error of $\delta m_{\tilde{\mu}_R} = 360$ MeV. This error can be considerably reduced by increasing the statistics. With a total luminosity of 100 fb^{-1} equally distributed over ten scan points, a precision of $\delta m_{\tilde{\mu}_R} = 175$ MeV is obtained. This result can be compared with Ref. [16] where an error on the determination of the smuon mass of 90 MeV was derived. While both results agree in the order of magnitude, in the present work a slightly lower precision is obtained as compared to Ref. [16]. This can be explained by differences in the considered scenarios and by the effect of background contributions.

Due to the low cross-section, a measurement of the left-chrial smuon mass from a threshold scan is not profitable. Here the precision obtained from endpoint kinematics in the continuum will clearly be superior.

Up to now it was assumed that the remaining MSSM model parameters besides the slepton masses are precisely known. This supposition, however, is not very realistic for the case of selectron production which depends on the neutralinos in the t-channel exchange contributions. Deviations in the neutralino parameters mainly affect the slope of the threshold excitation curve [17, 18]. In addition, they may change the size of the supersymmetric backgrounds. This opens up the possibility to disentangle these effects from the determination of the slepton masses, which is characterized by the starting point of the excitation curve.

The general concept can be demonstated by a formal expansion of the total cross-section σ in terms of the slepton velocity β,

$$\sigma = A + B\beta + \mathcal{O}(\beta^3). \tag{6.3}$$

The quantities A and B parametrize the background contributions and the overall slope of the threshold excitation curve. They include the complete dependence on the neutralino

parameters. If higher orders in β are sufficiently suppressed near threshold, the linear coefficient in β is then uniquely related to the slepton mass. It should be noted that (6.3) applies to the case of S-wave production. For particles that are produced in a P-wave, the leading coefficient would be $\propto \beta^3$ while the higher orders are of $\mathcal{O}(\beta^5)$.

Since the sleptons are unstable particles, the generalized velocities defined in (4.17) and (4.18) depend on the non-zero widths of the sleptons. Within a given scenario it is possible to obtain predictions for the widths from theoretical calculations. However, in an unbiased analysis the slepton width should also be regarded as an independent parameter.

A model-independent determination of the slepton masses could therefore be achieved with a four-parameter fit, where besides the mass $m_{\tilde{l}}$ a constant offset A, an overall scale factor B and the width $\Gamma_{\tilde{l}}$ are kept as free parameters. In order to explore the potential of this method, a number of "measurements" were performed using simulated threshold curves for different scenarios. While the underlying slepton mass values were always kept unchanged in all test scenarios, the neutralino parameters M_1, M_2 and μ have been varied within a factor two. In order to allow a direct comparison between the different test scenarios, the threshold cross-sections and slepton widths have been normalized to the case of the SPS1 scenario.

The resulting errors on the model-independent determination of the slepton masses are summarized in the third column of Tab. 6.1. The given error intervals always correspond to the worst case of the test scenarios. In all cases the achieved precision is only slightly reduced compared to the values that are obtained when all neutralino parameters are precisely known. Also shown in Tab. 6.1 are the resulting bounds on the slepton widths from the four-parameter fit. For the case of P-wave production processes, such as the pair production of R-selectrons or R-smuons in e^+e^- annihilation, one can obtain only rather weak constraints on the value of the slepton widths. On the other hand, it is possible to extract the widths of the sleptons with an error of 10–20% from the measurement of the $\tilde{e}_{\mathrm{R}}^-\tilde{e}_{\mathrm{R}}^-$ or $\tilde{e}_{\mathrm{R}}^\pm\tilde{e}_{\mathrm{L}}^\mp$ thresholds. It should be noted that the accuracy of the mass and width measurements crucially depends on the scan strategy. While for the extraction of the width it is advantageous to spend a large amount of the luminosity at or below the nominal threshold, the precision of the mass measurement can be increased by including scan points at higher centre-of-mass energies where the cross-section is larger.

It is interesting to study the influence of the finite widths and the Coulomb correction on the mass determination. Both effects enter non-linearly in the cross-section and can therefore not be incorporated into the parameters A and B in (6.3). An estimate of their impact is obtained by redoing the fit to the threshold excitation curve without finite width and Coulomb rescattering effects. In this case the R-selectron mass $m_{\tilde{e}_{\mathrm{R}}}$ extracted from the measurement of the $\tilde{e}_{\mathrm{R}}^-\tilde{e}_{\mathrm{R}}^-$ threshold in e^-e^- scattering deviates from the true underlying value by 150 MeV. This underlines the necessity to take into account these corrections. It should be noted that additional radiative corrections besides the dominant Coulomb corrections may be needed in order to match the experimental accuracy.

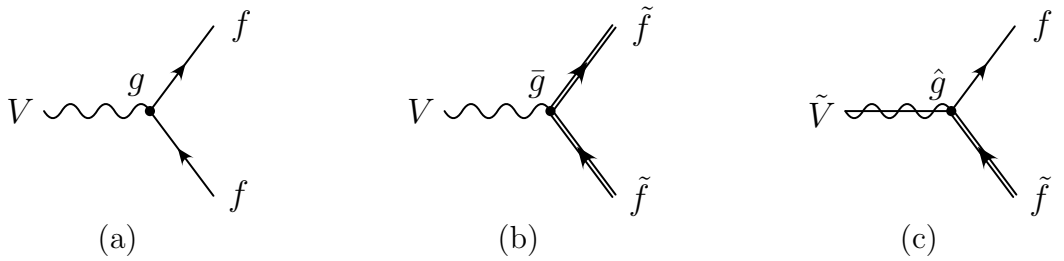

Figure 6.2: *Types of couplings in supersymmetric gauge theories. The arrow on the fermion and sfermion lines indicates lepton or baryon number flow.*

6.2 Testing the equivalence of SM gauge and MSSM Yukawa couplings

As well as precisely measuring the supersymmetry-breaking parameters—in particular sfermion and gaugino masses—it is essential to test that all other quantum numbers of the supersymmetric partners are identical to their Standard Model counterparts. For instance, supersymmetry requires the following couplings to be equal:

- The Standard Model gauge coupling g between a gauge boson V and a chiral fermion current f, Fig. 6.2 (a).
- The gauge coupling $\bar{g}$ between a gauge boson V and a scalar fermion current $\tilde{f}$, Fig. 6.2 (b).
- The Yukawa coupling $\hat{g}$ between gaugino $\tilde{V}$, fermion f and sfermion $\tilde{f}$, Fig. 6.2 (c).

Therefore, the exploration of supersymmetry at colliders requires the experimental verification of the relation $g = \bar{g} = \hat{g}$ for all gauge groups of the Standard Model. For the case of the SU(3) QCD sector, the relevant reference processes have been discussed elsewhere [14]. Here the focus is on the electroweak sector which comprises the hypercharge U(1) coupling g' and the SU(2) coupling g.

The Standard Model couplings g and g' are very accurately determined from low-energy and Z-peak observables. In the following, it will be discussed how precise values for the supersymmetry equivalents $\bar{g}^{(\prime)}$ and $\hat{g}^{(\prime)}$ can be obtained from the measurement of slepton pair production cross-sections in the continuum.

The pair production of smuons is particularly suited for the extraction of the gauge couplings $\bar{g}^{(\prime)}$, since this process is only mediated by the exchange of s-channel gauge bosons. By rephrasing the Born cross-section (3.3) for $\tilde{\mu}_\mathrm{R}$ production according to

$$\sigma[e^+ e^- \to \tilde{\mu}_\mathrm{R}^+ \tilde{\mu}_\mathrm{R}^-] = \frac{\alpha}{12s}\beta^3 \bar{g}'^2 \Bigg[c_\mathrm{W}^2 - \left(\tfrac{1}{2} - 2s_\mathrm{W}^2\right) \frac{s}{s - M_\mathrm{Z}^2} + \frac{1 + (1 - 4s_\mathrm{W}^2)^2}{16 c_\mathrm{W}^2} \left(\frac{s}{s - M_\mathrm{Z}^2}\right)^2 \Bigg], \tag{6.4}$$

it is apparent that it is directly proportional to the square of the U(1) coupling $\bar{g}'$. In this parametrization it is understood that the produced smuons are chiral eigenstates.

Alternatively, one could express the cross-section in terms of the photon- and Z-couplings. If in this case the electromagnetic charge of the smuons was assumed to be known, the cross-section would be sensitive to the weak isospin component of the smuons.

For the case of L-smuon production the situation is slightly more complicated because of the different photon- and Z-couplings,

$$\sigma[e^+e^- \to \tilde{\mu}_{\mathrm{L}}^+ \tilde{\mu}_{\mathrm{L}}^-] = \frac{\alpha}{48s}\beta^3 \Bigg[\bar{\lambda}_+^2 - \bar{\lambda}_+\bar{\lambda}_- \frac{1-4s_{\mathrm{W}}^2}{2s_{\mathrm{W}}c_{\mathrm{W}}} \frac{s}{s-M_{\mathrm{Z}}^2} + \bar{\lambda}_-^2 \frac{1+(1-4s_{\mathrm{W}}^2)^2}{16 s_{\mathrm{W}}^2 c_{\mathrm{W}}^2} \left(\frac{s}{s-M_{\mathrm{Z}}^2}\right)^2 \Bigg], \tag{6.5}$$

$$\bar{\lambda}_+ = c_{\mathrm{W}}\bar{g}' + s_{\mathrm{W}}\bar{g}, \qquad \bar{\lambda}_- = s_{\mathrm{W}}\bar{g}' - c_{\mathrm{W}}\bar{g}. \tag{6.6}$$

In the high-energy limit, the cross-sections for smuon production (6.4) and (6.5) get a particularly simple form,

$$\sigma[e^+e^- \to \tilde{\mu}_{\mathrm{R}}^+ \tilde{\mu}_{\mathrm{R}}^-] \xrightarrow{s\to\infty} \frac{5\alpha}{96s}\frac{\bar{g}'}{c_{\mathrm{W}}^2}, \tag{6.7}$$

$$\sigma[e^+e^- \to \tilde{\mu}_{\mathrm{L}}^+ \tilde{\mu}_{\mathrm{L}}^-] \xrightarrow{s\to\infty} \frac{\alpha}{384s}\left[\frac{5\bar{g}'}{c_{\mathrm{W}}^2} + \frac{2\bar{g}\bar{g}'}{s_{\mathrm{W}}c_{\mathrm{W}}} + \frac{\bar{g}}{s_{\mathrm{W}}^2}\right], \tag{6.8}$$

which has the virtue of being independent of any masses. However, also at realistic linear collider energies, the couplings $\bar{g}^{(\prime)}$ can be extracted without serious problems since the Z-boson mass M_{Z} and the weak mixing angles s_{W} are well-known quantities with almost negligible experimental errors.

In order to obtain a realistic picture of the attainable precision of the coupling determination, a detailed analysis has been performed using the methods of chapter 4. For instance, for the extraction of $\bar{g}'$ from $\tilde{\mu}_{\mathrm{R}}^+ \tilde{\mu}_{\mathrm{R}}^-$ production, the relevant experimental signature is $e^+e^- \to \mu^+\mu^- + \not{E}$. Standard Model and supersymmetric backgrounds have been taken into account and treated according to section 4.4. For this study the SPS1 scenario (see App. A) has been employed. No simulations of the detector acceptance are included.

It is assumed that 500 fb^{-1} of luminosity in the e^+e^- mode are spent at a centre-of-mass energy of $\sqrt{s} = 500$ GeV. By using an 80% right-polarized electron beam and a 50% left-polarized positron beam the cross-section is enhanced by a factor of 1.5. After application of appropriate cuts for background reduction this would result in about $N = 30000$ events with the given experimental signature. The statistical error $1/\sqrt{N}$ on the cross-section is very low, $\sim 0.6\%$.

There are also several sources for systematic errors. At first, the cross-section for smuon production depends crucially on the value of the smuon mass. Therefore, for the accurate determination of the smuon couplings, it is an important prerequisite to have precise measurements of the masses of the smuons. Taking the result of section 6.1, an error of $\delta m_{\tilde{\mu}_{\mathrm{R}}} = 360$ MeV has been assumed here. Furthermore the polarization uncertainty has to be taken into account. Here one can assume that the polarization degree may be determined to roughly 1%, using Compton scattering as a reference process.

Adding up both statistical and systematic errors, it turns out that the gauge coupling $\bar{g}'$ can be extracted from $\tilde{\mu}_{\mathrm{R}}^+ \tilde{\mu}_{\mathrm{R}}^-$ production with a total error of

$$\frac{\delta\bar{g}'}{\bar{g}'} \approx 1\%. \tag{6.9}$$

One could try to include detector effects by a simple global acceptance factor $\epsilon_{\mathrm{det}} = 0.5$. In fact this would only lead to a slight reduction of the expected accuracy down to $\delta\bar{g}'/\bar{g}' \approx 1.2\%$. This can be explained by the fact that the statistics are actually not the major limiting factor for the obtainable precision. The most important source for uncertainties is the error in the determination of the smuon mass $m_{\tilde{\mu}_{\mathrm{R}}}$.

The supersymmetric Yukawa couplings $\hat{g}^{(\prime)}$ can be determined from selectron production, since the t-/u-channel contributions, see Fig. 3.1 (b,c), directly depend on the Yukawa couplings. This has been considered for the e^+e^- mode in Ref. [116]. The e^-e^- mode has some advantages due to reduced background, larger cross-section, higher polarizability and no interfering s-channel contributions [119]; on the other hand, the expected luminosity in this case is substantially lower. Here both cases shall be studied carefully, taking into account the relevant backgrounds as mentioned before.

In comparison to the smuon case, additional complexity arises due to the dependence on the neutralino sector. In principle this difficulty could be avoided by going to high energies $\sqrt{s} \gg m_{\tilde{\chi}_i^0}$. From the general formula for $e^+e^- \to \tilde{e}_i^+\tilde{e}_i^-$, eq. (3.7), one obtains a universal leading logarithmic contribution

$$\sigma[e^+\,e^- \to \tilde{e}_{\mathrm{R}}^+\,\tilde{e}_{\mathrm{R}}^-] \xrightarrow{s\to\infty} \frac{\hat{g}'^4}{16\pi}\,\frac{\log s}{s} + \mathcal{O}\left(\frac{1}{s}\right), \tag{6.10}$$

$$\sigma[e^+\,e^- \to \tilde{e}_{\mathrm{L}}^+\,\tilde{e}_{\mathrm{L}}^-] \xrightarrow{s\to\infty} \frac{(\hat{g}^2+\hat{g}'^2)^2}{16\pi}\,\frac{\log s}{s} + \mathcal{O}\left(\frac{1}{s}\right). \tag{6.11}$$

In (6.10) and (6.11) all terms which depend on parameters of the neutralino sector have dropped out, as a consequence of the unitarity of the neutralino mixing matrix. However one can see from Fig. 6.3 that rather large values of $\sqrt{s}$ are needed to realize this model-independent procedure for determining the Yukawa couplings in practice. The figure shows the cross-section $\sigma(s)$ multiplied by s over a logarithmic scale for $\sqrt{s}$, so that a linear slope is obtained for the leading logarithmic term $\sim \log(s)/s$. In Fig. 6.3 (b) a constant offset term is subtracted [corresponding to the term of $\mathcal{O}(1/s)$ in $\sigma(s)$], so that the two curves overlap in the high-energy limit. A reasonable agreement between the asymptotic logarithmic contribution and the full cross-section is given only for $\sqrt{s} \gtrsim 2$ TeV.

For a realistic analysis of the determination of the Yukawa couplings from selectron production it is therefore necessary to use information about the neutralino sector. In the following it is assumed that the neutralino sector has the form of the MSSM. The neutralino mass matrix, see (2.34), essentially depends on three parameters, M_1, M_2 and μ. The dependence on $\tan\beta$ is relatively mild and can be neglected if the value of $\tan\beta$ can be extracted with moderate accuracy from some other measurement like Higgs decay branching ratios. All Standard Model parameters in (2.34) are known with high accuracy so that no uncertainties for these parameters need to be taken into account. The three parameters M_1, M_2 and μ can be inferred from three reference measurements, for example the masses of the two charginos $\tilde{\chi}_1^\pm$, $\tilde{\chi}_2^\pm$ and the mass of the lightest neutralino $\tilde{\chi}_1^0$. Simulations show [10, 15] that these three masses can be determined with high accuracy. Since the experimental accuracy can significantly depend on the chosen scenario, here slightly more conservative error estimates are taken,

$$\delta m_{\tilde{\chi}_1^\pm} = 100\ \mathrm{GeV}, \qquad \delta m_{\tilde{\chi}_2^\pm} = 400\ \mathrm{GeV}, \qquad \delta m_{\tilde{\chi}_1^0} = 100\ \mathrm{GeV}. \tag{6.12}$$

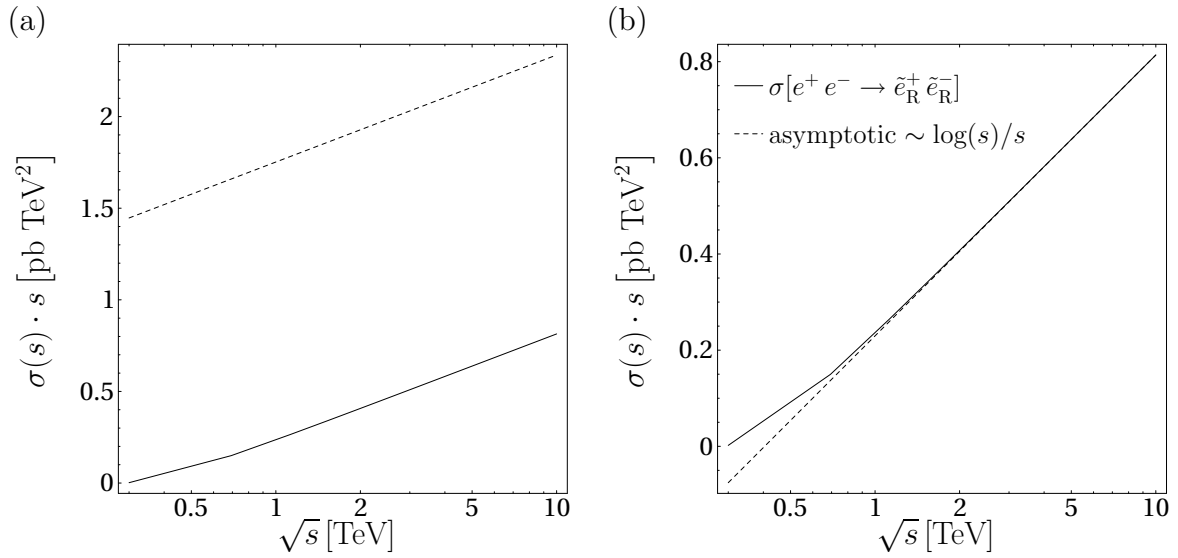

Figure 6.3: *Cross-section of $e^+e^- \to \tilde{e}_R^+ \tilde{e}_R^-$ for high centre-of-mass energies $\sqrt{s}$ in comparison with the asymptotic leading logarithmic contributions $\sim \log(s)/s$ (a), after subtraction of a constant offset term (b). Values for SPS1 scenario.*

Similar to the smuon case, the cross-section for selectron production sensitively depends on the selectron mass. Here the errors in the second column of Tab. 6.1 obtained from threshold scan fits are taken.

The total selectron cross-section and signal-to-background ratio can be enhanced by polarizing the incoming beams accordingly. The favourable polarization combinations for the production of right- and left-chiral selectron in e^+e^- and e^-e^- scattering have been discussed in section 4.4. It is assumed that the polarization degree can be controlled up to 1%.

Backgrounds both from Standard Model and supersymmetric processes are taken into account and can be reduced by the methods discussed in section 4.4. The various possible cross-sections and experimental signatures that could be used for measuring the Yukawa couplings in the selectron sector are listed in Tab. 6.2. For the discrimination between

process	polarization	L
$e^+e^- \to (\tilde{e}_R^+\tilde{e}_R^-) \to e^+e^-\,\tilde{\chi}_1^0\,\tilde{\chi}_1^0$	$P_{e^-} = +80\%$, $P_{e^+} = -50\%$	
$e^+e^- \to (\tilde{e}_R^\pm\tilde{e}_L^\mp) \to e^+e^-\,\tilde{\chi}_1^0\,\tilde{\chi}_2^0$	$P_{e^-} = -80\%$, $P_{e^+} = -50\%$	500 fb^{-1}
$\to e^+e^-\,\tau^+\tau^-\,\tilde{\chi}_1^0\,\tilde{\chi}_1^0$		
$e^-e^- \to (\tilde{e}_R^-\tilde{e}_R^-) \to e^-e^-\,\tilde{\chi}_1^0\,\tilde{\chi}_1^0$	$P_{e^-} = +80\%$	
$e^-e^- \to (\tilde{e}_L^-\tilde{e}_L^-) \to e^-e^-\,\tilde{\chi}_2^0\,\tilde{\chi}_2^0$	$P_{e^-} = -80\%$	50 fb^{-1}
$\to e^-e^-\,\tau\tau\tau\tau\,\tilde{\chi}_1^0\,\tilde{\chi}_1^0$		

Table 6.2: *Selectron production processes for different chirality combination used for extracting the supersymmetric Yukawa couplings. The optimal polarization combinations and the expected luminosity are also given.*

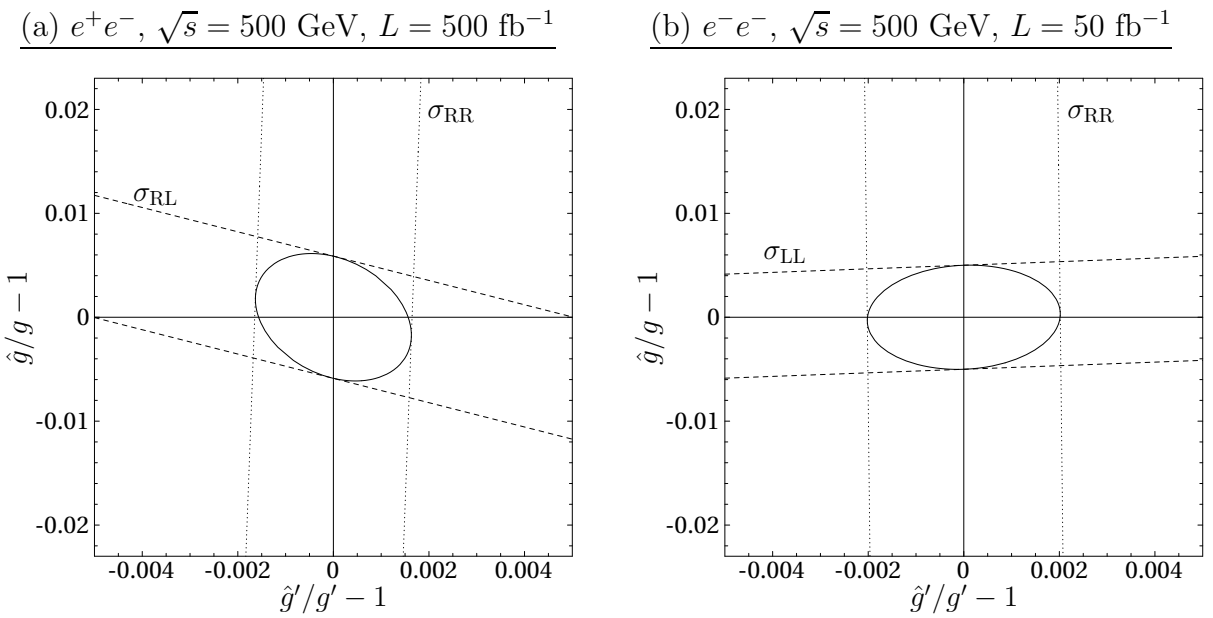

Figure 6.4: *1σ bounds on the determination of the supersymmetric Yukawa couplings $\hat{g}$ and $\hat{g}'$ from selectron cross-section measurements. The two plots compare the information obtained from the cross-sections $\sigma_{\mathrm{RR}} = \sigma[e^+ e^- \to \tilde{e}_{\mathrm{R}}^+ \tilde{e}_{\mathrm{R}}^-]$ and $\sigma_{\mathrm{RL}} = \sigma[e^+ e^- \to \tilde{e}_{\mathrm{R}}^\pm \tilde{e}_{\mathrm{L}}^\mp]$ in the e^+e^- mode (a) as well as $\sigma_{\mathrm{RR}} = \sigma[e^- e^- \to \tilde{e}_{\mathrm{R}}^- \tilde{e}_{\mathrm{R}}^-]$ and $\sigma_{\mathrm{LL}} = \sigma[e^- e^- \to \tilde{e}_{\mathrm{L}}^- \tilde{e}_{\mathrm{L}}^-]$ in the e^-e^- mode, respectively. Values for SPS1 scenario.*

left- and right-chiral states, beam polarization [18] and the decay of L-selectrons into taus, $\tilde{e}_{\mathrm{L}}^\pm \to e^\pm \tilde{\chi}_2^0 \to e^\pm \tau^+\tau^- \tilde{\chi}_1^0$, is employed. Because of the anti-pinch effect in the e^-e^- mode only one tenth of the designated e^+e^- luminosity is assumed for this case.

With this information and taking into account the aforementioned statistical and systematic errors, the resulting constraints on the Yukawa couplings $\hat{g}$ and $\hat{g}'$ from selectron cross-section measurements are shown in Fig. 6.4 for the case of the SPS1 scenario. From the overlap regions of the 1σ contours the following resulting accuracies can be read off,

$$e^+e^- : \qquad \frac{\delta\hat{g}'}{\hat{g}'} \approx 0.18\%, \qquad \frac{\delta\hat{g}}{\hat{g}} \approx 0.7\%, \tag{6.13}$$

$$e^-e^- : \qquad \frac{\delta\hat{g}'}{\hat{g}'} \approx 0.21\%, \qquad \frac{\delta\hat{g}}{\hat{g}} \approx 0.5\%. \tag{6.14}$$

The precisions obtained from measurements in the e^+e^- and e^-e^- mode are roughly comparable. The larger cross-sections and low background contamination in the e^-e^- mode are compensated by the higher luminosity in the e^+e^- mode. Nevertheless, the error for the determination of $\hat{g}$ in e^-e^- scattering is slightly lower than the error for e^+e^- annihilation. This can be understood by considering the different production processes. In the e^-e^- mode, the coupling $\hat{g}$ is extracted from the cross-section for $\tilde{e}_{\mathrm{L}}^-\tilde{e}_{\mathrm{L}}^-$ production. Since both produced selectrons are left-chiral, their couplings to neutralinos are both sensitive on $\hat{g}$. On the other hand, in the e^+e^- mode, $\hat{g}$ is determined from the cross-section for $\tilde{e}_{\mathrm{R}}^\pm\tilde{e}_{\mathrm{L}}^\mp$ production, which involves only one Yukawa-coupling depending on $\hat{g}$.

Alternatively, it is possible to extract the Yukawa couplings from the measurement of the cross-sections for neutralino pair production [123]. While the precision for the SU(2)-related Yukawa coupling g is comparable in both methods, the U(1)-related Yukawa coupling g' can be determined far more accurately in selectron pair production. In addition, the accuracy obtained from neutralino production will be somewhat reduced when including the decays of the neutralinos, which has not been done in [123].

As before, no simulation of the detector performance is included in this study. In order to roughly estimate the effect of the detector acceptance it is assumed that a final tau pair can be identified with an efficiency of $\epsilon_\tau = 80\%$. In addition a global acceptance factor $\epsilon_{\text{det}} = 0.5$ for the tagging of the electrons is included. With these refinements the resulting precision of the Yukawa coupling extraction is reduced to

$$e^+e^- : \qquad \frac{\delta\hat{g}'}{\hat{g}'} \approx 0.18\%, \qquad \frac{\delta\hat{g}}{\hat{g}} \approx 0.8\%, \tag{6.15}$$

$$e^-e^- : \qquad \frac{\delta\hat{g}'}{\hat{g}'} \approx 0.23\%, \qquad \frac{\delta\hat{g}}{\hat{g}} \approx 0.8\%. \tag{6.16}$$

The errors on the determination of $\hat{g}'$ and $\hat{g}$ are only slightly increased since the statistics are actually of minor importance for the overall errors. The obtainable precision is mainly limited by the uncertainty of the selectron masses $m_{\tilde{e}_{\text{R}}}$, $m_{\tilde{e}_{\text{L}}}$ and the beam polarization. Since the dependence on the statistical effects is rather weak, one may assume that the picture will not change substantially when replacing the crude estimate for the detector acceptance by a more detailed simulation.

The above studies on coupling determinations have been performed by using tree-level approximations for the matrix elements. For the impressive precision that can be achieved, see (6.9), (6.15) and (6.16), it is clearly necessary to include radiative corrections in the analysis. As a first step in this respect, complete next-to-leading order calculations for the pair production of right-chiral smuons and selectrons have been presented in chapter 5.

However the inclusion of radiative corrections in the analysis brings about additional subtleties. Since the virtual loop contributions involve almost the complete particle content of the MSSM, the one-loop prediction of the slepton cross-section depends on basically all parameters of the model. Accordingly the precise determination of supersymmetric couplings would require some knowledge on all these parameters. A consistent treatment would involve a simultaneous fit of the model to all available observables. Radiative corrections can then be included by an iterative procedure. Such a global analysis is however beyond the scope of this work. Nevertheless, in order to obtain a first estimate of the expected precision for the coupling determination, a tree-level analysis is sufficient.

Chapter 7

Conclusions

This thesis has presented a theoretical and phenomenological analysis of precision physics with the supersymmetric partners of the muons and electrons, scalar muons and scalar electrons, at future e^+e^- and e^-e^- linear colliders.

On one hand, a major task in the exploration of supersymmetry will be the determination of the supersymmetry-breaking parameters, in particular the masses of the superpartners. While it is obvious that supersymmetry needs to be broken if it is realized in nature, since none of the superpartners has been observed yet, the source of supersymmetry breaking is still unknown. Thus a large number of additional parameters is involved in the most general parametrization of soft supersymmetry breaking, posing an enormous experimental effort for their investigation. Furthermore, it is of particular importance to determine the soft-breaking parameters with high accuracy in order to be able to reconstruct the underlying breaking mechanism, which eventually involves extrapolations of the soft-breaking parameters to high energy scales.

For this purpose a clean experimental environment with high luminosity is required, which is provided by the concept of a high-energy e^+e^- linear collider. With such a machine it is possible to determine the masses of the scalar leptons with unparallelled precision from scans of the threshold excitation curves. Moreover, the measurement of cross-sections in the continuum provides accurate information about couplings and mixings of the sleptons.

As a consequence, accurate theoretical predictions of the pair production cross-sections are required. As two key points for a reliable computation near threshold, the inclusion of finite width effects and Coulomb corrections was discussed. Special attention was paid to the preservation of gauge invariance in the matrix elements. Backgrounds both from Standard Model and supersymmetric sources were computed including dominant contributions from pair production processes as well as sub-dominant contributions and interference effects. They can be controlled with suitable cuts and beam polarization. Nevertheless, a detailed simulation is necessary for estimating the remaining contributions.

Using these theoretical tools, an improved analysis of the measurement of slepton masses near threshold was performed. The excitations curves are characterized by their distinct rise proportional to the velocity or the third power of the velocity of the sleptons. The inclusion of sub-dominant backgrounds reduces the precision expected in previous studies. Nevertheless the measurement of the threshold cross-section proves to be the

favourable method for the precise determination of slepton masses. The resulting precision that can be expected is about a few 100 MeV for slepton masses around 200 GeV, corresponding to an accuracy at the per-mille level. In the particular case of the R-selectron mass a precision of even 2×10^{-4} can be obtained from the measurement in the e^-e^- mode, which benefits from the sharp rise of the excitation curve proportional to the selectron velocity.

Furthermore, a phenomenological method was developed which allows one to extract the masses without knowledge on other sectors of the MSSM, in particular the neutralino parameters. For the case of the selectrons, it is also possible to determine their decay widths with an error of 10–20%.

On the other hand, it was pointed out that one of the most important building blocks for establishing supersymmetry experimentally is the test of the equivalence between the Standard Model gauge couplings and their supersymmetric counterparts. Irrespective of the source of supersymmetry breaking, supersymmetric theories generally make the non-trivial prediction that the gauge coupling between a vector boson and a fermion or sfermion current is equal to the Yukawa coupling between the corresponding gaugino, fermion and sfermion. In order to test this relation, these couplings need to be determined with high precision, which can be achieved by measuring the production cross-sections for scalar leptons.

The pair production of scalar muons is particularly suited for extracting the gauge couplings of the smuons, since this process is mediated by s-channel gauge boson exchange. In contrast, the Yukawa couplings between electrons, selectrons and gauginos can be probed stringently in selectron pair production due to the t-channel gaugino exchange. In the analysis of the statistical and systematic uncertainties it was shown that from a measurement of the production cross-section these couplings can be extracted with a precision better than the per-cent level. In particular the accuracy that can be achieved in the determination of the U(1) gauge coupling and its Yukawa counterpart is superior to other methods.

On the theoretical side this requires the computation of precise predictions for the cross-sections. To this end, the complete next-to-leading order electroweak radiative corrections to the production of right-chiral smuons and selectrons in the MSSM have been calculated. Since in the continuum far above threshold, finite width effects are of minor importance, the final state sleptons have been treated on-shell. The size of the corrections were found to be sizeable, of the order of 5–10%. In a detailed analysis the dependence of the results on the soft-breaking parameters was discussed, notably non-decoupling contributions from virtual loops. While their effect was found to be non-negligible, it yet seems difficult to use them for inferring information on hypothetical heavy superpartners from the measurement of slepton cross-sections.

For the various investigations in this thesis, the production of scalar electrons in e^+e^- annihilation was compared to the corresponding processes in e^-e^- scattering. The e^-e^- mode turns out to be particularly favourable for the measurement of the selectron masses in threshold scans. Nevertheless, it also can provide complementary information on the selectron Yukawa couplings.

This thesis provides a first step towards the establishment of a firm theoretical basis for precision analyses in the scalar lepton sector at future linear colliders. It was shown

that important information about the masses and couplings of the sleptons can be obtained with high precision. More detailed studies, in particular in the field of radiative corrections, have to follow in order to match the experimental accuracy that is expected for the determination of the masses and couplings of the selectrons and smuons. Clearly they have to be supplemented with dedicated experimental simulations in order to obtain realistic results and to fully explore the phenomenology of the scalar leptons.

The precise determination of superpartner properties provides the basis for systematic extrapolations to higher scales in order to disentangle the physics that govern the breaking of supersymmetry. Since the breaking mechanism may eventually be related to gravitational interactions, one could thus obtain a window to the sector of gravity from collider particle physics.

Appendix A

Reference scenarios

Since the MSSM contains a large number of unknown soft-breaking parameters, it is impossible to perform a complete scan over the parameter space. Therefore, reference scenarios are used as typical examples of expected particle spectra. For the numerical results in this thesis, two reference scenarios were chosen.

The scenario 1 from the "Snowmass Points and Slopes" (SPS1) is part of a list of supersymmetric benchmark scenarios that was selected at the 2001 Snowmass workshop *"Summer Study on the Future of Particle Physics"* [124]. The SPS1 scenario is a typical mSUGRA scenario with relatively light sparticle masses. For the evolution of the breaking parameters down to weak scale the program *Isajet 7.58* [125] was specified. The low-scale parameters can be found in [126].

In order to emphasize the effect of finite slepton widths, the RR2 reference point of the Tesla study was chosen [10,127]. This scenario is an example of the fact that slepton widths can be relatively large, i.e. of the order $\mathcal{O}(1\text{ GeV})$ for slepton masses around 200 GeV. For the low-scale parameters, see [127].

The tree-level Higgs masses receive large radiative corrections (see also section 2.2.3). For the computation of the corrected masses, the program *FeynHiggs* [128] was employed, which encorporates full one-loop and leading two-loop corrections.

For the calculation of processes with multi-particle final states, the finite widths of the intermediate resonant particles is needed, see section 4.3. The Higgs decay widths including QCD corrections were computed with the program *Hdecay* [129]. In some cases, the lighter neutralinos and charginos can only decay into a three-particle final state[1]. The three-particle partial decay widths have been evaluated using the formulae of Ref. [130]. The remaining two-particle decay contributions can be calculated from simple tree-level formulae.

In the following the relevant particle masses, decay widths and branching ratios for this work are listed.

[1]Even if some two-particle decay channels are kinematically accessible, the effect of the three-particle decay modes may be non-negligible.

SPS 1 – mSUGRA scenario

Standard Model parameters:

$$\begin{aligned} M_{\rm Z} &= 91.1875 \text{ GeV}, & \sin^2\theta_{\rm W} &= 0.2309, \\ m_{\rm t} &= 175 \text{ GeV}, & \alpha(M_{\rm Z}) &= 1/127.70, \\ m_\tau &= 1.777 \text{ GeV}. \end{aligned} \tag{A.1}$$

Fundamental unification scale parameters:

$$m_0 = 100 \text{ GeV}, \quad M_{1/2} = 250 \text{ GeV}, \quad A_0 = -100 \text{ GeV}, \quad \tan\beta = 10, \quad \mu > 0. \tag{A.2}$$

Weak scale soft-breaking parameters of (2.18), generated with *Isajet 7.58* [126]:

$$\begin{aligned} M_1 &= 99.13 \text{ GeV}, & m_{\tilde{\rm e}_{\rm L}} = m_{\tilde{\mu}_{\rm L}} &= 196.64 \text{ GeV}, & m_{\tilde{\tau}_{\rm L}} &= 195.75 \text{ GeV}, \\ M_2 &= 192.74 \text{ GeV}, & m_{\tilde{\rm e}_{\rm R}} = m_{\tilde{\mu}_{\rm R}} &= 136.23 \text{ GeV}, & m_{\tilde{\tau}_{\rm R}} &= 133.55 \text{ GeV}, \\ \mu &= 352.39 \text{ GeV}, & m_{\tilde{\rm u}_{\rm L},\tilde{\rm d}_{\rm L}} = m_{\tilde{\rm c}_{\rm L},\tilde{\rm s}_{\rm L}} &= 539.86 \text{ GeV}, & m_{\tilde{\rm t}_{\rm L},\tilde{\rm b}_{\rm L}} &= 495.91 \text{ GeV}, \\ M_{\rm A^0} &= 393.63 \text{ GeV}, & m_{\tilde{\rm u}_{\rm R}} = m_{\tilde{\rm c}_{\rm R}} &= 521.66 \text{ GeV}, & m_{\tilde{\rm t}_{\rm R}} &= 424.83 \text{ GeV}, \\ \tan\beta &= 10, & m_{\tilde{\rm d}_{\rm R}} = m_{\tilde{\rm s}_{\rm R}} &= 519.53 \text{ GeV}, & m_{\tilde{\rm b}_{\rm R}} &= 516.86 \text{ GeV}, \end{aligned}$$

$$A_\tau = -254.20 \text{ GeV}, \qquad A_{\rm t} = -510.01 \text{ GeV}, \qquad A_{\rm b} = -772.66 \text{ GeV}. \tag{A.3}$$

Particle spectrum. Only the relevant data for this work are given:

Sfermions particle	mass m [GeV] width Γ [GeV]	decay modes
$\tilde{l}_{\rm R} = \tilde{e}_{\rm R}/\tilde{\mu}_{\rm R}$	$m = 142.97$ $\Gamma = 0.21$	$\tilde{l}_{\rm R}^- \to l^- \tilde{\chi}_1^0$ 100%
$\tilde{l}_{\rm L} = \tilde{e}_{\rm L}/\tilde{\mu}_{\rm L}$	$m = 202.14$ $\Gamma = 0.25$	$\tilde{l}_{\rm L}^- \to l^- \tilde{\chi}_1^0$ 48% $\to l^- \tilde{\chi}_2^0$ 19% $\to \nu_l \tilde{\chi}_1^-$ 33%
$\tilde{\nu}_l = \tilde{\nu}_e/\tilde{\nu}_\mu$	$m = 198.99$ $\Gamma = 0.16$	$\tilde{\nu}_l \to \nu_l \tilde{\chi}_1^0$ 88% $\to \nu_l \tilde{\chi}_2^0$ 3% $\to l^- \tilde{\chi}_1^+$ 9%

$\tilde{\tau}_1$	$m = 133.20$	$\tilde{u}_{\rm R}$	$m = 520.46$	$\tilde{t}_1$	$m = 375.72$
$\tilde{\tau}_2$	$m = 206.14$	$\tilde{u}_{\rm L}$	$m = 537.24$	$\tilde{t}_2$	$m = 585.16$
$\tilde{\nu}_\tau$	$m = 195.05$	$\tilde{d}_{\rm R}$	$m = 520.13$	$\tilde{b}_1$	$m = 488.00$
		$\tilde{d}_{\rm L}$	$m = 543.04$	$\tilde{b}_2$	$m = 528.24$

Neutralinos/Charginos particle	mass m [GeV] width Γ [GeV]	decay modes	
$\tilde{\chi}_1^0$	$m = 96.07$	—	
$\tilde{\chi}_2^0$	$m = 176.81$	$\tilde{\chi}_2^0 \to \tilde{e}_{\mathrm{R}}^{\pm}\, e^{\mp}$	6%
	$\Gamma = 0.020$	$\to \tilde{\mu}_{\mathrm{R}}^{\pm}\, \mu^{\mp}$	6%
		$\to \tilde{\tau}_1^{\pm}\, \tau^{\mp}$	88%
		$\to q\, \bar{q}\, \tilde{\chi}_1^0$	0.1%
$\tilde{\chi}_3^0$	$m = 358.81$	$\tilde{\chi}_3^0 \to \tilde{\chi}_1^{\pm}\, W^{\mp}$	59%
	$\Gamma = 2.02$	$\to \tilde{\chi}_1^0\, Z$	11%
		$\to \tilde{\chi}_2^0\, Z$	21%
$\tilde{\chi}_4^0$	$m = 377.80$	$\tilde{\chi}_4^0 \to \tilde{\chi}_1^{\pm}\, W^{\mp}$	52%
	$\Gamma = 2.80$	$\to \tilde{\chi}_1^0\, h_0$	7%
		$\to \tilde{\chi}_2^0\, h_0$	14%
		$\to \tilde{\nu}\, \bar{\nu},\ \tilde{\nu}^*\, \nu$	15%
$\tilde{\chi}_1^{\pm}$	$m = 176.22$	$\tilde{\chi}_1^+ \to \tilde{\tau}_1^+\, \nu_\tau$	100%
	$\Gamma = 0.014$		
$\tilde{\chi}_2^{\pm}$	$m = 378.24$	$\tilde{\chi}_2^+ \to \tilde{\chi}_1^0\, W^+$	6%
	$\Gamma = 2.65$	$\to \tilde{\chi}_2^0\, W^+$	29%
		$\to \tilde{\chi}_1^+\, Z$	24%
		$\to \tilde{\chi}_1^+\, h_0$	18%
		$\to \tilde{e}_{\mathrm{L}}^+\, \nu_e$	5%
		$\to \tilde{\mu}_{\mathrm{L}}^+\, \nu_\mu$	5%
		$\to \tilde{\tau}_2^+\, \nu_\tau$	6%

Higgs particle	tree-level mass [GeV]	mass from *FeynHiggs* [GeV]	width Γ from *HDECAY* [GeV]
h_0	89.28	122.61	0.0038
H_0	394.07	393.56	0.97
A_0	393.63	393.63	1.43

RR2 – mSUGRA scenario

Standard Model parameters:

$$\begin{aligned} M_{\mathrm{Z}} &= 91.187 \text{ GeV}, & \sin^2\theta_{\mathrm{W}} &= 0.2315, \\ m_{\mathrm{t}} &= 175 \text{ GeV}, & \alpha(M_{\mathrm{Z}}) &= 1/128.87, \\ m_{\tau} &= 1.777 \text{ GeV}. \end{aligned} \tag{A.4}$$

Fundamental unification scale parameters:

$$m_0 = 160 \text{ GeV}, \quad M_{1/2} = 200 \text{ GeV}, \quad A_0 = 600 \text{ GeV}, \quad \tan\beta = 30, \quad \mu > 0. \tag{A.5}$$

Weak scale soft-breaking parameters of (2.18), from [127]:

$$\begin{aligned} M_1 &= 78.0 \text{ GeV}, & m_{\tilde{\mathrm{e}}_{\mathrm{L}}} = m_{\tilde{\mu}_{\mathrm{L}}} &= 212 \text{ GeV}, & m_{\tilde{\tau}_{\mathrm{L}}} &= 189 \text{ GeV}, \\ M_2 &= 150 \text{ GeV}, & m_{\tilde{\mathrm{e}}_{\mathrm{R}}} = m_{\tilde{\mu}_{\mathrm{R}}} &= 179 \text{ GeV}, & m_{\tilde{\tau}_{\mathrm{R}}} &= 115 \text{ GeV}, \\ \mu &= 263 \text{ GeV}, & m_{\tilde{\mathrm{u}}_{\mathrm{L}},\tilde{\mathrm{d}}_{\mathrm{L}}} = m_{\tilde{\mathrm{c}}_{\mathrm{L}},\tilde{\mathrm{s}}_{\mathrm{L}}} &= 462 \text{ GeV}, & m_{\tilde{\mathrm{t}}_{\mathrm{L}},\tilde{\mathrm{b}}_{\mathrm{L}}} &= 409 \text{ GeV}, \\ M_{\mathrm{A}^0} &= 257 \text{ GeV}, & m_{\tilde{\mathrm{u}}_{\mathrm{R}}} = m_{\tilde{\mathrm{c}}_{\mathrm{R}}} &= 447 \text{ GeV}, & m_{\tilde{\mathrm{t}}_{\mathrm{R}}} &= 358 \text{ GeV}, \\ \tan\beta &= 30, & m_{\tilde{\mathrm{d}}_{\mathrm{R}}} = m_{\tilde{\mathrm{s}}_{\mathrm{R}}} &= 445 \text{ GeV}, & m_{\tilde{\mathrm{b}}_{\mathrm{R}}} &= 421 \text{ GeV}, \\ A_{\tau} &= 384 \text{ GeV}, & A_{\mathrm{t}} &= -258 \text{ GeV}, & A_{\mathrm{b}} &= -178 \text{ GeV}. \end{aligned} \tag{A.6}$$

Particle spectrum. Only the relevant data for this work are given:

Sfermions particle	mass m [GeV] width Γ [GeV]	decay modes
$\tilde{l}_{\mathrm{R}} = \tilde{e}_{\mathrm{R}}/\tilde{\mu}_{\mathrm{R}}$	$m = 184.39$	$\tilde{l}_{\mathrm{R}}^- \to l^- \tilde{\chi}_1^0$ 99%
	$\Gamma = 0.62$	$\to l^- \tilde{\chi}_2^0$ 0.8%
$\tilde{l}_{\mathrm{L}} = \tilde{e}_{\mathrm{L}}/\tilde{\mu}_{\mathrm{L}}$	$m = 217.19$	$\tilde{l}_{\mathrm{L}}^- \to l^- \tilde{\chi}_1^0$ 14%
	$\Gamma = 1.03$	$\to l^- \tilde{\chi}_2^0$ 34%
		$\to \nu_l \tilde{\chi}_1^-$ 52%
$\tilde{\nu}_l = \tilde{\nu}_e/\tilde{\nu}_{\mu}$	$m = 201.98$	$\tilde{\nu}_l \to \nu_l \tilde{\chi}_1^0$ 25%
	$\Gamma = 0.87$	$\to \nu_l \tilde{\chi}_2^0$ 20%
		$\to l^- \tilde{\chi}_1^+$ 55%

$\tilde{\tau}_1$	$m = 94.89$	$\tilde{u}_{\mathrm{R}}$	$m = 445.57$	$\tilde{t}_1$	$m = 354.91$
$\tilde{\tau}_2$	$m = 209.99$	$\tilde{u}_{\mathrm{L}}$	$m = 458.89$	$\tilde{t}_2$	$m = 476.01$
$\tilde{\nu}_{\tau}$	$m = 177.69$	$\tilde{d}_{\mathrm{R}}$	$m = 445.72$	$\tilde{b}_1$	$m = 367.08$
		$\tilde{d}_{\mathrm{L}}$	$m = 465.78$	$\tilde{b}_2$	$m = 462.57$

Neutralinos/Charginos particle	mass m [GeV] width Γ [GeV]	decay modes	
$\tilde{\chi}_1^0$	$m = 74.81$	—	
$\tilde{\chi}_2^0$	$m = 133.04$	$\tilde{\chi}_2^0 \to \tilde{\tau}_1^\pm \tau^\mp$	100%
	$\Gamma = 0.052$		
$\tilde{\chi}_3^0$	$m = 272.81$	$\tilde{\chi}_3^0 \to \tilde{\chi}_1^\pm W^\mp$	53%
	$\Gamma = 1.26$	$\to \tilde{\chi}_1^0 Z$	11%
		$\to \tilde{\chi}_2^0 Z$	14%
		$\to \tilde{\tau}_1^\pm \tau^\mp$	11%
		$\to \tilde{\tau}_2^\pm \tau^\mp$	4%
$\tilde{\chi}_4^0$	$m = 292.96$	$\tilde{\chi}_4^0 \to \tilde{\chi}_1^\pm W^\mp$	52%
	$\Gamma = 1.81$	$\to \tilde{\chi}_1^0 h_0$	6%
		$\to \tilde{\chi}_2^0 h_0$	10%
		$\to \tilde{\nu}\,\bar{\nu},\ \tilde{\nu}^*\,\nu$	14%
$\tilde{\chi}_1^\pm$	$m = 132.36$	$\tilde{\chi}_1^+ \to \tilde{\tau}_1^+ \nu_\tau$	100%
	$\Gamma = 0.044$		
$\tilde{\chi}_2^\pm$	$m = 294.84$	$\tilde{\chi}_2^+ \to \tilde{\chi}_1^0 W^+$	6%
	$\Gamma = 1.64$	$\to \tilde{\chi}_2^0 W^+$	30%
		$\to \tilde{\chi}_1^+ Z$	22%
		$\to \tilde{\chi}_1^+ h_0$	15%
		$\to \tilde{\tau}_2^+ \nu_\tau$	7%
		$\to \tilde{\nu}_\tau \tau^+$	7%

Higgs particle	tree-level mass [GeV]	mass from *FeynHiggs* [GeV]	width Γ from *HDECAY* [GeV]
h_0	90.96	123.38	0.0088
H_0	257.08	256.40	5.84
A_0	257.00	257.00	5.26

Bibliography

[1] S. L. Glashow, Nucl. Phys. **22** (1961) 579;
S. Weinberg, Phys. Rev. Lett. **19** (1967) 1264;
A. Salam, in *Elementary Particle Theory*, ed. N. Svartholm (Almquist and Wiksell, Stockholm, 1968) 367.

[2] S. L. Glashow, J. Iliopoulos and L. Maiani, Phys. Rev. D **2** (1970) 1285;
H. Fritzsch, M. Gell-Mann and H. Leutwyler, Phys. Lett. B **47** (1973) 365.

[3] H. Spiesberger, M. Spira and P. M. Zerwas, in *Scattering*, ed. P. Sabatier, Academic Press, London (2000) [hep-ph/0011255].

[4] J. Wess and B. Zumino, Phys. Lett. B **49** (1974) 52;
J. Wess and B. Zumino, Nucl. Phys. B **70** (1974) 39.

[5] R. Haag, J. T. Lopuszanski and M. Sohnius, Nucl. Phys. B **88** (1975) 257.

[6] L. Girardello and M. T. Grisaru, Nucl. Phys. B **194** (1982) 65.

[7] TESLA Technical Design Report, Part I, eds. F. Richard, J. R. Schneider, D. Trines and A. Wagner, DESY-2001-11A, [hep-ph/0106314].

[8] [NLC Collaboration], in *Proc. of the APS/DPF/DPB Summer Study on the Future of Particle Physics (Snowmass 2001)* eds. R. Davidson and C. Quigg, SLAC-R-571.

[9] N. Akasaka *et al.* [JLC Design Study Group], KEK-REPORT-97-1.

[10] TESLA Technical Design Report, Part III, eds. R. Heuer, D. J. Miller, F. Richard and P. M. Zerwas, DESY-2001-11C, [hep-ph/0106315].

[11] T. Abe *et al.* [American Linear Collider Working Group Collaboration], in *Proc. of the APS/DPF/DPB Summer Study on the Future of Particle Physics (Snowmass 2001)* eds. R. Davidson and C. Quigg, SLAC-R-570, [hep-ex/0106056].

[12] K. Abe *et al.* [ACFA Linear Collider Working Group Collaboration], KEK-REPORT-2001-11, [hep-ph/0109166].

[13] G. A. Blair, W. Porod and P. M. Zerwas, Phys. Rev. D **63** (2001) 017703 [hep-ph/0007107].

[14] M. Weber, Dissertation, Hamburg (2001), DESY-THESIS-2002-003;
M. Maniatis, Dissertation, Hamburg (2002), DESY-THESIS-2002-007;
A. Brandenburg, M. Maniatis, M. Weber and P. M. Zerwas, in preparation.

[15] H. U. Martyn and G. A. Blair, in *Proc. of the International Workshop on Linear Colliders*, Sitges, Spain (1999), [hep-ph/9910416].

[16] H. U. Martyn, contribution to *Workshop on Physics at TeV Colliders*, Les Houches, France (1999), [hep-ph/0002290].

[17] J. L. Feng and M. E. Peskin, Phys. Rev. D **64** (2001) 115002 [hep-ph/0105100].

[18] C. Blöchinger, H. Fraas, G. Moortgat-Pick and W. Porod, hep-ph/0201282.

[19] Y. Fukuda *et al.* [SuperKamiokande Collaboration], Phys. Rev. Lett. **82** (1999) 2644 [hep-ex/9812014];
S. Fukuda *et al.* [SuperKamiokande Collaboration], Phys. Rev. Lett. **86** (2001) 5651 [hep-ex/0103032]. Q. R. Ahmad *et al.* [SNO Collaboration], nucl-ex/0204009.

[20] E. Witten, Nucl. Phys. B **188** (1981) 513.

[21] M. E. Machacek and M. T. Vaughn, Nucl. Phys. B **222** (1983) 83;
M. E. Machacek and M. T. Vaughn, Nucl. Phys. B **236** (1984) 221;
M. E. Machacek and M. T. Vaughn, Nucl. Phys. B **249** (1985) 70.

[22] L. E. Ibáñez and G. G. Ross, Phys. Lett. B **105** (1981) 439;
L. E. Ibáñez, C. López and C. Muñoz, Nucl. Phys. B **256** (1985) 218;
M. B. Einhorn and D. R. Jones, Nucl. Phys. B **196** (1982) 475;
V. D. Barger, M. S. Berger and P. Ohmann, Phys. Rev. D **47** (1993) 1093 [hep-ph/9209232].

[23] U. Amaldi, W. de Boer and H. Fürstenau, Phys. Lett. B **260** (1991) 447;
W. de Boer, Prog. Part. Nucl. Phys. **33** (1994) 201 [hep-ph/9402266].

[24] D. Z. Freedman, P. van Nieuwenhuizen and S. Ferrara, Phys. Rev. D **13** (1976) 3214;
S. Deser and B. Zumino, Phys. Lett. B **62** (1976) 335;
P. van Nieuwenhuizen, Phys. Rept. **68** (1981) 189.

[25] H. P. Nilles, Phys. Rept. **110** (1984) 1.

[26] J. R. Ellis, J. S. Hagelin, D. V. Nanopoulos, K. A. Olive and M. Srednicki, Nucl. Phys. B **238** (1984) 453.

[27] F. Gabbiani and A. Masiero, Nucl. Phys. B **322** (1989) 235.

[28] M. Spira and P. M. Zerwas, lectures given at *36. Internationale Universitätswochen für Kernphysik und Teilchenphysik: Computing Particle Properties*, Schladming, Austria (1997) [hep-ph/9803257].

[29] H. E. Haber and R. Hempfling, Phys. Rev. Lett. **66** (1991) 1815;
Y. Okada, M. Yamaguchi and T. Yanagida, Prog. Theor. Phys. **85** (1991) 1;
J. R. Ellis, G. Ridolfi and F. Zwirner, Phys. Lett. B **257** (1991) 83;
J. R. Ellis, G. Ridolfi and F. Zwirner, Phys. Lett. B **262** (1991) 477;
A. Yamada, Phys. Lett. B **263** (1991) 233;
A. Brignole, J. R. Ellis, G. Ridolfi and F. Zwirner, Phys. Lett. B **271** (1991) 123;
P. Chankowski, S. Pokorski and J. Rosiek, Phys. Lett. B **274** (1992) 191;
P. Chankowski, S. Pokorski and J. Rosiek, Nucl. Phys. B **423** (1994) 437 [hep-ph/9303309].

[30] J. R. Espinosa and M. Quiros, Phys. Lett. B **266** (1991) 389;
R. Hempfling and A. H. Hoang, Phys. Lett. B **331** (1994) 99 [hep-ph/9401219];
J. A. Casas, J. R. Espinosa, M. Quiros and A. Riotto, Nucl. Phys. B **436** (1995) 3 [Erratum-ibid. B **439** (1995) 466] [hep-ph/9407389];
M. Carena, M. Quiros and C. E. Wagner, Nucl. Phys. B **461** (1996) 407 [hep-ph/9508343];
J. R. Espinosa and R. J. Zhang, Nucl. Phys. B **586** (2000) 3 [hep-ph/0003246];
G. Degrassi, P. Slavich and F. Zwirner, Nucl. Phys. B **611** (2001) 403 [hep-ph/0105096];
A. Brignole, G. Degrassi, P. Slavich and F. Zwirner, hep-ph/0112177.

[31] S. Heinemeyer, W. Hollik and G. Weiglein, Phys. Rev. D **58** (1998) 091701 [hep-ph/9803277];
S. Heinemeyer, W. Hollik and G. Weiglein, Phys. Lett. B **440** (1998) 296 [hep-ph/9807423];
S. Heinemeyer, W. Hollik and G. Weiglein, Eur. Phys. J. C **9** (1999) 343 [hep-ph/9812472].

[32] J. M. Frère, D. R. Jones and S. Raby, Nucl. Phys. B **222** (1983) 11;
M. Claudson, L. J. Hall and I. Hinchliffe, Nucl. Phys. B **228** (1983) 501;
C. Kounnas, A. B. Lahanas, D. V. Nanopoulos and M. Quiros, Nucl. Phys. B **236** (1984) 438;
J. F. Gunion, H. E. Haber and M. Sher, Nucl. Phys. B **306** (1988) 1.

[33] H. E. Haber and G. L. Kane, Phys. Rept. **117** (1985) 75.

[34] J. F. Gunion and H. E. Haber, Nucl. Phys. B **272** (1986) 1 [Erratum-ibid. B **402** (1993) 567];
J. F. Gunion and H. E. Haber, Nucl. Phys. B **278** (1986) 449;
J. F. Gunion and H. E. Haber, Nucl. Phys. B **307** (1988) 445 [Erratum-ibid. B **402** (1993) 569].

[35] J. Küblbeck, M. Böhm and A. Denner, Comput. Phys. Commun. **60** (1990) 165;
T. Hahn, Comput. Phys. Commun. **140** (2001) 418 [hep-ph/0012260];
T. Hahn, *FeynArts 3 User's Guide* (2001), [`http://www.feynarts.de`].

[36] A. Denner, H. Eck, O. Hahn and J. Küblbeck, Nucl. Phys. B **387** (1992) 467.

[37] T. Hahn and C. Schappacher, Comput. Phys. Commun. **143** (2002) 54 [hep-ph/0105349].

[38] S. Ferrara, L. Girardello and F. Palumbo, Phys. Rev. D **20** (1979) 403.

[39] D. Z. Freedman and P. van Nieuwenhuizen, Phys. Rev. D **14** (1976) 912;
E. Cremmer, B. Julia, J. Scherk, S. Ferrara, L. Girardello and P. van Nieuwenhuizen, Nucl. Phys. B **147** (1979) 105;
E. Cremmer, S. Ferrara, L. Girardello and A. Van Proeyen, Nucl. Phys. B **212** (1983) 413.

[40] L. J. Hall, J. Lykken and S. Weinberg, Phys. Rev. D **27** (1983) 2359.

[41] K. Inoue, A. Kakuto, H. Komatsu and S. Takeshita, Prog. Theor. Phys. **68** (1982) 927 [Erratum-ibid. **70** (1983) 330];
S. P. Martin and M. T. Vaughn, Phys. Rev. D **50** (1994) 2282 [hep-ph/9311340];
Y. Yamada, Phys. Rev. D **50** (1994) 3537 [hep-ph/9401241];
D. M. Pierce, J. A. Bagger, K. T. Matchev and R. j. Zhang, Nucl. Phys. B **491** (1997) 3 [hep-ph/9606211].

[42] M. Dine and W. Fischler, Phys. Lett. B **110** (1982) 227;
C. R. Nappi and B. A. Ovrut, Phys. Lett. B **113** (1982) 175;
L. Alvarez-Gaumé, M. Claudson and M. B. Wise, Nucl. Phys. B **207** (1982) 96;
M. Dine and A. E. Nelson, Phys. Rev. D **48** (1993) 1277 [hep-ph/9303230].

[43] S. Ambrosanio, G. D. Kribs and S. P. Martin, Phys. Rev. D **56** (1997) 1761 [hep-ph/9703211].

[44] L. Randall and R. Sundrum, Nucl. Phys. B **557** (1999) 79 [hep-th/9810155];
G. F. Giudice, M. A. Luty, H. Murayama and R. Rattazzi, JHEP **9812** (1998) 027 [hep-ph/9810442];
M. Dine, A. E. Nelson, Y. Nir and Y. Shirman, Phys. Rev. D **53** (1996) 2658 [hep-ph/9507378].

[45] I. Hinchliffe and L. Littenberg, in *Proc. of DPF Summer Study on Elementary Particle Physics and Future Facilities, Aspen, Colorado, 1982*, LBL-15022;
R. M. Barnett, H. E. Haber and K. S. Lackner, Phys. Rev. D **29** (1984) 1381;
T. Kobayashi and M. Kuroda, Phys. Lett. B **134** (1984) 271;
D. H. Schiller and D. Wähner, Nucl. Phys. B **255** (1985) 505.

[46] A. Ballestrero and E. Maina, Phys. Lett. B **173** (1986) 341.

[47] M. Glück and E. Reya, Phys. Lett. B **130** (1983) 423.

[48] A. Bartl, H. Fraas and W. Majerotto, Z. Phys. C **34** (1987) 411;
B. de Carlos and M. A. Diaz, Phys. Lett. B **417** (1998) 72 [hep-ph/9511421].

[49] M. K. Gaillard, L. J. Hall and I. Hinchliffe, Phys. Lett. B **116** (1982) 279 [Erratum-ibid. B **119** (1982) 471];
M. Kuroda, K. Ishikawa, T. Kobayashi and S. Yamada, Phys. Lett. B **127** (1983) 467 [Erratum-ibid. B **154** (1983) 457];
I. Hayashibara, F. Takasaki, Y. Shimizu and M. Kuroda, Phys. Lett. B **158** (1985) 349;
A. R. Allan, N. Brown and A. D. Martin, Z. Phys. C **31** (1986) 479;
K. Hidaka, H. Komatsu and P. Ratcliffe, Nucl. Phys. B **304** (1988) 417.

[50] T. Schimert and X. Tata, Phys. Rev. D **32** (1985) 721.

[51] A. Datta and A. Djouadi, hep-ph/0111466.

[52] T. Tsukamoto, K. Fujii, H. Murayama, M. Yamaguchi and Y. Okada, Phys. Rev. D **51** (1995) 3153.

[53] W. Beenakker and A. Denner, Int. J. Mod. Phys. A **9** (1994) 4837.

[54] W. Beenakker *et al.*, in *Physics at LEP2*, eds. G. Altarelli, T. Sjöstrand, F. Zwirner (CERN-96-01), Vol. 1, 79 [hep-ph/9602351].

[55] A. Denner, S. Dittmaier, M. Roth and D. Wackeroth, Nucl. Phys. B **560** (1999) 33 [hep-ph/9904472].

[56] M. J. Veltman, Physica **29** (1963) 186;
R. G. Stuart, Phys. Lett. B **262** (1991) 113;
A. Aeppli, G. J. van Oldenborgh and D. Wyler, Nucl. Phys. B **428** (1994) 126 [hep-ph/9312212].

[57] W. Beenakker, F. A. Berends and A. P. Chapovsky, Nucl. Phys. B **548** (1999) 3 [hep-ph/9811481];
A. Denner, S. Dittmaier, M. Roth and D. Wackeroth, Nucl. Phys. B **587** (2000) 67 [hep-ph/0006307].

[58] N. Nakanishi, Prog. Theo. Phys. **19** (1958) 159;
T. Kinoshita, J. Math. Phys. **3** (1962) 650;
T. D. Lee and M. Nauenberg, Phys. Rev. **133** (1964) B1549.

[59] E. A. Kuraev and V. S. Fadin, Sov. J. Nucl. Phys. **41** (1985) 466 [Yad. Fiz. **41** (1985) 733];
G. Altarelli and G. Martinelli, in *Physics at LEP*, eds. J. Ellis and R. Peccei (CERN-86-02), Vol. 1, p. 47.

[60] F. A. Berends *et al*, in *Z Physics at LEP 1*, eds. G. Altarelli, R. Kleiss and C. Verzegnassi (CERN-89-08), p. 89.

[61] M. Skrzypek and S. Jadach, Z. Phys. C **49** (1991) 577;
M. Skrzypek, Acta Phys. Polon. B **23** (1992) 135;
M. Cacciari, A. Deandrea, G. Montagna and O. Nicrosini, Europhys. Lett. **17** (1992) 123.

[62] T. Ohl, Comput. Phys. Commun. **101** (1997) 269 [hep-ph/9607454].

[63] D. Schulte, CERN-PS-99-014.

[64] A. Sommerfeld, *Atombau und Spektrallinien*, Bd. 2, (Vieweg, Braunschweig, 1939);
A. D. Sakharov, Zh. Eksp. Teor. Fiz. **18** (1948) 631 [Sov. Phys. Usp. **34** (1948) 375].

[65] V. S. Fadin and V. A. Khoze, JETP Lett. **46** (1987) 525 [Pisma Zh. Eksp. Teor. Fiz. **46** (1987) 417];
V. S. Fadin and V. A. Khoze, Sov. J. Nucl. Phys. **48** (1988) 309 [Yad. Fiz. **48** (1988) 487].

[66] V. S. Fadin, V. A. Khoze and A. D. Martin, Phys. Lett. B **311** (1993) 311;
V. S. Fadin, V. A. Khoze and A. D. Martin, Phys. Lett. B **320** (1994) 141 [hep-ph/9309234].

[67] D. Y. Bardin, W. Beenakker and A. Denner, Phys. Lett. B **317** (1993) 213.

[68] V. S. Fadin, V. A. Khoze, A. D. Martin and A. Chapovsky, Phys. Rev. D **52** (1995) 1377 [hep-ph/9501214].

[69] R. Kleiss and W. J. Stirling, Nucl. Phys. B **262** (1985) 235.

[70] E. Byckling and K. Kajantie, *Particle Kinematics*, Wiley & Sons, London (1973).

[71] F. A. Berends, P. H. Daverveldt and R. Kleiss, Nucl. Phys. B **253** (1985) 441;
F. A. Berends, P. H. Daverveldt and R. Kleiss, Comput. Phys. Commun. **40** (1986) 285;
J. Hilgart, R. Kleiss and F. Le Diberder, Comput. Phys. Commun. **75** (1993) 191.
F. A. Berends, R. Pittau and R. Kleiss, Nucl. Phys. B **424** (1994) 308 [hep-ph/9404313].

[72] R. Kleiss and R. Pittau, Comput. Phys. Commun. **83** (1994) 141 [hep-ph/9405257].

[73] H.-U. Martyn, in *Conceptual Design of a 500 GeV e^+e^- Linear Collider*, eds. R. Brinkmann, G. Materlik, J. Rossbach and A. Wagner, DESY 1997-048 and ECFA 1997-182.

[74] A. Freitas, D. J. Miller and P. M. Zerwas, Eur. Phys. J. C **21** (2001) 361 [hep-ph/0106198].

[75] F. Cuypers, G. J. van Oldenborgh and R. Rückl, Nucl. Phys. B **409** (1993) 128 [hep-ph/9305287].

[76] V. D. Barger and T. Han, Phys. Lett. B **212** (1988) 117;
V. D. Barger, T. Han and R. J. Phillips, Phys. Rev. D **39** (1989) 146;
A. Tofighi-Niaki and J. F. Gunion, Phys. Rev. D **39** (1989) 720.

[77] A. Freitas, D. J. Miller and P. M. Zerwas, in *2nd ECFA/DESY Linear Collider Study*, DESY Hamburg (2000), LC Note LC-TH-2001-011;
A. Freitas and D. J. Miller, in *Proc. of the APS/DPF/DPB Summer Study on the Future of Particle Physics (Snowmass 2001)* ed. R. Davidson and C. Quigg, [hep-ph/0111430].

[78] J. Guasch, W. Hollik and J. Solà, Phys. Lett. B **510** (2001) 211 [hep-ph/0101086].

[79] C. G. Bollini and J. J. Giambiagi, Nuovo Cim. B **12** (1972) 20;
J. F. Ashmore, Lett. Nuovo Cim. **4** (1972) 289;
G. 't Hooft and M. J. Veltman, Nucl. Phys. B **44** (1972) 189.

[80] W. Hollik, E. Kraus and D. Stöckinger, Eur. Phys. J. C **23** (2002) 735 [arXiv:hep-ph/0007134].

[81] W. Hollik and D. Stöckinger, Eur. Phys. J. C **20** (2001) 105 [hep-ph/0103009].

[82] S. P. Martin and M. T. Vaughn, Phys. Lett. B **318** (1993) 331 [hep-ph/9308222].

[83] W. Siegel, Phys. Lett. B **84** (1979) 193.

[84] D. M. Capper, D. R. Jones and P. van Nieuwenhuizen, Nucl. Phys. B **167** (1980) 479.

[85] W. Siegel, P. K. Townsend and P. van Nieuwenhuizen, in *Proc. of Cambridge meeting on superspace and supergravity (Cambridge 1980)* p. 165–175, ITP-SB-80-65;
R. van Damme and G. 't Hooft, Phys. Lett. B **150** (1985) 133.

[86] I. Jack, D. R. Jones and K. L. Roberts, Z. Phys. C **62** (1994) 161 [hep-ph/9310301];
I. Jack, D. R. Jones and K. L. Roberts, Z. Phys. C **63** (1994) 151 [hep-ph/9401349].

[87] L. V. Avdeev, G. A. Chochia and A. A. Vladimirov, Phys. Lett. B **105** (1981) 272.

[88] W. Siegel, Phys. Lett. B **94** (1980) 37.

[89] A. Denner, Fortsch. Phys. **41** (1993) 307.

[90] H. Eberl, A. Bartl and W. Majerotto, Nucl. Phys. B **472** (1996) 481 [hep-ph/9603206];
A. Djouadi, W. Hollik and C. Jünger, Phys. Rev. D **55** (1997) 6975 [hep-ph/9609419].

[91] J. Guasch, J. Solà and W. Hollik, Phys. Lett. B **437** (1998) 88 [hep-ph/9802329].

[92] H. Rzehak, Diplomarbeit, Karlsruhe (2001) [`http://www-itp.physik.uni-karlsruhe.de/prep/diploma/`].

[93] D. Pierce and A. Papadopoulos, Phys. Rev. D **50** (1994) 565 [hep-ph/9312248]. D. Pierce and A. Papadopoulos, Nucl. Phys. B **430** (1994) 278 [hep-ph/9403240].

[94] H. Eberl, M. Kincel, W. Majerotto and Y. Yamada, Phys. Rev. D **64** (2001) 115013 [hep-ph/0104109].

[95] T. Fritzsche and W. Hollik, hep-ph/0203159.

[96] B. A. Kniehl and A. Pilaftsis, Nucl. Phys. B **474** (1996) 286 [hep-ph/9601390].

[97] A. Freitas and D. Stöckinger, hep-ph/0205281.

[98] A. Dabelstein, Z. Phys. C **67** (1995) 495 [hep-ph/9409375].

[99] P. Chankowski, S. Pokorski and J. Rosiek, Nucl. Phys. B **423** (1994) 437 [hep-ph/9303309].

[100] L. H. Wan, W. G. Ma, R. Y. Zhang and J. Yi, Phys. Rev. D **64** (2001) 115004 [hep-ph/0107089].

[101] M. Frank, S. Heinemeyer, W. Hollik and G. Weiglein, hep-ph/0202166.

[102] H. Kluberg-Stern and J. B. Zuber, Phys. Rev. D **12** (1975) 467; O. Piguet and K. Sibold, Nucl. Phys. B **253** (1985) 517.

[103] Y. Yamada, Phys. Lett. B **530** (2002) 174 [hep-ph/0112251].

[104] R. Häussling and E. Kraus, Z. Phys. C **75** (1997) 739 [hep-th/9608160].

[105] M. Carena, S. Heinemeyer, C. E. Wagner and G. Weiglein, hep-ph/9912223.

[106] J. A. Coarasa, D. Garcia, J. Guasch, R. A. Jiménez and J. Solà, Eur. Phys. J. C **2** (1998) 373 [hep-ph/9607485].

[107] R. Mertig, M. Böhm and A. Denner, Comput. Phys. Commun. **64** (1991) 345.

[108] T. Hahn and M. Pérez-Victoria, Comput. Phys. Commun. **118** (1999) 153 [hep-ph/9807565].

[109] T. Hahn, *FormCalc 3 User's Guide* (2001), [`http://www.feynarts.de/formcalc`].

[110] F. del Aguila, A. Culatti, R. Muñoz Tapia and M. Pérez-Victoria, Nucl. Phys. B **537** (1999) 561 [hep-ph/9806451].

[111] G. Passarino and M. J. Veltman, Nucl. Phys. B **160** (1979) 151.

[112] G. 't Hooft and M. J. Veltman, Nucl. Phys. B **153** (1979) 365; A. Denner, U. Nierste and R. Scharf, Nucl. Phys. B **367** (1991) 637.

[113] G. J. van Oldenborgh and J. A. Vermaseren, Z. Phys. C **46** (1990) 425;
T. Hahn, *LoopTools 2 User's Guide* (2001),
[`http://www.feynarts.de/looptools`].

[114] A. v. Manteuffel, Diplomarbeit, Hamburg (2002).

[115] T. Appelquist and J. Carazzone, Phys. Rev. D **11** (1975) 2856.

[116] M. M. Nojiri, K. Fujii and T. Tsukamoto, Phys. Rev. D **54** (1996) 6756 [hep-ph/9606370].

[117] H. C. Cheng, J. L. Feng and N. Polonsky, Phys. Rev. D **56** (1997) 6875 [hep-ph/9706438].

[118] M. J. Veltman, Nucl. Phys. B **123** (1977) 89;
M. E. Peskin and T. Takeuchi, Phys. Rev. Lett. **65** (1990) 964;
M. E. Peskin and T. Takeuchi, Phys. Rev. D **46** (1992) 381.

[119] H. C. Cheng, J. L. Feng and N. Polonsky, Phys. Rev. D **57** (1998) 152 [hep-ph/9706476].

[120] M. Dima *et al.*, Phys. Rev. D **65** (2002) 071701 [hep-ex/0112017].

[121] J. K. Mizukoshi, H. Baer, A. S. Belyaev and X. Tata, Phys. Rev. D **64** (2001) 115017 [hep-ph/0107216].

[122] S. Baker and R. D. Cousins, Nucl. Instrum. Meth. A **221** (1984) 437.

[123] S. Y. Choi, J. Kalinowski, G. Moortgat-Pick and P. M. Zerwas, Eur. Phys. J. C **22** (2001) 563 [hep-ph/0108117].

[124] B. C. Allanach *et al.*, in *Proc. of the APS/DPF/DPB Summer Study on the Future of Particle Physics (Snowmass 2001)* ed. R. Davidson and C. Quigg, [hep-ph/0202233].

[125] H. Baer, F. E. Paige, S. D. Protopopescu and X. Tata, hep-ph/0001086.

[126] N. Ghodbane and H. U. Martyn, in *Proc. of the APS/DPF/DPB Summer Study on the Future of Particle Physics (Snowmass 2001)* ed. R. Davidson and C. Quigg, [hep-ph/0201233].

[127] S. Ambrosanio, G. A. Blair and P. M. Zerwas, *A Study of mSUGRA for the Linear Collider* (1998) [`http://www.hep.ph.rhbnc.ac.uk/ blair/susy`].

[128] S. Heinemeyer, W. Hollik and G. Weiglein, Comput. Phys. Commun. **124** (2000) 76 [hep-ph/9812320].

[129] A. Djouadi, J. Kalinowski and M. Spira, Comput. Phys. Commun. **108** (1998) 56 [hep-ph/9704448].

[130] A. Bartl, H. Fraas and W. Majerotto, Z. Phys. C **30** (1986) 441;
A. Bartl, H. Fraas and W. Majerotto, Nucl. Phys. B **278** (1986) 1.

Acknowledgements

First of all I am very much obliged to my thesis advisor Peter Zerwas for the suggestion of the project and support throughout this work. I have profited from his experience and his help to bring me into fruitful contact with the high energy physics community.

I am grateful to Andreas von Manteuffel, David John Miller and Dominik Stöckinger for a pleasant and prolific collaboration in various parts of this project and for numerous discussions. Many thanks to David John Miller and Georg Weiglein for proof-reading parts of the draft.

Many thanks to all my colleagues and friends at DESY for the pleasant and relaxed working atmosphere. During my work I have learned a lot from many discussions with Klaus Desch, Stefan Dittmaier, Thomas Fritzsche, Markos Maniatis, Hans-Ulrich Martyn, Gudrid Moortgat-Pick and Benedikt Plümper. I have also enjoyed the fruitful and cooperative communications within the ECFA/DESY Linear Collider Study.

Special thanks to the Spontaneous Harmony Breakers, Jenny Böhme, Laura Covi, Markus Diehl, Babette Dörmer, Birgit Eberle, Stefan Fredenhagen, Markus Knodel, Sabine Lammers, Fantina Madricardo, Gudrid Moortgat-Pick, Mauro Papinutto, Matthias de Riese, Christiane Risler, Luigi Scorzato, Michael "Pfeil" Spira, Sören Wiesenfeldt and Jan Würthner, for some spontaneous syllable breaking and many marvellous spontaneous harmonies [131].

To my parents I'm particularly grateful for their continuous encouragement and support over the years.

[131] J. Böhme *et al.* [the Spontaneous Harmony Breakers], contribution to *the 10th International Conference on Supersymmetry and Unification of Fundamental Interactions*, Hamburg, Germany (2002).